Predictor-Based Cooperative Adaptive Cruise Control of Vehicular Platoons with Actuation and Communication Delays

by

Amirhossein Samii

A dissertation
submitted in partial fulfillment of the
requirements for the degree of

Doctor of Philosophy
in
Technical University of Crete
School of Electrical and Computer Engineering

Committee in Charge:
Professor Nikolaos Bekiaris-Liberis (Supervisor)
Professor Thrasyvoulos Spyropoulos
Professor Eftichis Koutroulis

Chania, September 2025

Thesis Committee Members:

Professor Nikolaos Bekiaris-Liberis
Technical University of Crete, School of ECE

Professor Thrasyvoulos Spyropoulos
Technical University of Crete, School of ECE

Professor Eftichis Koutroulis
Technical University of Crete, School of ECE

Professor Michail Lagoudakis
Technical University of Crete, School of ECE

Professor Stefania Santini
University of Napoli Federico II

Professor Meng Wang
Technische Universitat Dresden

Professor Themistoklis Charalambous
University of Cyprus

Abstract

Traffic flow efficiency and safety can be significantly improved via Cooperative Adaptive Cruise Control (CACC) of vehicular platoons. One critical property in vehicle platooning is *string stability*, which is essential for ensuring both safety and efficiency. String stability serves as a key indicator of how efficiently disturbances are attenuated as they propagate upstream in a platoon. However, the benefits of string (and vehicle) stability may be compromised in the presense of delays in actuation, sensing, or communication.

This research aims to develop *predictor-based* CACC designs to compensate the negative effects of *long actuation and communication delays* in vehicular platoons. The proposed control design framework is applied to heterogeneous vehicular platoons, where each vehicle's dynamics are modeled by a third-order linear system with input delay. For each design we develop, we establish vehicle stability, string stability, and tracking of the desired speed/spacing. The proofs of individual vehicle stability, string stability, and regulation rely mainly on employment of an input-output approach on the frequency/time domains. We present consistent simulation results, including validations with real traffic data. We further provide experimental validation results, in a pair of real vehicles, of one of our predictor-based CACC designs.

Acknowledgements

Besides hard work, creativity and luck, the completion of this endeavour required proper guidance and support. For the last two, I'm thankful to Professor Bekiaris-Liberis, a true professional, for his support throughout the last 3 years of my work in our lab. I would also like to acknowledge my colleagues, Panagiotis A. Karafotis and Redmer de Haan, for thier fruitful suggestions and assistance to enhance the quality of my work. I am equally thankful to the members of my thesis committee, Prof. Koutroulis and Prof. Spyropoulos, for their constructive feedback and essential suggestions.

This thesis is a reflection of the unwavering support and boundless love I received from my family and friends during this challenging academic pursuit. I owe an immense debt of gratitude to my parents, who nurtured my curiosity and supported my educational endeavours from the very beginning. To my wife, Fatemeh, your endless patience and understanding, especially during the most demanding phases of this research, have been my anchor. My appreciation also goes to my friends in the Technical University of Crete, whose resources and assistance have been invaluable. Their collective wisdom and encouragement have been a cornerstone of my research experience.

This work was supported by the Hellenic Foundation for Research and Innovation (H.F.R.I.) under the "2nd Call for H.F.R.I. Research Projects to Support Faculty Members & Researchers" (Project Number: 3537/ORAMA). Co-funded by the European Union (ERC, C-NORA, 101088147). Views and opinions expressed are however those of the authors only and do not necessarily reflect those of the European Union or the European Research Council. Neither the European Union nor the granting authority can be held responsible for them.

True knowledge is that which leads you to perfection, not that which merely adds to your information.

–Avicenna (Ibn Sina)

Contents

Abstract iv
Acknowledgements v

1 Introduction **1**
1.1 Motivation 1
1.2 Literature 1
1.3 Contributions 2
1.4 Organization 5
1.5 Notation and Definitions 5

2 Robustness of String Stability of Linear Predictor-Feedback CACC to Communication Delay **7**
2.1 Chapter Organization 7
2.2 Robustness of Predictor-Feedback CACC for Heterogeneous Platoons to Communication Delay 8
2.2.1 Vehicle Model and Predictor-Feedback CACC Design 8
2.2.2 Main Result 10
2.3 Simulation Results 16
2.4 Chapter Conclusions and Related Publications 20

3 Simultaneous Compensation of Actuation and Communication Delays for Heterogeneous Platoons **22**
3.1 Chapter Organization 23
3.2 Predictor-Feedback CACC for Heterogeneous Platoons with Both Actuator and Communication Delays 23
3.2.1 Vehicle Model and Nominal Delay-Free Design 23
3.2.2 Communication Delay-Compensating Predictor-Feedback Control Design 24
3.3 String Stability Despite Actuation and Communication Delays 25

3.4 Numerical Illustration of String Stability 36
3.5 Simulation Results 37
3.5.1 Predictor-Feedback CACC with Simultaneous Compensation of Actuator/Communication Delays 38
3.5.2 Predictor-Feedback without Compensation of Communication Delay 41
3.5.3 Validation with NGSIM Data 43
3.6 Chapter Conclusions and Related Publications 44

4 Numerical Investigation of Head-to-Tail String Stability 46
4.1 Chapter Organization 46
4.2 Predictor-Based ACC for Mixed Traffic 47
4.2.1 Automated Vehicle Model and Nominal Delay-Free Control Design 47
4.2.2 Predictor-Based ACC Design with Actuator Delay 48
4.2.3 Human-Driven Vehicle Model 49
4.3 Head-to-Tail String Stability of Mixed Traffic 49
4.4 Stability and String Stability 51
4.4.1 Automated Vehicles 51
4.4.2 Human-Driven Vehicles 52
4.5 Numerical Investigation of Head-To-Tail String Stability 52
4.6 Simulation and Optimal Choice of Controller Parameters 54
4.7 Chapter Conclusions and Related Publications 59

5 Predictor-Based CACC Design for Heterogeneous Vehicles with Distinct Input Delays 60
5.1 Chapter Organization 61
5.2 Predictor-Based CACC for Heterogeneous Platoons with Distinct Actuator Delays 61
5.2.1 Vehicle Model and Nominal Delay-Free Design 61
5.2.2 Predictor-Based Control Design for Compensation of Distinct Actuation Delays 62
5.3 String Stability Despite Distinct Actuation Delays 63
5.4 Numerical Illustration of String Stability 68
5.5 Simulation Results 70
5.5.1 Predictor-Based CACC Design 70
5.5.2 Predictor-Feedback Control Design 74
5.5.3 Predictor-Based CACC Design Validation with the OpenACC Dataset 76
5.5.4 Predictor-Based ACC Design 79

5.6 Robustness of String Stability of Predictor-Based CACC for Distinct Input Delays to Distinct Communication Delays . . . 82
5.6.1 Numerical Illustration of String Stability . . . 83
5.6.2 Simulation Results . . . 84
5.7 Chapter Conclusions and Related Publications . . . 86

6 Exact Predictor-Feedback CACC of Heterogeneous Vehicular Platoons 87
6.1 Chapter Organization . . . 88
6.2 Exact Predictor-Feedback CACC for Heterogeneous Platoons with Distinct Delays . . . 88
6.2.1 Vehicle Model and Nominal Delay-Free Design . . . 88
6.2.2 Exact Predictor-Feedback CACC for Distinct Delays . . . 89
6.3 String Stability Despite Distinct Actuation Delays . . . 93
6.4 Illustrative Example . . . 96
6.5 Simulation Results . . . 99
6.5.1 Exact Predictor-Feedback CACC Design with Leader's Intention . . . 99
6.5.2 Predictor-Based CACC Design . . . 102
6.5.3 Robustness of String Stability of Predictor-Feedback CACC to Parameters Mismatches . . . 103
6.5.4 Validation with the OpenACC Dataset . . . 104
6.5.5 Validation with NGSIM Dataset . . . 106
6.6 Chapter Conclusions and Related Publications . . . 108

7 Experimental Implementation and Validation of Predictor-Based CACC for Vehicular Platoons 109
7.1 Chapter Organization . . . 109
7.2 CACC for Heterogeneous Platoons with Distinct Actuation Delays . . . 110
7.2.1 Vehicle Model and Available Measurements . . . 110
7.2.2 Continuous Predictor-Based CACC Design . . . 111
7.2.3 Predictor-Based CACC Design for Distinct Delays Implemented with Zero-Order Hold . . . 112
7.3 Numerical Investigation of String Stability in Discrete Time And Simulation Results . . . 113
7.3.1 Choice of Control Parameters . . . 114
7.3.2 Simulation Results . . . 115
7.4 Experimental Implementation and Validation . . . 119
7.4.1 Description of the Experimental Setup . . . 119

7.4.2 Experimental Results 120
7.5 Chapter Conclusions and Related Publications 122

8 Perspectives **123**

Bibliography **124**

Complete List of Publications **131**

Chapter 1

Introduction

1.1 Motivation

String stability[1] is a crucial requirement that serves as an indicator of the safety and efficiency properties of platoons consisting of vehicles equipped with Adaptive Cruise Control (ACC) and Cooperative Adaptive Cruise Control (CACC) capabilities; see, for example, [12], [39], [42]. This property is imperiled in the presence of delays that affect actuation, sensing, or communication of vehicular systems; see, for example, [4], [14], [19], [35], [41], [55], [57], [62], [67]. Lack of string (or vehicle) stability in a platoon may, in particular, imply increased fuel consumption and decreased safety properties, due to, e.g., the emergence of stop-and-go waves [4], [7], [46]. For this reason, in the thesis we develop CACC laws to compensate long actuation and communication delays in vehicular platoons.

1.2 Literature

Existing works address small actuation delays only [24, 55], or small communication delays only [1], [10], [41], [43], or both [13], [19], [32], [39], [59], [61]. To address larger actuation or communication delays a predictor-based approach is required. Predictor-based control designs addressing long actuation and communication delays can be found in [4], [7], [14], [18], [36], [35], [51], [57], [58], [60], and [62]. The problem of compensation of long and *distinct* (for each vehicle) actuation delays is addressed in [14] and [63]. In [14] a distributed, sampled-data predictor-based controller is introduced and [63] employs a

[1]String stability refers to the property that any small disturbance in the lead car's speed is either damped or remains the same as it propagates down the line. This ensures that no following car overreacts, allowing traffic to flow smoothly.

switching type delay-adaptive predictor, which is designed to estimate the unknown input delay for each vehicle. As compared with the related existing results, this thesis makes the following contributions: (a) develops new, less complex predictor-feedback CACC designs, b) achieves simultaneous compensation of large actuation/communication delays, c) achieves complete compensation of large/distinct actuation delays, d) develops constructive and systematic approaches for establishing individual vehicles' stability, string stability, and regulation of the closed-loop systems, and e) validates the designs with real traffic data and in actual experiments. Table 1.1 illustrates the distinctions between the present thesis and related, existing works.

Table 1.1: Various types of delays addressed in literature

Delays Types \ References	[7], [4], [14], [18], [36], [35], [51], [57], [60]	[58]	[62] and current thesis	[1], [13], [10], [19], [24], [32], [39], [41], [43], [55], [59], [61]	[14, 62, 63], and current thesis
Small actuation and/or communication delays				✓	
Large actuation delay *only*	✓				
Large communication delay *only*		✓			
Simultaneous large actuation and communication delays			✓		
Distinct/large actuation delays					✓

1.3 Contributions

In the present thesis, we first start studying robustness of string stability of predictor-feedback CACC, which is developed for compensation of actuator delay, to the presence of communication delays. In particular, complementing [4], we perform this study for heterogeneous vehicles with third-order dynamics. We also provide consistent simulations of the responses of vehicles in a platoon, with respect to initial conditions deviations from equilibrium and leading vehicle's maneuvers.

To achieve full compensation for both actuation and communication delays, we then construct a linear, predictor-feedback CACC law augmented with an integral term of the difference between the preceding vehicle's, delayed, by an amount equal to the respective communication delay, speed and its current speed. In particular, we consider platoons of vehicles with heterogeneous dynamics described by a third-order linear system with actuation delay, subject to communication delays. The control design developed achieves $\mathcal{L}_2$ string stability with respect to speed/acceleration errors propagation (and with respect to spacing errors propagation as well, in the particular case of homogeneous vehicles). Furthermore, the control design achieves stability of individual vehicles (which is a prerequisite for string stability) and zero, steady-state speed and spacing tracking errors, for a constant leader's speed. To achieve zero, steady-state spacing tracking error it is required to reduce the original time-headway by an amount equal to the respective communication delay, which imposes a condition that the desired time-headway is larger than the respective communication delay.

We next investigate a mixed traffic scenario in which we use a linearized optimal velocity model (OVM) with input delay for human-driven vehicles, while for the ACC-equipped vehicle at the tail of the platoon a linear, second-order system under input delay is used. Due to technical challenges associated with analytically investigating head-to-tail string stability and performance, we conduct a numerical study. In particular, employing the ACC law in [7], we perform an exhaustive search on three metrics quantifying performance in terms of fuel consumption, safety, and comfort. Additionally, utilizing the recommended optimal/allowable control parameters, we present consistent simulation results for a platoon of four vehicles.

Furthermore, due to the heterogeneous nature of actuation delays among vehicles in a platoon in real-world scenarios, we construct predictor-based CACC laws, which achieve input delay compensation, for platoons of heterogeneous vehicles whose dynamics are described by a third-order linear system with actuation delays that may be different for each individual vehicle. The control design developed achieves $\mathcal{L}_2$ string stability with respect to speed/acceleration errors propagation, under specific conditions that we derive on the ego vehicle's controller/model parameters, as well as on the model parameters of the preceding vehicle and the difference between the delay values of the ego vehicle and its preceding vehicle (no restriction is imposed on the size of each individual input delay). Furthermore, the control design achieves stability of individual vehicles (which is a prerequisite for string stability) and zero, steady-state speed and spacing tracking errors, for a constant leader's speed. We also present numerical and simulation results. Furthermore, we present simulation results of a platoon of seven vehicles, for the practical

scenario in which a vehicle cut in the platoon (described by considering initial conditions deviations from equilibrium) and subsequently performs an acceleration/deceleration maneuver. Moreover, we study numerically the robustness of $\mathcal{L}_2$ string stability of our predictor-based CACC design, in the presence of communication delays.

Since the predictor-based CACC design imposes a restriction on the values of the delay differences between consecutive vehicles (for guaranteeing string stability), we then develop CACC designs, which achieve complete input delay compensation, for platoons of heterogeneous vehicles whose dynamics are described by a third-order linear system with actuation delays that may be different/arbitrary for each individual vehicle. The design utilizes V2V (vehicle-to-vehicle) and V2X (vehicle-to-everything) communication, where the ego vehicle employs measurements and information about the delay/lag and control parameter values from all consecutive vehicles ahead that have a smaller input delay and from the first vehicle ahead that features a larger delay. Despite these requirements, because the control input of each vehicle achieves exact delay compensation, vehicle and string stability can be studied as in the nominal, delay-free case, considering pairs of vehicles, which is an advantage with respect to analysis' complexity. In particular, the control design developed achieves $\mathcal{L}_2$ string stability with respect to speed/acceleration errors propagation, stability of individual vehicles (which is a prerequisite for string stability), and zero steady-state, spacing/speed error, for a constant leader's speed. We also provide simulation results for a platoon of three vehicles. Moreover, we compare the performance of our developed design with the conventional predictor-based CACC design, which cannot guarantee string stability for large delay differences among vehicles. Furthermore, we present simulation results in even more realistic scenarios. In particular, real traffic data are used for the trajectory of the leading vehicle, taken from two different datasets, namely the OpenACC [33] and NGSIM [37] datasets, as well as the platoon consists of six vehicles.

Finally, to experimentally validate our approach in a real-world setup, we provide the explicit formulae of the respective predictor-based CACC design, when it is applied through zero-order hold employing sampled measurements. For such a sampled-data implementation we obtain vehicle and string stability conditions numerically, via derivation of the respective transfer functions relating the speeds of pairs of consecutive vehicles. We present consistent simulation results for a platoon of five vehicles, under digital implementation of the controller. We then present the description of the experimental setup, including the measurements/sensors employed, the parameters of control implementation, and the parameters identified for the model of the vehicles; we also present the results of the experimental implementation and validation of our controller in a pair of real vehicles.

The experimental results confirm that vehicle stability and string stability in speed error propagation are achieved despite long and distinct actuation delays affecting the vehicles.

1.4 Organization

In Chapter 2, we present robustness results of string stability of predictor-feedback CACC, which is developed for compensation of a fixed homogeneous actuator delay, to the presence of communication delays. In Chapter 3, we develop a linear predictor-feedback CACC law, augmented with an integral term, to simultaneously compensate for both actuation and communication delays. In Chapter 4, we investigate string stability in a mixed traffic scenario with both ACC-equipped and human-driven vehicles. In Chapters 5 and 6, we construct predictor-based CACC laws, which achieve input delay compensation, for platoons of heterogeneous vehicles with actuation delays that may be different for each individual vehicle. In Chapter 7, we implement and validate the predictor-based design introduced in Chapter 5 in a pair of full-scale real vehicles. We provide remarks for future research in Chapter 8.

1.5 Notation and Definitions

In the vehicular platoons considered, each vehicle is indexed by $i = 1, ..., N$, where $s_i = x_{i-1} - x_i - l_i$ and x_i is the position of vehicle i and l_i is its length, v_i is vehicle speed, a_i is vehicle acceleration, τ_i is lag, capturing engine dynamics, and u_i is the individual vehicle's control variable. Note that for the leading vehicle we assume similarly that it has the same type of third-order dynamics as the rest of the vehicles[2]. The difference is that u_l acts as a time-varying, exogenous input rather than as feedback control input. We adopt the convention that $v_0 = v_l$ and $a_0 = a_l$ are the speed and acceleration of the string leader, respectively.

We recall the definition of string stability employed in this thesis. A platoon of vehicles following each other within one lane without overtaking, is $\mathcal{L}_2$ string stable, if the following conditions hold

$$\sup_{\omega} |G_i(j\omega)| \leq 1, \qquad i = 1, ..., N, \tag{1.1}$$

where $G_i(j\omega)$ denotes the transfer function between the i-th vehicle's speed and the speed of its preceding vehicle $i-1$ (see, e.g., [12], [19]). It should be noted that string stability

[2]The respective design can be modified in a straightforward manner when this is not true.

of a platoon in the heterogeneous case depends on the selection of states used to analyze the propagation of disturbances (upstream in the platoon). Here we choose to study $\mathcal{L}_2$ string stability with respect to speed errors propagation for simplicity and because this is the most commonly used definition, see, for example, [19], [42], [62]. Note also that the respective transfer functions, corresponding to acceleration states, are identical to those for speed states, while for homogeneous platoons string stability with respect to spacing errors is equivalent to string stability with respect to speed/acceleration errors.

Chapter 2

Robustness of String Stability of Linear Predictor-Feedback CACC to Communication Delay

Linear predictor-feedback CACC achieves actuator delay compensation in vehicular platoons, provided that there is no V2V communication delay. In the present chapter, we establish robustness of string stability of predictor-feedback CACC to (uncertain) communication delay. The robustness property is established for heterogeneous vehicular platoons, in which, each individual vehicle's dynamics are described by a third-order linear system with input delay. The proof of robustness relies on employment of an input-output approach in the frequency domain, which enables derivation of explicit conditions on the value of communication delay, which guarantee string stability, depending on control laws and vehicle models parameters. The theoretical guarantees of string stability and the respective conditions on parameters are thoroughly illustrated also numerically.

2.1 Chapter Organization

The outline of the chapter is as follows. Section 2.2 presents the considered model of a heterogeneous platoon and the predictor-feedback designs, together with the main robustness result. In Section 2.3 we present numerical experiments for validation of the theoretical results and in Section 2.4 we provide concluding remarks.

2.2 Robustness of Predictor-Feedback CACC for Heterogeneous Platoons to Communication Delay

2.2.1 Vehicle Model and Predictor-Feedback CACC Design

a) Vehicle dynamics: We consider the following third-order, linear system with actuator delay that describes vehicle dynamics (see, e.g., [1], [57], [58], [59])

$$\dot{s}_i(t) = v_{i-1}(t) - v_i(t), \tag{2.1}$$

$$\dot{v}_i(t) = a_i(t), \tag{2.2}$$

$$\dot{a}_i(t) = -\frac{1}{\tau_i}a_i(t) + \frac{1}{\tau_i}u_i(t-D), \tag{2.3}$$

where $D \geq 0$ is actuator delay, and $t \geq 0$ is time.

b) Available measurements: For CACC platoons the measurements available to the ego vehicle i are its own spacing s_i, speed v_i, and acceleration a_i, as well as the speed of the preceding vehicle v_{i-1}. It is possible to obtain this information through on-board sensors. Furthermore, the control input of the preceding vehicle and its acceleration are also available and are denoted by $u_{i-1,\mathrm{m}}$ and $a_{i-1,\mathrm{m}}$ respectively. These measurements are transmitted from the preceding vehicle, through V2V communication. Due to the presence of communication delay these measurements are defined as $a_{i-1,\mathrm{m}}(t) = a_{i-1}(t-D_{\mathrm{c,i-1}})$ and $u_{i-1,\mathrm{m}}(\theta) = u_{i-1}(\theta - D_{\mathrm{c,i-1}}), \theta \in [t-D, t]$, respectively, where $D_{\mathrm{c,i-1}} \geq 0$, $i = 1, ..., N$, are fixed communication delays that may be different in each vehicle.

c) Nominal control design: Without actuation delay, the following control strategy is constructed

$$u_i(t) = \tau_i\alpha_i\left(\frac{s_i(t)}{h_i} - v_i(t)\right) + \tau_i b_i(v_{i-1}(t) - v_i(t)) + \tau_i c_i a_i(t), \tag{2.4}$$

where $\alpha_i > 0$, $b_i > 0$, and $c_i \in \mathbb{R}$ are design parameters, and $h_i > 0$ is the desired time-headway.

d) Predictor-feedback CACC design: The predictor-based control laws, under communication delay, for system (2.1)–(2.3) are given by

$$u_i(t) = \frac{\tau_i\alpha_i}{h_i}q_{i,1}(t) - \tau_i(\alpha_i + b_i)q_{i,2}(t) + \tau_i b_i q_{i,3}(t) + \tau_i c_i q_{i,4}(t), \tag{2.5}$$

$$q_i(t) = \mathrm{e}^{\Gamma_i D}\bar{x}_i(t) + \int_{t-D}^{t}\mathrm{e}^{\Gamma_i(t-\theta)}B_i u_i(\theta)\,d\theta + \int_{t-D}^{t}\mathrm{e}^{\Gamma_i(t-\theta)}B_{1i}u_{i-1,\mathrm{m}}(\theta)\,d\theta, \tag{2.6}$$

where

$$q_i = \begin{bmatrix} q_{i,1} & q_{i,2} & q_{i,3} & q_{i,4} & q_{i,5} \end{bmatrix}^{\mathrm{T}}, \quad \bar{x}_i = \begin{bmatrix} s_i & v_i & v_{i-1} & a_i & a_{i-1,\mathrm{m}} \end{bmatrix}^{\mathrm{T}}, \tag{2.7}$$

$$B_i = \begin{bmatrix} 0 & 0 & 0 & \frac{1}{\tau_i} & 0 \end{bmatrix}^{\mathrm{T}}, \quad B_{1i} = \begin{bmatrix} 0 & 0 & 0 & 0 & \frac{1}{\tau_{i-1}} \end{bmatrix}^{\mathrm{T}}, \tag{2.8}$$

$$\Gamma_i = \begin{bmatrix} 0 & -1 & 1 & 0 & 0 \\ 0 & 0 & 0 & 1 & 0 \\ 0 & 0 & 0 & 0 & 1 \\ 0 & 0 & 0 & -\frac{1}{\tau_i} & 0 \\ 0 & 0 & 0 & 0 & -\frac{1}{\tau_{i-1}} \end{bmatrix}. \tag{2.9}$$

Note that for control implementation the value of the communication delay is not needed. Control laws (2.5), in the absence of communication delay, correspond to an exact predictor-feedback CACC design. In the present case, due to communication delay, the states q_i are not exact, D time-units predictor states anymore. In Figure 2.1, we present a block diagram that illustrates how each ego vehicle constructs each own controller, as well as which information is needed.

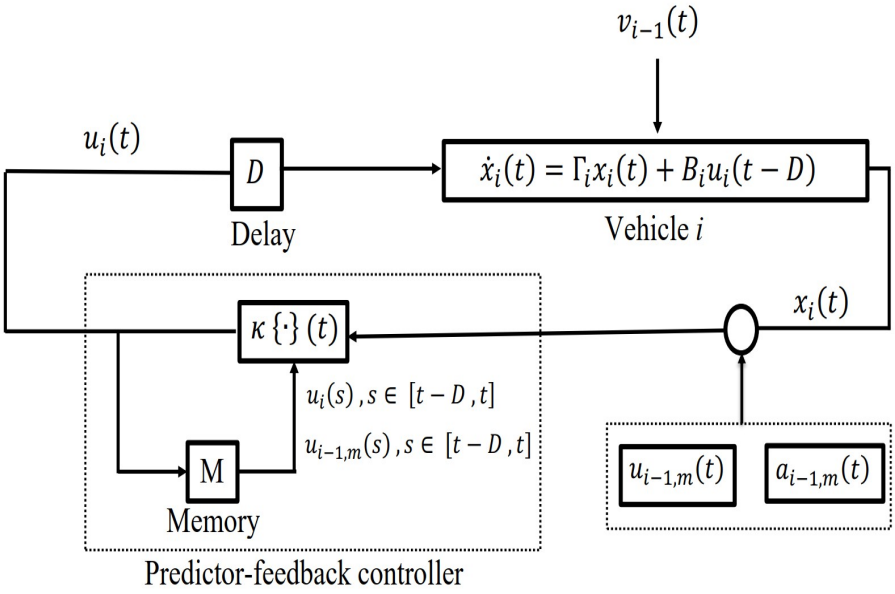

Figure 2.1: Block diagram of the predictor-feedback control design. The operator $\kappa\{\cdot\}$ defines the predictor-feedback law of each ego vehicle that utilizes the available past actuation command of the ego vehicle and preceding vehicle. Moreover, the right dashed box illustrates all the needed information from the preceding vehicle, which is obtained via V2V communication.

2.2.2 Main Result

We are now ready to state the main result of the chapter.

Theorem 2.1: Consider a platoon of vehicles with heterogeneous dynamics modeled by (2.1)–(2.3), under control laws (2.5) with (2.6)–(2.9). There exists a positive constant ϵ such that for all $0 \leq D_{c,i-1} < \epsilon$, $i = 1, ..., N$, and any $D \geq 0$, $h_i > 0$, $i = 1, ..., N$, the platoon is $\mathcal{L}_2$ string stable provided that the following conditions hold for $i = 1, ..., N$:

$$\frac{1}{\tau_i} - c_i > 0, \tag{2.10}$$

$$\left(\frac{1}{\tau_i} - c_i\right)(\alpha_i + b_i) - \frac{\alpha_i}{h_i} > 0, \tag{2.11}$$

$$\left(c_i - \frac{1}{\tau_i}\right)^2 - 2(\alpha_i + b_i) > 0, \tag{2.12}$$

$$\frac{2}{h_i}\left(c_i - \frac{1}{\tau_i}\right) + 2b_i + \alpha_i > 0. \tag{2.13}$$

Remark 2.1: The first two conditions of Theorem 2.1, which come from the Routh-Hurwitz criterion, guarantee the individual stability of each vehicle i, which is a prerequisite for string stability of the platoon; while the remaining two conditions are derived from the string stability criterion, for the nominal case without communication delay. Conditions (2.10)–(2.13) can be satisfied for any given $h_i > 0$ with a proper choice of α_i, b_i, c_i. To see this note that conditions (2.10)–(2.13) can be satisfied provided that for a given $h_i > 0$ the parameter $\gamma_i = \frac{1}{\tau_i} - c_i$ can be chosen to satisfy $\gamma_i \in \left(\max\left\{\frac{\alpha_i}{(\alpha_i+b_i)h_i}, \sqrt{2(\alpha_i+b_i)}\right\}, \frac{h_i(2b_i+\alpha_i)}{2}\right)$, which in turn can be guaranteed, for example, by a sufficiently large choice of b_i. Note that these conditions concern the nominal, delay-free design (2.4) and not the predictor-based design, owing to the delay-compensating property of our controller.

Remark 2.2: Theorem 2.1 implies that communication delay does not affect individual vehicle stability (this is shown via derivation of transfer function (2.14) given in (2.37)). This is, in fact, consistent, because, as it is evident from (2.5), (2.6), communication delay affects only the feedforward and not the feedback terms in each ego vehicle's controller, i.e., it affects only measurements of the preceding vehicle's states. In addition, this is consistent with the fact that the dependence of the predictor-feedback controller on a_{i-1}, u_{i-1} originates in that predictor feedback is constructed to predict also the preceding vehicle's speed v_{i-1}, involved in the nominal delay-free controller (2.4), and which affects only tracking performance and string stability, but not individual vehicle's stability. Moreover, this is also consistent with the fact that the predictor-feedback controller is input-to-state stable (see, for example, [5], [27]) with respect to exogenous inputs and the states of the

preceding vehicle, namely v_{i-1}, a_{i-1}, and u_{i-1}, act as such, when viewed from the ego vehicle's dynamics perspective.

Proof of Theorem 2.1: In order to studying stability and string stability, we first compute the transfer functions

$$G_i(s) = \frac{V_i(s)}{V_{i-1}(s)}, \quad i = 1, ..., N, \tag{2.14}$$

viewing as input the preceding vehicle's speed and as output the current vehicle's speed. Taking Laplace transform of the predictor states (2.6) we get

$$Q_i(s) = \mathrm{e}^{\Gamma_i D}\bar{X}_i(s) + M_{1,i}(s)U_i(s) + M_{2,i}(s)U_{i-1}(s), \tag{2.15}$$

where

$$M_{1,i}(s) = (sI_{5\times5} - \Gamma_i)^{-1}\left(I_{5\times5} - \mathrm{e}^{\Gamma_i D}\mathrm{e}^{-sD}\right)B_i, \tag{2.16}$$

$$M_{2,i}(s) = (sI_{5\times5} - \Gamma_i)^{-1}\left(I_{5\times5} - \mathrm{e}^{\Gamma_i D}\mathrm{e}^{-s(D+D_{c,i-1})}\right)B_{1i}, \tag{2.17}$$

$$\mathrm{e}^{\Gamma_i D} = \begin{bmatrix} 1 & -D & D & E_{14} & E_{15} \\ 0 & 1 & 0 & E_{24} & 0 \\ 0 & 0 & 1 & 0 & \tau_{i-1}\left(1 - \mathrm{e}^{\frac{-D}{\tau_{i-1}}}\right) \\ 0 & 0 & 0 & \mathrm{e}^{\frac{-D}{\tau_i}} & 0 \\ 0 & 0 & 0 & 0 & \mathrm{e}^{\frac{-D}{\tau_{i-1}}} \end{bmatrix}, \tag{2.18}$$

$$E_{14} = \tau_i^2\left(1 - \frac{D}{\tau_i} - \mathrm{e}^{\frac{-D}{\tau_i}}\right), \tag{2.19}$$

$$E_{15} = \tau_{i-1}^2\left(\mathrm{e}^{\frac{-D}{\tau_{i-1}}} + \frac{D}{\tau_{i-1}} - 1\right), \tag{2.20}$$

$$E_{24} = \tau_i\left(1 - \mathrm{e}^{\frac{-D}{\tau_i}}\right). \tag{2.21}$$

Using (2.8), (2.9), (2.16), and (2.17) we get

$$(sI_{5\times5}-\Gamma_i)^{-1}=\frac{1}{s^2}\begin{bmatrix} s & -1 & 1 & -\frac{\tau_i}{s\tau_i+1} & \frac{\tau_{i-1}}{s\tau_{i-1}+1} \\ 0 & s & 0 & \frac{s\tau_i}{s\tau_i+1} & 0 \\ 0 & 0 & s & 0 & \frac{s\tau_{i-1}}{s\tau_{i-1}+1} \\ 0 & 0 & 0 & \frac{s^2\tau_i}{s\tau_i+1} & 0 \\ 0 & 0 & 0 & 0 & \frac{s^2\tau_{i-1}}{s\tau_{i-1}+1} \end{bmatrix}, \tag{2.22}$$

$$M_{1,i}(s)=\begin{bmatrix} M_{11,i}(s) & M_{21,i}(s) & 0 & M_{41,i}(s) & 0 \end{bmatrix}^{\mathrm{T}}, \tag{2.23}$$

$$M_{2,i}(s)=\begin{bmatrix} m_{11,i}(s) & 0 & m_{31,i}(s) & 0 & m_{51,i}(s) \end{bmatrix}^{\mathrm{T}}, \tag{2.24}$$

where

$$M_{11,i}(s)=\frac{\mathrm{e}^{-sD}\left(\tau_i-\tau_i e^{\frac{-D}{\tau_i}}\right)}{s^2\tau_i}+\frac{\mathrm{e}^{-sD}\left(\tau_i^2\mathrm{e}^{\frac{-D}{\tau_i}}+D\tau_i-\tau_i^2\right)}{s\tau_i}+\frac{\tau_i\left(\mathrm{e}^{-\frac{D}{\tau_i}}\mathrm{e}^{-sD}-1\right)}{s^2\tau_i(s\tau_i+1)}, \tag{2.25}$$

$$M_{21,i}(s)=-\frac{\mathrm{e}^{-sD}(\tau_i-\tau_i\mathrm{e}^{\frac{-D}{\tau_i}})}{s\tau_i}-\frac{\tau_i\left(\mathrm{e}^{\frac{-D}{\tau_i}}\mathrm{e}^{-sD}-1\right)}{s\tau_i(s\tau_i+1)}, \tag{2.26}$$

$$M_{41,i}(s)=-\frac{\mathrm{e}^{\frac{-D}{\tau_i}}\mathrm{e}^{-sD}-1}{s\tau_i+1}, \tag{2.27}$$

$$m_{11,i}(s)=-\frac{\mathrm{e}^{-s(D+D_{\mathrm{c},i-1})}\left(\tau_{i-1}-\tau_{i-1}\mathrm{e}^{\frac{-D}{\tau_{i-1}}}\right)}{s^2\tau_{i-1}}-\frac{\mathrm{e}^{-s(D+D_{\mathrm{c},i-1})}\left(\tau_{i-1}^2\mathrm{e}^{\frac{-D}{\tau_{i-1}}}+D\tau_{i-1}-\tau_{i-1}^2\right)}{s\tau_{i-1}} \tag{2.28}$$

$$-\frac{\tau_{i-1}\left(\mathrm{e}^{-\frac{D}{\tau_{i-1}}}\mathrm{e}^{-s(D+D_{\mathrm{c},i-1})}-1\right)}{s^2\tau_{i-1}(s\tau_{i-1}+1)},$$

$$m_{31,i}(s)=-\frac{\mathrm{e}^{-s(D+D_{\mathrm{c},i-1})}\left(\tau_{i-1}-\tau_{i-1}\mathrm{e}^{\frac{-D}{\tau_{i-1}}}\right)}{s\tau_{i-1}}-\frac{\tau_{i-1}\left(\mathrm{e}^{\frac{-D}{\tau_{i-1}}}\mathrm{e}^{-s(D+D_{\mathrm{c},i-1})}-1\right)}{s\tau_{i-1}(s\tau_{i-1}+1)}, \tag{2.29}$$

$$m_{51,i}(s)=-\frac{\mathrm{e}^{\frac{-D}{\tau_{i-1}}}\mathrm{e}^{-s(D+D_{\mathrm{c},i-1})}-1}{s\tau_{i-1}+1}. \tag{2.30}$$

Using the i-th vehicle's model (2.1)–(2.3) we obtain

$$\begin{bmatrix} S_i(s) \\ V_i(s) \\ A_i(s) \end{bmatrix}=\left(sI_{3\times3}-\bar{\Gamma}_i\right)^{-1}\left(\begin{bmatrix} 0 \\ 0 \\ \frac{1}{\tau_i} \end{bmatrix}\mathrm{e}^{-sD}U_i(s)+\begin{bmatrix} 1 \\ 0 \\ 0 \end{bmatrix}V_{i-1}(s)\right), \tag{2.31}$$

where

$$\bar{\Gamma}_i = \begin{bmatrix} 0 & -1 & 0 \\ 0 & 0 & 1 \\ 0 & 0 & -\frac{1}{\tau_i} \end{bmatrix}, \tag{2.32}$$

and hence

$$\begin{bmatrix} S_i(s) \\ V_i(s) \\ A_i(s) \end{bmatrix} = \begin{bmatrix} -\frac{1}{s^2(s\tau_i+1)} \\ \frac{1}{s(s\tau_i+1)} \\ \frac{1}{s\tau_i+1} \end{bmatrix} \mathrm{e}^{-sD} U_i(s) + \begin{bmatrix} \frac{1}{s} \\ 0 \\ 0 \end{bmatrix} V_{i-1}(s). \tag{2.33}$$

Using control laws (2.5), together with (2.15)–(2.30), we arrive at

$$\begin{aligned} U_i(s) = {} & \frac{\tau_i\alpha_i}{h_i} S_i(s) - \left(\tau_i(\alpha_i+b_i) + \frac{D\tau_i\alpha_i}{h_i}\right) V_i(s) + \left(\tau_i b_i + \frac{D\tau_i\alpha_i}{h_i}\right) V_{i-1}(s) \\ & + \left(\tau_i c_i \mathrm{e}^{\frac{-D}{\tau_i}} - \tau_i(\alpha_i+b_i)\left(\tau_i - \tau_i \mathrm{e}^{\frac{-D}{\tau_i}}\right) - \frac{\tau_i\alpha_i}{h_i}\left(\tau_i^2 \mathrm{e}^{\frac{-D}{\tau_i}} + D\tau_i - \tau_i^2\right)\right) A_i(s) \\ & + \left(\tau_i b_i \left(\tau_{i-1} - \tau_{i-1}\mathrm{e}^{\frac{-D}{\tau_{i-1}}}\right) + \frac{\tau_i\alpha_i}{h_i}\left(\tau_{i-1}^2 \mathrm{e}^{\frac{-D}{\tau_{i-1}}} + D\tau_{i-1} - \tau_{i-1}^2\right)\right) \mathrm{e}^{-D_{c,i-1}s} A_{i-1}(s) \\ & + g_{1,i}(s) U_i(s) + g_{2,i}(s) U_{i-1}(s), \end{aligned} \tag{2.34}$$

where

$$g_{1,i}(s) = \left(\frac{\tau_i\alpha_i}{h_i} M_{11,i}(s) - \tau_i(\alpha_i+b_i) M_{21,i}(s) + \tau_i c_i M_{41,i}(s)\right), \tag{2.35}$$

$$g_{2,i}(s) = \left(\frac{\tau_i\alpha_i}{h_i} m_{11,i}(s) + \tau_i b_i m_{31,i}(s)\right). \tag{2.36}$$

Hence, substituting (2.33) in (2.34) we derive $\frac{U_i}{U_{i-1}}$, which, multiplying it by $\frac{s\tau_{i-1}+1}{s\tau_i+1}$, gives

$$G_i(s) = \frac{\mu_{1,i}(s)s + \mu_{2,i}(s)}{s^3 + \left(\frac{1}{\tau_i} - c_i\right)s^2 + (\alpha_i+b_i)s + \frac{\alpha_i}{h_i}}, \tag{2.37}$$

where

$$\mu_{1,i}(s) = \left(- D\frac{\alpha_i}{h_i}\mathrm{e}^{-(D+D_{c,i-1})s} + D\frac{\alpha_i}{h_i}\mathrm{e}^{-Ds} - b_i\mathrm{e}^{-(D+D_{c,i-1})s} + b_i\mathrm{e}^{-Ds} + b_i\right), \tag{2.38}$$

$$\mu_{2,i}(s) = \left(\frac{\alpha_i}{h_i}\mathrm{e}^{-Ds} - \frac{\alpha_i}{h_i}\mathrm{e}^{-(D+D_{c,i-1})s} + \frac{\alpha_i}{h_i}\right). \tag{2.39}$$

String stability in $\mathcal{L}_2$ is guaranteed when $|G_i(j\omega)| \leq 1$, for all $\omega \geq 0$. The condition is satisfied for $\omega = 0$ since $|G_i(0)| = 1$. Moreover, from (2.37) we have

$$G_i(j\omega) = \frac{f_{1,i}(\omega) + jf_{2,i}(\omega)}{f_{3,i}(\omega) + jf_{4,i}(\omega)}, \tag{2.40}$$

$$f_{1,i}(\omega) = \frac{\alpha_i}{h_i} + \frac{\alpha_i}{h_i}(\cos(\omega D) - \cos(\omega(D + D_{\mathrm{c},i-1}))) + \omega\left(\frac{\alpha_i D}{h_i} + b_i\right)(\sin(\omega D) - \sin(\omega(D + D_{\mathrm{c},i-1}))), \tag{2.41}$$

$$f_{2,i}(\omega) = b_i\omega - \frac{\alpha_i}{h_i}(\sin(\omega D) - \sin(\omega(D + D_{\mathrm{c},i-1}))) + \omega\left(\frac{\alpha_i D}{h_i} + b_i\right)(\cos(\omega D) - \cos(\omega(D + D_{\mathrm{c},i-1}))), \tag{2.42}$$

$$f_{3,i}(\omega) = \omega^2\left(\mathrm{c}_i - \frac{1}{\tau_i}\right) + \frac{\alpha_i}{h_i}, \tag{2.43}$$

$$f_{4,i}(\omega) = \omega(\alpha_i + b_i) - \omega^3. \tag{2.44}$$

For a given ω, based on the mean-value theorem [25], it can be concluded that, for each i, there exist $\xi_i(\omega)$ and $\zeta_i(\omega)$ such that

$$\cos(\omega D) - \cos(\omega(D + D_{\mathrm{c},i-1})) = \omega D_{\mathrm{c},i-1}\sin(\omega\xi_i(\omega)), \quad \xi_i \in (D, D + D_{\mathrm{c},i-1}) \tag{2.45}$$

$$\sin(\omega D) - \sin(\omega(D + D_{\mathrm{c},i-1})) = -\omega D_{\mathrm{c},i-1}\cos(\omega\zeta_i(\omega)), \quad \zeta_i \in (D, D + D_{\mathrm{c},i-1}). \tag{2.46}$$

Hence, (2.41), (2.42) can also be written as

$$f_{1,i}(\omega) = \frac{\alpha_i}{h_i} + \frac{\alpha_i}{h_i}\omega D_{\mathrm{c},i-1}\sin(\omega\xi_i(\omega)) - \omega^2\left(\frac{\alpha_i D}{h_i} + b_i\right)D_{\mathrm{c},i-1}\cos(\omega\zeta_i(\omega)), \tag{2.47}$$

$$f_{2,i}(\omega) = b_i\omega + \frac{\alpha_i}{h_i}\omega D_{\mathrm{c},i-1}\cos(\omega\zeta_i(\omega)) + \omega^2\left(\frac{\alpha_i D}{h_i} + b_i\right)D_{\mathrm{c},i-1}\sin(\omega\xi_i(\omega)). \tag{2.48}$$

Therefore, the condition for string stability becomes $f_{1,i}(\omega)^2 + f_{2,i}(\omega)^2 < f_{3,i}(\omega)^2 + f_{4,i}(\omega)^2$, $\omega > 0$, $i = 1, ..., N$, and hence, after straightforward computations, we get the following condition that has to hold for all $\omega > 0$ and $i = 1, ..., N$

$$\omega^6 + \omega^4 f_{5,i}(\omega) + \omega^3 f_{6,i}(\omega) + \omega^2 f_{7,i}(\omega) + \omega f_{8,i}(\omega) > 0, \tag{2.49}$$

where

$$f_{5,i}(\omega) = \left(c_i - \frac{1}{\tau_i}\right)^2 - 2(\alpha_i + b_i) - D_{\mathrm{c},i-1}^2 \left(\cos(\omega\zeta_i(\omega))^2 + \sin(\omega\xi_i(\omega))^2\right) \left(b_i^2 + \frac{2D\alpha_i b_i}{h_i} + \frac{D^2\alpha_i^2}{h_i^2}\right), \tag{2.50}$$

$$f_{6,i}(\omega) = D_{\mathrm{c},i-1} \sin(\omega\xi_i(\omega)) \left(-2b_i^2 - \frac{2D\alpha_i b_i}{h_i}\right), \tag{2.51}$$

$$f_{7,i}(\omega) = \alpha_i^2 + 2\alpha_i b_i - \frac{2\alpha_i}{h_i\tau_i} + \frac{2\alpha_i c_i}{h_i} - \frac{D_{\mathrm{c},i-1}^2\alpha_i^2}{h_i^2}\left(\cos(\omega\zeta_i(\omega))^2 + \sin(\omega\xi_i(\omega))^2\right) + \frac{2DD_{\mathrm{c},i-1}\alpha_i^2\cos(\omega\zeta_i(\omega))}{h_i^2}, \tag{2.52}$$

$$f_{8,i}(\omega) = -\frac{2D_{\mathrm{c},i-1}\alpha_i^2\sin(\omega\xi_i(\omega))}{h_i^2}. \tag{2.53}$$

Using the facts that $|\sin(x)| \leq |x|$, for all $x \in \mathbb{R}$, that $\omega, \xi_i > 0$, and that $\xi_i < D + D_{\mathrm{c},i-1}$ we get from (2.51), (2.53)

$$f_{6,i}(\omega) \geq -\omega D_{\mathrm{c},i-1}\left(2b_i^2 + \frac{2D\alpha_i b_i}{h_i}\right)(D + D_{\mathrm{c},i-1}), \tag{2.54}$$

$$f_{8,i}(\omega) \geq -\omega\frac{2D_{\mathrm{c},i-1}\alpha_i^2}{h_i^2}(D + D_{\mathrm{c},i-1}). \tag{2.55}$$

Thus, condition (2.49) is satisfied if for all $\omega > 0$

$$\omega^4 + \omega^2\left(f_{5,i}(\omega) - D_{\mathrm{c},i-1}\left(2b_i^2 + \frac{2D\alpha_i b_i}{h_i}\right)(D + D_{\mathrm{c},i-1})\right) + \left(f_{7,i}(\omega) - \frac{2D_{\mathrm{c},i-1}\alpha_i^2}{h_i^2}(D + D_{\mathrm{c},i-1})\right) > 0. \tag{2.56}$$

Since from (2.50), (2.52) we have that

$$f_{5,i}(\omega) \geq \left(c_i - \frac{1}{\tau_i}\right)^2 - 2(\alpha_i + b_i) - 2D_{\mathrm{c},i-1}^2\left(b_i^2 + \frac{2D\alpha_i b_i}{h_i} + \frac{D^2\alpha_i^2}{h_i^2}\right), \tag{2.57}$$

$$f_{7,i}(\omega) \geq \alpha_i^2 + 2\alpha_i b_i - \frac{2\alpha_i}{h_i\tau_i} + \frac{2\alpha_i c_i}{h_i} - \frac{2D_{\mathrm{c},i-1}^2\alpha_i^2}{h_i^2} - \frac{2DD_{\mathrm{c},i-1}\alpha_i^2}{h_i^2}, \tag{2.58}$$

condition (2.56) holds if the following two conditions hold for $i = 1, ..., N$

$$\left(c_i - \frac{1}{\tau_i}\right)^2 - 2(\alpha_i + b_i) - 2D_{\mathrm{c},i-1}^2 \left(b_i^2 + \frac{2D\alpha_i b_i}{h_i} + \frac{D^2\alpha_i^2}{h_i^2}\right)$$
$$- D_{\mathrm{c},i-1}\left(2b_i^2 + \frac{2D\alpha_i b_i}{h_i}\right)(D + D_{\mathrm{c},i-1}) > 0, \tag{2.59}$$
$$\alpha_i\left(\alpha_i + 2b_i + \frac{2}{h_i}\left(c_i - \frac{1}{\tau_i}\right)\right) - 4D_{\mathrm{c},i-1}\frac{\alpha_i^2}{h_i^2}(D + D_{\mathrm{c},i-1}) > 0. \tag{2.60}$$

The left-hand side of (2.59), (2.60) are continuous functions of $D_{\mathrm{c},i-1}$ and equal to positive values when $D_{\mathrm{c},i-1} = 0$, under the conditions on the parameters a_i, b_i, c_i, τ_i, h_i of Theorem 1. Thus, there exists a sufficiently small $\epsilon > 0$ such that for all $0 < D_{\mathrm{c},i-1} < \epsilon$, $i = 1, ..., N$ the left-hand side of (2.59), (2.60) is positive, which completes the proof. □

2.3 Simulation Results

This section illustrates numerically the performance of the predictor-feedback CACC design. Note that the simulations are conducted in Matlab R2022b, where integrals in the predictor-based controller (2.6) are computed using the trapezoidal rule. Moreover, third-order models for vehicles' dynamics, as described in (2.1)–(2.3), are implemented using the Euler method. Additionally, in this section, a fixed time step of $T_s = 0.01$ is selected to align with typical sampling times of control execution and measurements, see, e.g., [22], [23]. We consider a homogeneous platoon of four vehicles in order to make the numerical example more accessible and to more clearly illustrate the benefits of predictor feedback, without distracting the reader with definition of various different numerical parameters. For a homogeneous platoon of four vehicles with third-order dynamics given by (2.1)–(2.3), we consider a case in which $\tau_i = \tau = 0.1$, $D_{\mathrm{c},i-1} = D_{\mathrm{c}}$, $i = 1, 2, 3, 4$, and $D = 0.7$. We choose for all i

$$\alpha_i = -hp^3, \tag{2.61}$$
$$b_i = hp^3 + 3p^2, \tag{2.62}$$
$$c_i = \frac{1}{\tau} + 3p, \tag{2.63}$$

for some $p < 0$ and $h_i = h$ within the range $[0.5, 1.4]$. This choice results in the characteristic polynomial of G in (2.37) being $(s - p)^3$.

Figure 2.2 depicts $\sup_\omega |G(j\omega)|$ as a function of p and h. In the nominal case without communication delay the conditions in Theorem 2.1, reduce to condition $h^2p^2+6hp+6<0$, which should hold to guarantee string stability. In the top plot of Figure 2.2, the region between the red curves indicates where condition $h^2p^2+6hp+6<0$ is satisfied. Similarly, in Figure 2.2, bottom plot, we show $\sup_\omega |G(j\omega)|$ with $D_{\rm c}=0.1$. We observe that, increasing $D_{\rm c}$ makes the allowable region, which guarantees string stability, to shrink.

In Figure 2.3 we set $h=0.75$, $p=-3$, and, $D_{\rm c}=0.1$. According to bottom plot of Figure 2.2, this choice satisfies the $\mathcal{L}_2$ string stability criterion. We consider a scenario in which $a_{i-1,m}(s)=0, s\in[-D_{\rm c},0]$, and $u_{i0}\equiv 0$, for each vehicle i, while we set $v_{i0}=15\left(\frac{m}{s}\right)$, $i=1,2,3$ and $v_{\rm l0}=\frac{2v_{i0}}{3}=10\left(\frac{m}{s}\right)$, and $s_{i0}=hv_{i0}=h\times 15\ m$, $i=2,3$, $s_{10}=13.5\ m$. Additionally, the leading vehicle performs a deceleration and acceleration maneuver. As Figure 2.3 shows, despite acceleration and speed responses exhibiting oscillations, $\mathcal{L}_2$ string stability is maintained.

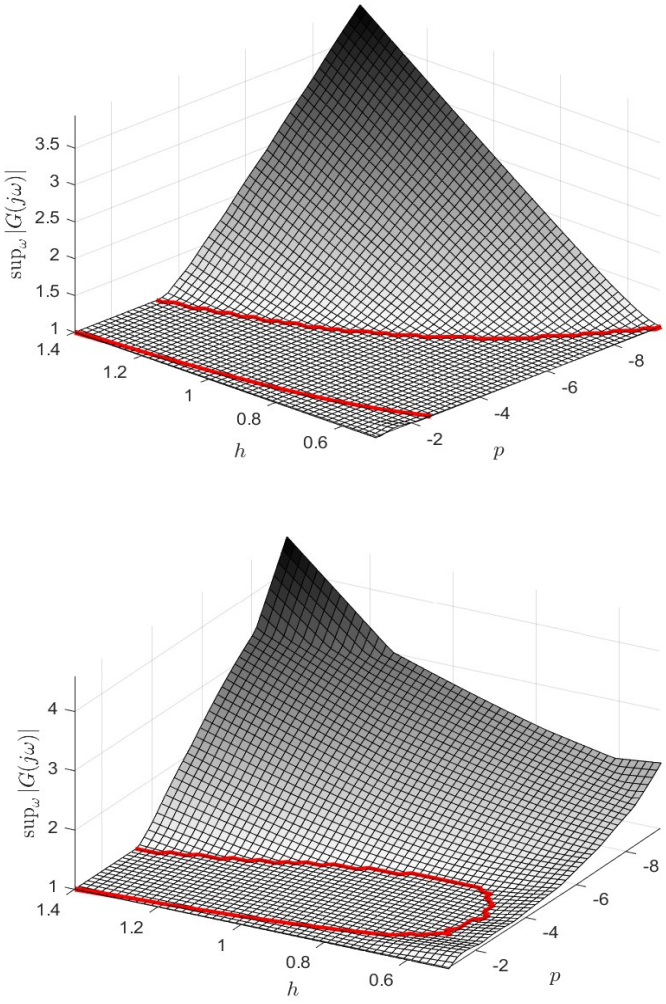

Figure 2.2: The values of function $\sup_\omega |G(j\omega)|$ corresponding to transfer function (2.37) for homogeneous vehicles, for different values of time-headway h and p. Top: $\sup_\omega |G(j\omega)|$ as function of h and p with constant communication delay $D_c = 0$. Bottom: $\sup_\omega |G(j\omega)|$ as function of h and p with constant communication delay $D_c = 0.1$.

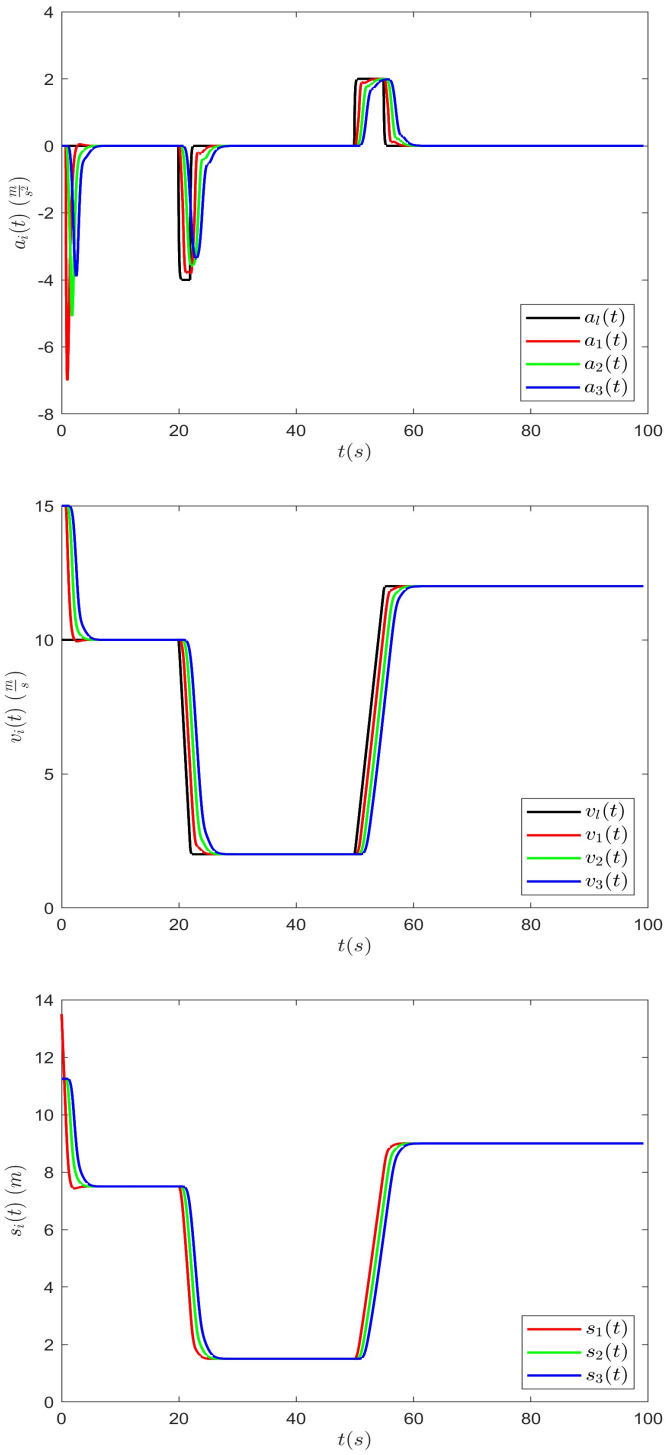

Figure 2.3: Acceleration (top), speed (middle), and spacing (bottom) of four vehicles, with dynamics described by (2.1)–(2.3), where $D = 0.7$, $\tau = 0.1$, following a leader that performs an acceleration/deceleration maneuver, under the CACC control laws (2.5), where $D_c = 0.1$. The desired time-headway is $h = 0.75$ while control parameters are chosen according to (2.61)–(2.63) with $p = -3$. Initial conditions are $v_{i0} = 15\left(\frac{m}{s}\right)$, $i = 1, 2, 3$, $v_{l0} = \frac{2v_{i0}}{3} = 10\left(\frac{m}{s}\right)$, $s_{i0} = hv_{i0} = h \times 15\ m$, $i = 2, 3$, $s_{10} = 13.5\ m$, and $u_{i0} = 0$, for $i = 1, 2, 3$.

To further numerically analyze the $\mathcal{L}_2$ string stability property of the closed-loop system, as this is described by (2.37), we define different scenarios that illustrate the impact of D, $D_{\rm c}$, and h on $\mathcal{L}_2$ string stability. In Figure 2.4, top plot, we show the values of $\sup_\omega |G(j\omega)|$ as function of $0.5 \geq \ D_{\rm c} \geq 0$ and $1 \geq D \geq 0$, with fixed $h = 0.75$ and $p = -3$. The red line shows the distinction between string stability and instability. In the same manner, the bottom plot shows $\sup_\omega |G(j\omega)|$ as function of $0.5 \geq \ D_{\rm c} \geq 0$, and $1.4 \geq h \geq 0.5$ with fixed $D = 0.7$ and $p = -3$, confirming that for a small communication delay string stability, in the presence of a large actuator delay, is preserved. It is interesting to observe that the upper limit of the communication delay considered in Figure 2.4 and ensures string stability, is, usually, higher than what conditions (2.59), (2.60) may predict, due to the conservatism of the derived bounds. Nevertheless, Figure 2.4 is consistent with conditions (2.59), (2.60). For example, conditions (2.59), (2.60) indicate that string stability is preserved for increasing $D_{\rm c}$ when D decreases or when h increases.

2.4 Chapter Conclusions and Related Publications

In the present chapter, we establish robustness of $\mathcal{L}_2$ string stability of predictor-feedback CACC design, which is originally developed in [4] to compensate actuation delay only, to communication delay. We derive analytical conditions on control law parameters and the parameters of the vehicle models, including actuation and communication delays, which guarantee $\mathcal{L}_2$ string stability. We demonstrate numerically the $\mathcal{L}_2$ string stability properties of the platoon, including characterization of the domains, in the parameters' space, which guarantee string stability.

This chapter is an adaptation of material appearing in

A. Samii and N. Bekiaris-Liberis, "Robustness of string stability of linear predictor-feedback CACC to communication delay", *IEEE International Conference on Intelligent Transportation Systems*, Bilbao, Spain, 2023.

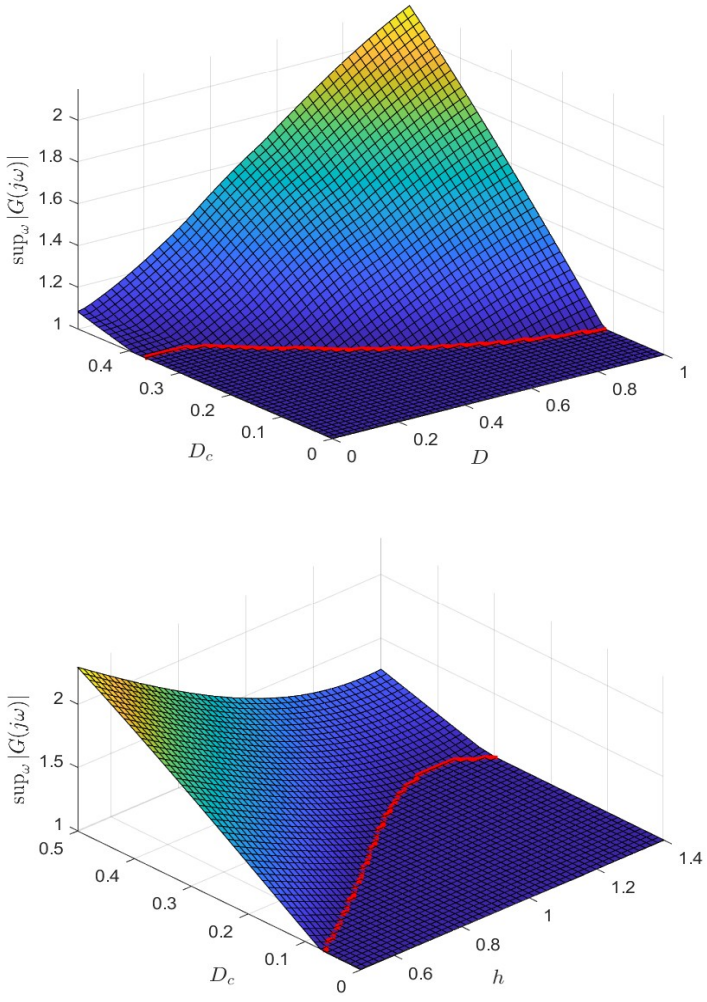

Figure 2.4: The values of $\sup_\omega |G(j\omega)|$ corresponding to transfer function (2.37) for homogeneous vehicles. Top: $\sup_\omega |G(j\omega)|$ for different actuator delays and communication delays with $h = 0.75$ and $p = -3$. Bottom: $\sup_\omega |G(j\omega)|$ as function of communication delay and time-headway with $D = 0.7$ and $p = -3$.

Chapter 3

Simultaneous Compensation of Actuation and Communication Delays for Heterogeneous Platoons via Predictor-Feedback CACC with Integral Action

We construct a predictor-feedback cooperative adaptive cruise control (CACC) design with integral action, which achieves simultaneous compensation of long, actuation and communication delays, for platoons of heterogeneous vehicles whose dynamics are described by a third-order linear system with input delay. The key ingredients in our design are an underlying predictor-feedback law that achieves actuation delay compensation and an integral term of the difference between the delayed (by an amount equal to the respective communication delay) and current speed of the preceding vehicle. The latter, essentially, creates a virtual spacing variable, which can be regulated utilizing only delayed position and speed measurements from the preceding vehicle. We establish individual vehicle stability, string stability, and regulation for vehicular platoons, under the control design developed. The proofs rely on combining an input-output approach (in the frequency domain), with derivation of explicit solutions for the closed-loop systems, and they are enabled by the actuation and communication delays-compensating property of the design. We demonstrate numerically the control and model parameters' conditions of string stability, while we also present simulation results, in realistic scenarios, including a scenario in which the leading vehicle's trajectory is obtained from NGSIM data. All case studies confirm the effectiveness of the design developed.

3.1 Chapter Organization

The outline of the chapter is as follows. Section 3.2 presents the model of heterogeneous platoons considered and the communication/actuation delays-compensating predictor-feedback design with integral action. In Section 3.3, we state our main result, which is stability, string stability, and regulation under the CACC law developed. In Section 3.4 we present numerical experiments for validation of the string stability guarantees. Simulation results are presented in Section 3.5 and in Section 3.6 we provide concluding remarks.

3.2 Predictor-Feedback CACC for Heterogeneous Platoons with Both Actuator and Communication Delays

3.2.1 Vehicle Model and Nominal Delay-Free Design

a) Vehicle dynamics: We consider a heterogeneous string of vehicles (see Figure 3.1) each one modeled by the following third-order, linear system with actuator delay that describes vehicle dynamics (see, e.g., [1], [57], [58], [59])

$$\dot{s}_i(t) = v_{i-1}(t) - v_i(t), \tag{3.1}$$

$$\dot{v}_i(t) = a_i(t), \tag{3.2}$$

$$\dot{a}_i(t) = -\frac{1}{\tau_i} a_i(t) + \frac{1}{\tau_i} u_i(t - D), \tag{3.3}$$

where $D \geq 0$ is input delay, and $t \geq 0$ is time.

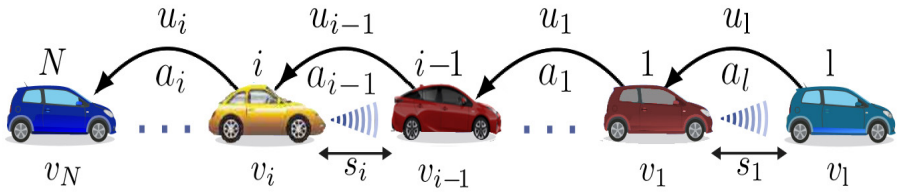

Figure 3.1: Platoon of $N + 1$ heterogeneous vehicles following each other in a single lane without overtaking. The dynamics of each vehicle $i = 1, ..., N$ are governed by system (3.1)–(3.3). Each vehicle can measure its own speed, the relative speed with the preceding vehicle, and the spacing with respect to the preceding vehicle. The control input and acceleration of each vehicle is communicated to the following vehicle via V2V communication.

b) Available measurements: For CACC platoons the measurements available to the ego vehicle i are its own spacing s_i, speed v_i, acceleration a_i, and control input u_i as well as the speed of the preceding vehicle v_{i-1}. It is possible to obtain this information through on-board sensors (for a more low level description of the ways of acquiring such measurements in practical applications the reader is referred to, e.g., [15], [16], [17]). Furthermore, the control input of the preceding vehicle, as well as its acceleration and speed are also available and are denoted by $u_{i-1,\mathrm{m}}$, $a_{i-1,\mathrm{m}}$, and $v_{i-1,\mathrm{m}}$ respectively. These measurements are transmitted from the preceding vehicle, through V2V communication. Due to the presence of communication delay these measurements are modeled by $v_{i-1,\mathrm{m}}(t) = v_{i-1}(t - D_{\mathrm{c},i-1})$, $a_{i-1,\mathrm{m}}(t) = a_{i-1}(t - D_{\mathrm{c},i-1})$ and $u_{i-1,\mathrm{m}}(\theta) = u_{i-1}(\theta - D_{\mathrm{c},i-1}), \theta \in [t - D, t]$, respectively, where $D_{\mathrm{c},i-1} \geq 0$, $i = 1, ..., N$, are communication delays[1].

c) Nominal control design: Without input delay, the following control strategy is constructed

$$u_i(t) = \tau_i \alpha_i \left(\frac{s_i(t)}{h_i} - v_i(t) \right) + \tau_i b_i (v_{i-1}(t) - v_i(t)) + \tau_i c_i a_i(t), \tag{3.4}$$

where $\alpha_i > 0$, $b_i > 0$, and $c_i \in \mathbb{R}$ are design parameters, and $h_i > 0$ is time-headway.

3.2.2 Communication Delay-Compensating Predictor-Feedback Control Design

The predictor-based control laws with communication delay compensation for system (3.1)–(3.3) are given by

$$u_i(t) = \frac{\tau_i \alpha_i}{h_i} q_{i,1}(t) - \tau_i(\alpha_i + b_i) q_{i,2}(t) + \tau_i b_i q_{i,3}(t) + \tau_i c_i q_{i,4}(t) + \frac{\tau_i \alpha_i}{h_i} \sigma_i(t), \tag{3.5}$$

$$\dot{\sigma}_i(t) = v_{i-1,\mathrm{m}}(t) - v_{i-1}(t), \tag{3.6}$$

$$q_i(t) = \mathrm{e}^{\Gamma_i D} \bar{x}_i(t) + \int_{t-D}^{t} \mathrm{e}^{\Gamma_i (t-\theta)} B_i u_i(\theta)\, d\theta + \int_{t-D}^{t} \mathrm{e}^{\Gamma_i (t-\theta)} B_{1i} u_{i-1,\mathrm{m}}(\theta)\, d\theta, \tag{3.7}$$

[1]The initial conditions $v_{i-1}(s) = v_{i-1_0}(s)$, $s \in [-D_{\mathrm{c},i-1}, 0]$, $a_{i-1}(s) = a_{i-1_0}(s)$, $s \in [-D_{\mathrm{c},i-1}, 0]$ and $u_{i-1}(s) = u_{i-1_0}(s)$, $s \in [-D - D_{\mathrm{c},i-1}, 0)$ are assumed to be continuous functions.

where

$$q_i = \begin{bmatrix} q_{i,1} & q_{i,2} & q_{i,3} & q_{i,4} & q_{i,5} \end{bmatrix}^{\mathrm{T}}, \quad \bar{x}_i = \begin{bmatrix} s_i & v_i & v_{i-1,\mathrm{m}} & a_i & a_{i-1,\mathrm{m}} \end{bmatrix}^{\mathrm{T}}, \tag{3.8}$$

$$B_i = \begin{bmatrix} 0 & 0 & 0 & \frac{1}{\tau_i} & 0 \end{bmatrix}^{\mathrm{T}}, B_{1i} = \begin{bmatrix} 0 & 0 & 0 & 0 & \frac{1}{\tau_{i-1}} \end{bmatrix}^{\mathrm{T}}, \tag{3.9}$$

$$\Gamma_i = \begin{bmatrix} 0 & -1 & 1 & 0 & 0 \\ 0 & 0 & 0 & 1 & 0 \\ 0 & 0 & 0 & 0 & 1 \\ 0 & 0 & 0 & -\frac{1}{\tau_i} & 0 \\ 0 & 0 & 0 & 0 & -\frac{1}{\tau_{i-1}} \end{bmatrix}. \tag{3.10}$$

It is important to note that we employ in our control design two different measurements for the preceding vehicle speed, one from on-board sensors v_{i-1} and one from V2V communication $v_{i-1,\mathrm{m}}$. Note that for control implementation the value of the communication delay is not needed, because $v_{i-1,\mathrm{m}}$ can be obtained directly from V2V communication. If $D_{\mathrm{c},i-1}$ is known to vehicle i, then one could, alternatively, employ $v_{i-1,\mathrm{m}}(t)$ via $v_{i-1,\mathrm{m}}(t) = v_{i-1}(t - D_{\mathrm{c},i-1})$.

Control laws (3.5), in the absence of communication delay, correspond to an exact predictor-feedback CACC design. In the present case, due to communication delay, the states q_i are not exact, D-time units predictor states anymore. Nevertheless, simultaneous compensation of input and communication delays is achieved, as stated in the next section, in which we also include details on the mechanism embedded in our controller that enables input/communication delays compensation.

3.3 String Stability Despite Actuation and Communication Delays

We now state our main result.

Theorem 3.1: Consider a platoon of vehicles with heterogeneous dynamics modeled by (3.1)–(3.3), under control laws (3.5) with (3.6)–(3.10). Let the leading vehicle's speed be uniformly bounded and continuous. For any $D \geq 0$, $h_i > 0$, $i = 1, ..., N$, the platoon is $\mathcal{L}_2$ string stable with respect to speed errors propagation provided that the following

conditions hold for $i = 1, ..., N$:

$$\frac{1}{\tau_i} - c_i > 0, \tag{3.11}$$

$$\left(\frac{1}{\tau_i} - c_i\right)(\alpha_i + b_i) - \frac{\alpha_i}{h_i} > 0, \tag{3.12}$$

$$\left(c_i - \frac{1}{\tau_i}\right)^2 - 2(\alpha_i + b_i) > 0, \tag{3.13}$$

$$\frac{2}{h_i}\left(c_i - \frac{1}{\tau_i}\right) + 2b_i + \alpha_i > 0. \tag{3.14}$$

Furthermore, all states remain bounded and, for a constant leading vehicle's speed, say v^*, regulation is achieved with $\lim_{t\to+\infty} a_i(t) = 0$, $\lim_{t\to\infty} v_i(t) = v^*$, and $\lim_{t\to+\infty} s_i(t) = h_i v^* - \lim_{t\to+\infty} \sigma_i(t)$, where $\lim_{t\to+\infty} \sigma_i(t) = \sigma_i(0) + \int_{-D_{\mathrm{c},i-1}}^{0} v_{i-1_0}(s)ds - D_{\mathrm{c},i-1}v^*$, .

Remark 3.1: Communication delay is compensated by regulating the speed of the ego vehicle to match the speed of the preceding vehicle, also accounting for the respective communication delay (see Remarks 3.2 and 3.3). This regulatory action in the presence of communication delays alters the equilibrium point, resulting in loss of zero, steady-state tracking error, as the controller aims to regulate $s_i + \sigma_i$ (rather than s_i) to $h_i v_i$ (this phenomenon also appears in, e.g., [58]). To address steady-state error when communication delay is known (e.g., as a known, average network delay), we can set $\sigma_i(0) = -\int_{-D_{\mathrm{c},i-1}}^{0} v_{i-1_0}(s)ds$ and $h_i = h_{i,\mathrm{des}} - D_{\mathrm{c},i-1}$ (assuming $h_{i,\mathrm{des}} > D_{\mathrm{c},i-1}$, which is a reasonable requirement given that the controller reacts with $D_{\mathrm{c},i-1}$ delay and that, typically, the values of communication delay are much smaller that the desired headways), which results in a steady-state value for s_i to be $h_{i,\mathrm{des}}v^*$. Note that the choice for $\sigma_i(0)$ can be implemented at $t = 0$ using the past measurements of v_{i-1}, which are available. On the other hand, if $D_{\mathrm{c},i-1}$ is unknown, we can set $\sigma_i(0) = 0$. This results in a steady-state error for s_i of $D_{\mathrm{c},i-1}v^* - \int_{-D_{\mathrm{c},i-1}}^{0} v_{i-1_0}(s)ds$. Nevertheless, it is worth noting that, in practice, $D_{\mathrm{c},i-1}$ is typically much smaller than h_i, and thus, the steady-state error is expected not to be large, particularly when the initial condition for speed is close to the leader's equilibrium speed or, at least, an estimate $\hat{D}_{\mathrm{c},i-1}$ of actual communication delay $D_{\mathrm{c},i-1}$ is available.

Remark 3.2: Note that the conditions in the statements of Theorem 3.1 do not depend on the delays values. To better understand the structure of our controller that allows simultaneous actuation and communication delays compensation we proceed as follows.

We re-formulate the control laws (3.5) as[2]

$$u_i(t) = K_i p_i(t) + K_i \left(\mathrm{e}^{\Gamma_i D} \begin{bmatrix} \sigma_i(t) \\ 0 \\ \Delta v_{i-1}(t) \\ 0 \\ \Delta a_{i-1}(t) \end{bmatrix} + \int_{t-D}^{t} \mathrm{e}^{\Gamma_i (t-\theta)} B_{1i} \Delta u_{i-1}(\theta)\, d\theta \right), \tag{3.15}$$

where

$$p_i(t) = \mathrm{e}^{\Gamma_i D} \tilde{x}_i(t) + \int_{t-D}^{t} \mathrm{e}^{\Gamma_i (t-\theta)} B_i u_i(\theta)\, d\theta + \int_{t-D}^{t} \mathrm{e}^{\Gamma_i (t-\theta)} B_{1i} u_{i-1}(\theta)\, d\theta, \tag{3.16}$$

$$\tilde{x}_i = \begin{bmatrix} s_i & v_i & v_{i-1} & a_i & a_{i-1} \end{bmatrix}^T, \tag{3.17}$$

$$\Delta v_{i-1}(t) = v_{i-1,\mathrm{m}}(t) - v_{i-1}(t), \tag{3.18}$$

$$\Delta a_{i-1}(t) = a_{i-1,\mathrm{m}}(t) - a_{i-1}(t), \tag{3.19}$$

$$\Delta u_{i-1}(s) = u_{i-1,\mathrm{m}}(s) - u_{i-1}(s), \quad s \in [t-D, t], \tag{3.20}$$

$$K_i = \begin{bmatrix} \frac{\tau_i \alpha_i}{h_i} & -\tau_i(\alpha_i + b_i) & \tau_i b_i & \tau_i c_i & 0 \end{bmatrix}. \tag{3.21}$$

The terms (3.18)–(3.20) in parentheses of (3.15) are viewed as error due to the communication delays $D_{\mathrm{c},i-1}$, because in the nominal case $D_{\mathrm{c},i-1} = 0$, terms (3.18)–(3.20) are zero and p_i is the exact predictor of $\tilde{x}_i$, D-time units in advance. Structure of (3.15) reveals the reason for which Theorem 3.1 implies that communication delay does not affect individual vehicle stability. As it is evident from (3.15), communication delay affects only the feedforward and not the feedback terms in each ego vehicle's controller, i.e., it affects only measurements of the preceding vehicle's states; while the part $K_i p_i$ achieves input delay compensation and individual vehicle stability. This is consistent with the fact that the predictor-feedback controller is input-to-state stable (see, for example, [5], [27]) with respect to exogenous inputs and the states of the preceding vehicle, namely σ_i, Δv_{i-1}, Δa_{i-1}, and Δu_{i-1}, act as such, when viewed from the ego vehicle's dynamics perspective.

Remark 3.3: We next proceed to explaining how string stability is achieved. The states σ_i, Δv_{i-1}, and Δa_{i-1} involved in (3.15), for $t \geq \max_i \{D_{\mathrm{c},i-1}\}$ satisfy the following

[2]Using (3.21), relation (3.5) is written as $u_i(t) = K_i q_i(t) + \frac{\tau_i \alpha_i}{h_i} \sigma_i(t)$. Using (3.7), from definitions (3.8) and (3.17)–(3.20) we get $q_i(t) = \mathrm{e}^{\Gamma_i D} \tilde{x}_i(t) + \mathrm{e}^{\Gamma_i D} \begin{bmatrix} 0 & 0 & \Delta v_{i-1}(t) & 0 & \Delta a_{i-1}(t) \end{bmatrix}^T + \int_{t-D}^{t} \mathrm{e}^{\Gamma_i (t-\theta)} B_i u_i(\theta)\, d\theta + \int_{t-D}^{t} \mathrm{e}^{\Gamma_i (t-\theta)} B_{1i} u_{i-1}(\theta)\, d\theta + + \int_{t-D}^{t} \mathrm{e}^{\Gamma_i (t-\theta)} B_{1i} \Delta u_{i-1}(\theta)\, d\theta$. With definitions (3.16), (3.36), and noting that $K_i \mathrm{e}^{\Gamma_i D} \begin{bmatrix} \sigma_i(t) & 0 & 0 & 0 & 0 \end{bmatrix}^T = \frac{\tau_i \alpha_i}{h_i} \sigma_i(t)$, we get (3.15).

dynamics

$$\dot{\sigma}_i(t) = \Delta v_{i-1}(t), \tag{3.22}$$

$$\Delta\dot{v}_{i-1}(t) = \Delta a_{i-1}(t), \tag{3.23}$$

$$\Delta\dot{a}_{i-1}(t) = -\frac{1}{\tau_{i-1}}\Delta a_{i-1}(t) + \frac{1}{\tau_{i-1}}\Delta u_{i-1}(t-D). \tag{3.24}$$

Then, we define the new signal $\bar{p}_i$, as the predictor of states σ_i, Δv_{i-1}, and Δa_{i-1}, over a D-time units horizon, treating Δu_{i-1} as input, in the following manner

$$\bar{p}_i(t) = \mathrm{e}^{\bar{\Gamma}_i D}\hat{x}_i(t) + \int_{t-D}^{t} \mathrm{e}^{\bar{\Gamma}_i(t-\theta)}\bar{B}_{1i}\Delta u_{i-1}(\theta)d\theta, \tag{3.25}$$

where

$$\bar{p}_i = \begin{bmatrix} \bar{p}_{i,1} \\ \bar{p}_{i,2} \\ \bar{p}_{i,3} \end{bmatrix}, \quad \hat{x}_i = \begin{bmatrix} \sigma_i \\ \Delta v_{i-1} \\ \Delta a_{i-1} \end{bmatrix}, \tag{3.26}$$

$$\bar{B}_{1i} = \begin{bmatrix} 0 \\ 0 \\ \frac{1}{\tau_{i-1}} \end{bmatrix}, \quad \bar{\Gamma}_i = \begin{bmatrix} 0 & 1 & 0 \\ 0 & 0 & 1 \\ 0 & 0 & -\frac{1}{\tau_{i-1}} \end{bmatrix}. \tag{3.27}$$

Substituting (3.25) in the parentheses of (3.15) we get

$$u_i(t) = K_i p_i(t) + K_i \begin{bmatrix} \bar{p}_{i,1} \\ 0 \\ \bar{p}_{i,2} \\ 0 \\ \bar{p}_{i,3} \end{bmatrix}. \tag{3.28}$$

Thus, (3.15) is written for $t \geq \max_i \{D_{\mathrm{c},i-1}\}$ as

$$\begin{aligned} u_i(t) = {} & \frac{\tau_i\alpha_i}{h_i}s_i(t+D) - \tau_i(\alpha_i+b_i)v_i(t+D) + \tau_i b_i v_{i-1}(t+D) + \tau_i c_i a_i(t+D) \\ & + \frac{\tau_i\alpha_i}{h_i}\sigma_i(t+D) + \tau_i b_i\left(v_{i-1,\mathrm{m}}(t+D) - v_{i-1}(t+D)\right). \end{aligned} \tag{3.29}$$

Hence, for $t \geq \max_i \{D_{\mathrm{c},i-1}\}$ we have

$$u_i(t) = \tau_i \alpha_i \left(\frac{\bar{s}_i(t+D)}{h_i} - v_i(t+D) \right) + \tau_i b_i \left(v_{i-1,\mathrm{m}}(t+D) - v_i(t+D) \right) + \tau_i c_i a_i(t+D), \tag{3.30}$$

where

$$\bar{s}_i(t) = s_i(t) + \sigma_i(t). \tag{3.31}$$

Noting that $\dot{\bar{s}}_i(t) = v_{i-1,\mathrm{m}}(t) - v_i(t)$, one could observe comparing (3.30) with the nominal controller (3.4) the following. First, all involved states are predicted by D-time units for input delay compensation. Second, communication delay is compensated through aiming at regulation of the ego's vehicle speed v_i to $v_{i-1,\mathrm{m}}$ rather than v_{i-1}. This is evident by the fact that $v_{i-1,\mathrm{m}}$ is involved in (3.30) (instead of v_{i-1}), together with the fact that $\bar{s}_i$ satisfies $\dot{\bar{s}}_i = v_{i-1,\mathrm{m}} - v_i$, which is viewed as the counterpart of s_i, under communication delay. One of the key aspects of the proposed controller, which makes it beneficial to string stability, is that the controller aims at regulating v_i to $v_{i-1,\mathrm{m}}$, while, simultaneously, aiming at regulating $\bar{s}_i$ (and not s_i) to $h_i v_i$. In other words, the controller regulates both speed and position of vehicle i taking into account the past (by $D_{\mathrm{c},i-1}$) speed and position (note that $\bar{s}_i$ could be viewed as $x_{i-1}(t - D_{\mathrm{c},i-1}) - x_i(t)$) of vehicle $i-1$, because this is the available information for the reference trajectory to vehicle i at time t (and it depends on the past preceding vehicle's speed/position). This, in a way, aligns the objectives of speed and spacing regulation, i.e., we regulate both, accounting for delayed information, rather than regulating speed but not spacing, using delayed information. This matching/synchronization is beneficial for string stability, because each vehicle's controller reacts uniformly, with respect to time, to speed and spacing deviations. Moreover, the way that the effect of the current speed of vehicle $i-1$ is being canceled from the spacing dynamics is by subtracting, via σ_i (having units of spacing), the term v_{i-1}. We note here that it is anticipated that, this characteristic of the controller, may not be beneficial for safety, due to the fact that the controller reacts to past and not to the current speed/spacing of the preceding vehicle.

Remark 3.4: The stability and string stability conditions of Theorem 3.1 are identical to those in Theorem 2.1, and thus, can be satisfied for any given $h_i > 0$ with a proper choice of design parameters α_i, b_i, c_i.

Proof of Theorem 3.1: In order to studying stability and string stability of speed error propagation, we first compute the transfer functions

$$G_i(s) = \frac{V_i(s)}{V_{i-1}(s)}, \quad i = 1, ..., N, \tag{3.32}$$

viewing as input the preceding vehicle's speed and as output the current vehicle's speed. Taking Laplace transform of the predictor states (3.7) we get

$$Q_i(s) = \mathrm{e}^{\Gamma_i D}\bar{X}_i(s) + M_{1,i}(s)U_i(s) + M_{2,i}(s)U_{i-1}(s)\mathrm{e}^{-sD_{\mathrm{c},i-1}}, \tag{3.33}$$

where

$$M_{1,i}(s) = (sI_{5\times5} - \Gamma_i)^{-1}\left(I_{5\times5} - \mathrm{e}^{\Gamma_i D}\mathrm{e}^{-sD}\right)B_i, \tag{3.34}$$

$$M_{2,i}(s) = (sI_{5\times5} - \Gamma_i)^{-1}\left(I_{5\times5} - \mathrm{e}^{\Gamma_i D}\mathrm{e}^{-sD}\right)B_{1i}, \tag{3.35}$$

$$\mathrm{e}^{\Gamma_i D} = \begin{bmatrix} 1 & -D & D & E_{14} & E_{15} \\ 0 & 1 & 0 & E_{24} & 0 \\ 0 & 0 & 1 & 0 & \tau_{i-1}\left(1 - \mathrm{e}^{\frac{-D}{\tau_{i-1}}}\right) \\ 0 & 0 & 0 & \mathrm{e}^{\frac{-D}{\tau_i}} & 0 \\ 0 & 0 & 0 & 0 & \mathrm{e}^{\frac{-D}{\tau_{i-1}}} \end{bmatrix}, \tag{3.36}$$

$$E_{14} = \tau_i^2\left(1 - \frac{D}{\tau_i} - \mathrm{e}^{\frac{-D}{\tau_i}}\right), \tag{3.37}$$

$$E_{15} = \tau_{i-1}^2\left(\mathrm{e}^{\frac{-D}{\tau_{i-1}}} + \frac{D}{\tau_{i-1}} - 1\right), \tag{3.38}$$

$$E_{24} = \tau_i\left(1 - \mathrm{e}^{\frac{-D}{\tau_i}}\right). \tag{3.39}$$

Using (3.8), (3.10), (3.34), and (3.35) we get

$$(sI_{5\times5} - \Gamma_i)^{-1} = \begin{bmatrix} s & 1 & -1 & 0 & 0 \\ 0 & s & 0 & -1 & 0 \\ 0 & 0 & s & 0 & -1 \\ 0 & 0 & 0 & s + \frac{1}{\tau_i} & 0 \\ 0 & 0 & 0 & 0 & s + \frac{1}{\tau_{i-1}} \end{bmatrix}^{-1} = \frac{1}{s^2}\begin{bmatrix} s & -1 & 1 & -\frac{\tau_i}{s\tau_i+1} & -\frac{\tau_{i-1}}{s\tau_{i-1}+1} \\ 0 & s & 0 & \frac{s\tau_i}{s\tau_i+1} & 0 \\ 0 & 0 & s & 0 & \frac{s\tau_{i-1}}{s\tau_{i-1}+1} \\ 0 & 0 & 0 & \frac{s^2\tau_i}{s\tau_i+1} & 0 \\ 0 & 0 & 0 & 0 & \frac{s^2\tau_{i-1}}{s\tau_{i-1}+1} \end{bmatrix}, \tag{3.40}$$

$$M_{1,i}(s) = \begin{bmatrix} M_{11,i}(s) & M_{21,i}(s) & 0 & M_{41,i}(s) & 0 \end{bmatrix}^{\mathrm{T}}, \tag{3.41}$$

$$M_{2,i}(s) = \begin{bmatrix} m_{11,i}(s) & 0 & m_{31,i}(s) & 0 & m_{51,i}(s) \end{bmatrix}^{\mathrm{T}}, \tag{3.42}$$

where

$$M_{11,i}(s) = \frac{\mathrm{e}^{-sD}\left(\tau_i - \tau_i e^{\frac{-D}{\tau_i}}\right)}{s^2\tau_i} + \frac{\mathrm{e}^{-sD}\left(\tau_i^2\mathrm{e}^{\frac{-D}{\tau_i}} + D\tau_i - \tau_i^2\right)}{s\tau_i} + \frac{\tau_i\left(\mathrm{e}^{-\frac{D}{\tau_i}}\mathrm{e}^{-sD} - 1\right)}{s^2\tau_i(s\tau_i+1)}, \quad (3.43)$$

$$M_{21,i}(s) = -\frac{\mathrm{e}^{-sD}(\tau_i - \tau_i\mathrm{e}^{\frac{-D}{\tau_i}})}{s\tau_i} - \frac{\tau_i\left(\mathrm{e}^{\frac{-D}{\tau_i}}\mathrm{e}^{-sD} - 1\right)}{s\tau_i(s\tau_i+1)}, \quad (3.44)$$

$$M_{41,i}(s) = -\frac{\mathrm{e}^{\frac{-D}{\tau_i}}\mathrm{e}^{-sD} - 1}{s\tau_i + 1}, \quad (3.45)$$

$$m_{11,i}(s) = -\frac{\mathrm{e}^{-sD}\left(\tau_{i-1} - \tau_{i-1}\mathrm{e}^{\frac{-D}{\tau_{i-1}}}\right)}{s^2\tau_{i-1}} - \frac{\mathrm{e}^{-sD}\left(\tau_{i-1}^2\mathrm{e}^{\frac{-D}{\tau_{i-1}}} + D\tau_{i-1} - \tau_{i-1}^2\right)}{s\tau_{i-1}} - \frac{\tau_{i-1}\left(\mathrm{e}^{-\frac{D}{\tau_{i-1}}}\mathrm{e}^{-sD} - 1\right)}{s^2\tau_{i-1}(s\tau_{i-1}+1)}, \quad (3.46)$$

$$m_{31,i}(s) = -\frac{\mathrm{e}^{-sD}\left(\tau_{i-1} - \tau_{i-1}\mathrm{e}^{\frac{-D}{\tau_{i-1}}}\right)}{s\tau_{i-1}} - \frac{\tau_{i-1}\left(\mathrm{e}^{\frac{-D}{\tau_{i-1}}}\mathrm{e}^{-sD} - 1\right)}{s\tau_{i-1}(s\tau_{i-1}+1)}, \quad (3.47)$$

$$m_{51,i}(s) = -\frac{\mathrm{e}^{\frac{-D}{\tau_{i-1}}}\mathrm{e}^{-sD} - 1}{s\tau_{i-1} + 1}. \quad (3.48)$$

Using the i-th vehicle's model (3.1)–(3.3) we obtain

$$\begin{bmatrix} S_i(s) \\ V_i(s) \\ A_i(s) \end{bmatrix} = \left(sI_{3\times3} - \hat{\Gamma}_i\right)^{-1}\left(\begin{bmatrix} 0 \\ 0 \\ \frac{1}{\tau_i} \end{bmatrix}\mathrm{e}^{-sD}U_i(s) + \begin{bmatrix} 1 \\ 0 \\ 0 \end{bmatrix}V_{i-1}(s)\right), \quad (3.49)$$

where

$$\hat{\Gamma}_i = \begin{bmatrix} 0 & -1 & 0 \\ 0 & 0 & 1 \\ 0 & 0 & -\frac{1}{\tau_i} \end{bmatrix}, \quad (3.50)$$

and hence

$$\begin{bmatrix} S_i(s) \\ V_i(s) \\ A_i(s) \end{bmatrix} = \begin{bmatrix} -\frac{1}{s^2(s\tau_i+1)} \\ \frac{1}{s(s\tau_i+1)} \\ \frac{1}{s\tau_i+1} \end{bmatrix}\mathrm{e}^{-sD}U_i(s) + \begin{bmatrix} \frac{1}{s} \\ 0 \\ 0 \end{bmatrix}V_{i-1}(s). \quad (3.51)$$

Using control laws (3.5), together with (3.33)–(3.48), we arrive at

$$\begin{aligned}U_i(s) = {} & \frac{\tau_i\alpha_i}{h_i}S_i(s) - \left(\tau_i(\alpha_i+b_i) + \frac{D\tau_i\alpha_i}{h_i}\right)V_i(s) - \frac{\tau_i\alpha_i}{sh_i}V_{i-1}(s) \\ & + \left(\tau_i b_i + \frac{D\tau_i\alpha_i}{h_i} + \frac{\tau_i\alpha_i}{sh_i}\right)\mathrm{e}^{-D_{c,i-1}s}V_{i-1}(s) + \left(\tau_i c_i \mathrm{e}^{\frac{-D}{\tau_i}} - \tau_i(\alpha_i+b_i)\left(\tau_i - \tau_i\mathrm{e}^{\frac{-D}{\tau_i}}\right)\right. \\ & \left. - \frac{\tau_i\alpha_i}{h_i}\left(\tau_i^2\mathrm{e}^{\frac{-D}{\tau_i}} + D\tau_i - \tau_i^2\right)\right)A_i(s) \\ & + \left(\tau_i b_i\left(\tau_{i-1} - \tau_{i-1}\mathrm{e}^{\frac{-D}{\tau_{i-1}}}\right) + \frac{\tau_i\alpha_i}{h_i}\left(\tau_{i-1}^2\mathrm{e}^{\frac{-D}{\tau_{i-1}}} + D\tau_{i-1} - \tau_{i-1}^2\right)\right)\mathrm{e}^{-D_{c,i-1}s}A_{i-1}(s) \\ & + g_{1,i}(s)U_i(s) + g_{2,i}(s)U_{i-1}(s)\mathrm{e}^{-D_{c,i-1}s}, \end{aligned} \tag{3.52}$$

where

$$g_{1,i}(s) = \left(\frac{\tau_i\alpha_i}{h_i}M_{11,i}(s) - \tau_i(\alpha_i+b_i)M_{21,i}(s) + \tau_i c_i M_{41,i}(s)\right), \tag{3.53}$$

$$g_{2,i}(s) = \left(\frac{\tau_i\alpha_i}{h_i}m_{11,i}(s) + \tau_i b_i m_{31,i}(s)\right). \tag{3.54}$$

Hence, substituting (3.51) in (3.52) we derive $\frac{U_i}{U_{i-1}}$, which, multiplying it by $\frac{s\tau_{i-1}+1}{s\tau_i+1}$, gives

$$G_i(s) = \frac{\left(b_i s + \frac{\alpha_i}{h_i}\right)\mathrm{e}^{-D_{c,i-1}s}}{s^3 + \left(\frac{1}{\tau_i} - c_i\right)s^2 + (\alpha_i+b_i)s + \frac{\alpha_i}{h_i}}. \tag{3.55}$$

String stability in $\mathcal{L}_2$ is guaranteed when $|G_i(j\omega)| \leq 1$, for all $\omega \geq 0$. The condition is satisfied for $\omega = 0$ since $|G_i(0)| = 1$. Moreover, from (3.55) we have

$$G_i(j\omega) = \frac{f_{1,i} + jf_{2,i}(\omega)}{f_{3,i}(\omega) + jf_{4,i}(\omega)}\mathrm{e}^{-D_{c,i-1}j\omega}, \tag{3.56}$$

$$f_{1,i} = \frac{\alpha_i}{h_i}, \tag{3.57}$$

$$f_{2,i}(\omega) = b_i\omega, \tag{3.58}$$

$$f_{3,i}(\omega) = \omega^2\left(\mathrm{c}_i - \frac{1}{\tau_i}\right) + \frac{\alpha_i}{h_i}, \tag{3.59}$$

$$f_{4,i}(\omega) = \omega(\alpha_i+b_i) - \omega^3. \tag{3.60}$$

By using the fact that $\sup_\omega |\mathrm{e}^{-D_{c,i-1}j\omega}| = 1$, the condition for string stability becomes $f_{1,i}^2 + f_{2,i}(\omega)^2 < f_{3,i}(\omega)^2 + f_{4,i}(\omega)^2$, $\omega > 0$, $i = 1, ..., N$, and hence, after straightforward computations, we get the following condition that has to hold for all $\omega > 0$ and $i = 1, ..., N$

$$\omega^6 + \omega^4 f_{5,i} + \omega^2 f_{6,i} > 0, \tag{3.61}$$

where

$$f_{5,i} = \left(c_i - \frac{1}{\tau_i}\right)^2 - 2(\alpha_i + b_i), \tag{3.62}$$

$$f_{6,i} = \alpha_i \left(\alpha_i + 2b_i + \frac{2}{h_i}\left(c_i - \frac{1}{\tau_i}\right)\right). \tag{3.63}$$

Relation (3.61) holds for all $\omega > 0$, under the conditions on the parameters a_i, b_i, c_i, τ_i, h_i of Theorem 3.1.

We next show that boundedness of all states is achieved. Using the delay-compensating property of predictor feedback (see e.g., [5]), we have, using (3.29), that for $t \geq \max\left\{D, \max_i \{D_{\mathrm{c},i-1}\}\right\} = \bar{D}$ (note that, due to linearity of systems (3.1)–(3.3) and controllers (3.5), no finite escape time phenomenon can appear for $t < \bar{D}$) it holds

$$\begin{aligned}\begin{bmatrix}\dot{s}_i(t)\\ \dot{v}_i(t)\\ \dot{a}_i(t)\end{bmatrix} =& \begin{bmatrix}0 & -1 & 0\\ 0 & 0 & 1\\ \frac{a_i}{h_i} & -(a_i+b_i) & c_i - \frac{1}{\tau_i}\end{bmatrix}\begin{bmatrix}s_i(t)\\ v_i(t)\\ a_i(t)\end{bmatrix}\\ &+ \begin{bmatrix}1\\0\\0\end{bmatrix} v_{i-1}(t) + \begin{bmatrix}0\\0\\b_i\end{bmatrix} v_{i-1,\mathrm{m}}(t) + \begin{bmatrix}0\\0\\\frac{a_i}{h_i}\end{bmatrix}\sigma_i(t),\end{aligned} \tag{3.64}$$

$$\dot{\sigma}_i(t) = v_{i-1,\mathrm{m}}(t) - v_{i-1}(t). \tag{3.65}$$

The solution to (3.64), (3.65) is given as

$$\begin{aligned}\begin{bmatrix}s_i(t)\\ v_i(t)\\ a_i(t)\end{bmatrix} =& \mathrm{e}^{\bar{A}_i\left(t-\bar{D}\right)}\begin{bmatrix}s_i\left(\bar{D}\right)\\ v_i\left(\bar{D}\right)\\ a_i\left(\bar{D}\right)\end{bmatrix} + \int_{\bar{D}}^{t}\mathrm{e}^{\bar{A}_i(t-s)}\left(\begin{bmatrix}1\\0\\0\end{bmatrix} v_{i-1}(s) + \begin{bmatrix}0\\0\\b_i\end{bmatrix} v_{i-1,\mathrm{m}}(s)\right.\\ &\left. + \begin{bmatrix}0\\0\\\frac{a_i}{h_i}\end{bmatrix}\sigma_i(s)\right) ds,\end{aligned} \tag{3.66}$$

$$\sigma_i(t) = \sigma_i\left(\bar{D}\right) + \int_{\bar{D}}^{t}\left(v_{i-1,\mathrm{m}}(s) - v_{i-1}(s)\right) ds, \tag{3.67}$$

where $\bar{A}_i = \begin{bmatrix}0 & -1 & 0\\ 0 & 0 & 1\\ \frac{a_i}{h_i} & -(a_i+b_i) & c_i - \frac{1}{\tau_i}\end{bmatrix}$. Under the conditions in Theorem 3.1, $\bar{A}_i$ always has all its eigenvalues with strictly negative real part, which means that the states s_i,

v_i, a_i remain bounded, provided that σ_i and v_{i-1} are bounded. We establish next the boundedness of σ_1 under the assumption that the leader's speed, denoted as v_0, is bounded by, say, M_{v_0}, i.e., $|v_0(s)| \leq \mathrm{M}_{v0}$, for all $s \geq -D_{\mathrm{c},0}$. We derive

$$\sigma_1(t) = \sigma_1(0) + \int_0^t \left(v_0(s - D_{\mathrm{c},0}) - v_0(s)\right) ds = \sigma_1(0) + \int_{-D_{\mathrm{c},0}}^{t-D_{\mathrm{c},0}} v_0(s)ds - \int_0^t v_0(s)ds, \tag{3.68}$$

and thus,

$$\sigma_1(t) = \sigma_1(0) + \int_{-D_{\mathrm{c},0}}^{0} v_0(s)ds - \int_{t-D_{\mathrm{c},0}}^{t} v_0(s)ds. \tag{3.69}$$

Considering the assumption on the leader's speed being bounded we can derive that

$$\int_{t-D_{\mathrm{c},0}}^{t} |v_0(s)|\, ds \leq \int_{t-D_{\mathrm{c},0}}^{t} \mathrm{M}_{v_0} ds = \mathrm{M}_{v_0} D_{\mathrm{c},0}. \tag{3.70}$$

Thus, considering (3.69), (3.70), it follows that σ_1 is uniformly bounded, with $|\sigma_1(t)| \leq \mathrm{M}_{\sigma_1}$, where $\mathrm{M}_{\sigma_1} = \sigma_1(0) + 2\mathrm{M}_{v_0} D_{\mathrm{c},0}$, $t \geq 0$. For showing boundedness of v_1 we proceed as follows. By using (3.66) for $i = 1$, with the fact that $\left|\mathrm{e}^{\bar{A}_1\left(t-\bar{D}\right)}\right| \leq k_1 \mathrm{e}^{-\lambda_1\left(t-\bar{D}\right)}$, for some positive constants k_1, λ_1 (because A_1 is Hurwitz, see, e.g., [29]) we get for $t \geq \bar{D}$

$$|v_1(t)| \leq r_{1,1}(t) + r_{2,1}(t) \leq \bar{v}_1(t), \tag{3.71}$$

where

$$r_{1,1}(t) = k_1 \mathrm{e}^{-\lambda_1\left(t-\bar{D}\right)} \left(\left|s_1\left(\bar{D}\right)\right| + \left|v_1\left(\bar{D}\right)\right| + \left|a_1\left(\bar{D}\right)\right|\right), \tag{3.72}$$

$$r_{2,1}(t) = \int_{\bar{D}}^{t} k_1 \mathrm{e}^{-\lambda_1(t-s)} \left(|v_0(s)| + |b_1 v_{0,\mathrm{m}}(s)| + \left|\frac{\alpha_1}{h_1}\sigma_1(s)\right|\right) ds, \tag{3.73}$$

$$\bar{v}_1(t) = r_{1,1}(t) + \frac{(1+b_1)\, k_1}{\lambda_1}\mathrm{M}_{v_0} + \frac{k_1\alpha_1}{\lambda_1 h_1}\mathrm{M}_{\sigma_1}. \tag{3.74}$$

Relations (3.71)–(3.74) imply that v_1 is uniformly bounded with $|v_1(s)| \leq \mathrm{M}_{v_1}$, $s \geq -D_{\mathrm{c},1}$. This assertion is based on the observation that v_1 is bounded by constant terms $\frac{(1+b_1)k_1}{\lambda_1}\mathrm{M}_{v_0}$, $\frac{k_1\alpha_1}{\lambda_1 h_1}\mathrm{M}_{\sigma_1}$, and an exponentially decaying term, as well as using the fact that $v_1(s)$, $s \in [-D_{\mathrm{c},1}, 0]$ is also bounded (by assumption). Then, we need to show that σ_2 is

uniformly bounded. We derive

$$\sigma_2(t) = \sigma_2(0) + \int_0^t \left(v_1(s - D_{\mathrm{c},1}) - v_1(s)\right) ds = \sigma_2(0) + \int_{-D_{\mathrm{c},1}}^{0} v_1(s) ds - \int_{t-D_{\mathrm{c},1}}^{t} v_1(s) ds. \tag{3.75}$$

Following a similar argument as for the boundedness of σ_1 and since

$$\int_{t-D_{\mathrm{c},1}}^{t} |v_1(s)|\, ds \leq \int_{t-D_{\mathrm{c},1}}^{t} \mathrm{M}_{v_1} ds = \mathrm{M}_{v_1} D_{\mathrm{c},1}, \tag{3.76}$$

we conclude that σ_2 is uniformly bounded. We next show that v_2 is bounded. Similarly to derivation of (3.71)–(3.74), there exist some positive constants k_2 and λ_2, such that for $t \geq \bar{D}$

$$|v_2(t)| \leq r_{1,2}(t) + r_{2,2}(t) \leq \bar{v}_2(t), \tag{3.77}$$

where

$$r_{1,2}(t) = k_2 \mathrm{e}^{-\lambda_2\left(t-\bar{D}\right)} \left(\left|s_2\left(\bar{D}\right)\right| + \left|v_2\left(\bar{D}\right)\right| + \left|a_2\left(\bar{D}\right)\right|\right), \tag{3.78}$$

$$r_{2,2}(t) = \int_{\bar{D}}^{t} k_2 \mathrm{e}^{-\lambda_2(t-s)} \left(|v_1(s)| + |b_2 v_{1,\mathrm{m}}(s)| + \left|\frac{\alpha_2}{h_2}\sigma_2(s)\right|\right) ds, \tag{3.79}$$

$$\bar{v}_2(t) = r_{1,2}(t) + \frac{(1+b_2)\, k_2}{\lambda_2} \mathrm{M}_{v_1} + \frac{k_2 \alpha_1}{\lambda_2 h_2} \mathrm{M}_{\sigma_2}. \tag{3.80}$$

This pattern continues iteratively up to $i = N$. Consequently, we can deduce by induction that v_i and σ_i, $i = 1, ..., N$, are bounded. From (3.66) and the fact that the $\bar{A}_i$ matrices are Hurwitz we conclude that the system's states s_i and a_i are also bounded.

Next, we demonstrate how control law (3.5) regulates s_i, v_i, a_i, and σ_i, and we also compute their steady-state values. Regulation follows starting with $i = 1$ and considering $v_0 \equiv v^*$ as the leader's speed having constant value. This assumption leads to bounded limits for each σ_i and, subsequently, results in finite limits for v_i, s_i, and a_i. To clarify this, we begin with σ_1, which is constant (given a constant v_0). This enables us to recursively compute finite limits for v_1, s_1, and a_1, based on (3.66) and the fact that $\bar{A}_1$ is Hurwitz. Then, using (3.75), together with the continuity of v_1 (for $t \geq \bar{D}$) and the fact that v_1 has a finite limit, we obtain that σ_2 has a finite limit. By considering (3.66) and the finite limit of states v_1 and σ_2, as well as the fact that $\bar{A}_2$ is Hurwitz, we deduce that v_2, s_2, and a_2 have finite limits. This process continues recursively, leading to the conclusion that s_i, v_i, a_i, and σ_i, $i = 1, 2, ..., N$, have finite limits. Moreover, we can derive $\lim_{t\to+\infty} \dot{s}_i(t) = \lim_{t\to+\infty} \dot{v}_i(t) = \lim_{t\to+\infty} \dot{a}_i(t) = 0$,

$i = 1, 2, ..., N$. This is established by applying, for example, Barbalat's lemma, (see, e.g., [49]), given that s_i, v_i, and a_i have finite limits and by using (3.64), (3.65), which allow us to conclude boundedness of $\ddot{s}_i$, $\ddot{v}_i$, $\ddot{a}_i$. Subsequently, by using (3.64) we deduce that $\lim_{t\to+\infty} v_i(t) = \lim_{t\to+\infty} v_{i-1}(t) = v^*$, and $\lim_{t\to+\infty} v_{i-1,\mathrm{m}}(t) = \lim_{t\to+\infty} v_{i-1}(t) = v^*$. Moreover, we conclude that $\lim_{t\to+\infty} s_i(t) = \lim_{t\to+\infty} (h_i v_i(t) - \sigma_i(t))$, where

$$\lim_{t\to+\infty} \sigma_i(t) = \sigma_i(0) + \int_{-D_{\mathrm{c},i-1}}^{0} v_{i-1_0}(s)ds - \lim_{t\to+\infty} \int_{-D_{\mathrm{c},i-1}}^{0} v_{i-1}(s+t)ds. \tag{3.81}$$

Due to the fact that v_{i-1} is a continuous function on the time interval $\left(\bar{D},\ +\infty\right)$ and uniformly bounded, we can derive

$$\lim_{t\to+\infty} \sigma_i(t) = \sigma_i(0) + \int_{-D_{\mathrm{c},i-1}}^{0} v_{i-1_0}(s)ds - D_{\mathrm{c},i-1}v^*, \tag{3.82}$$

which completes the proof. □

3.4 Numerical Illustration of String Stability

In this section, we numerically analyze the string stability properties of the closed-loop system, according to Theorem 3.1. The transfer function $G_i = \frac{V_i}{V_{i-1}}$, which corresponds to the closed-loop systems described by equations (3.1)–(3.3), (3.5)–(3.10), along with choices (made for simplicity of illustration)

$$\alpha_i = -h_i p_i^3, \tag{3.83}$$

$$b_i = h_i p_i^3 + 3p_i^2, \tag{3.84}$$

$$c_i = \frac{1}{\tau_i} + 3p_i, \tag{3.85}$$

for some $p_i < 0$ and all i, is determined as

$$G_i(s) = \frac{V_i(s)}{V_{i-1}(s)} = \frac{-p_i^3 + p_i^2(p_i h_i + 3)s}{(s - p_i)^3} \mathrm{e}^{-sD_{\mathrm{c},i-1}}. \tag{3.86}$$

The numerical performance of the predictor-feedback CACC design (3.5) is showcased, focusing on $\mathcal{L}_2$ string stability definition in relation to (3.86). Figure 3.2 depicts $\sup_\omega |G_i(j\omega)|$ as a function of p_i and h_i, where G_i is defined in (3.86). The conditions in Theorem 3.1, reduce to condition $h_i^2 p_i^2 + 6h_i p_i + 6 < 0$, which should hold to guarantee string stability. In Figure 3.2, the region between the red curves indicates where condition $h_i^2 p_i^2 + 6h_i p_i + 6 < 0$ is satisfied.

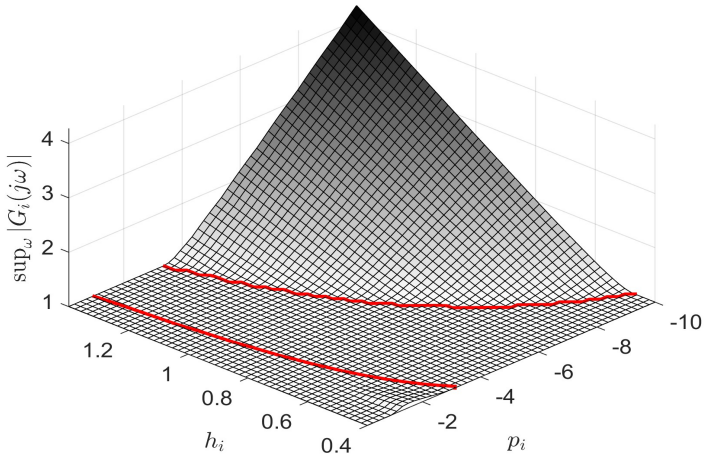

Figure 3.2: The values of function $\sup_\omega |G_i(j\omega)|$ corresponding to transfer function (3.86) for heterogeneous vehicles, for different values of time-headway h_i and control parameter p_i.

In fact, string stability in $\mathcal{L}_p$, $p \in [1, +\infty]$, is also established. This follows based on the facts that $G_i(0) = 1$ and that (3.86) corresponds to a non-negative impulse response (see, e.g., [12]). As inferred from [48] (Theorem 5; case Type D-1), the validity of the latter is confirmed when the subsequent condition holds

$$-\frac{1}{p_i} \geq -\frac{h_i}{p_i}\left(p_i + \frac{3}{h_i}\right) \geq 0, \tag{3.87}$$

which can be also written as $-\frac{3}{h_i} \leq p_i \leq -\frac{2}{h_i}$ (that also guarantees $h_i^2 p_i^2 + 6h_i p_i + 6 < 0$). Note that all conditions for string stability do not depend on communication delay $D_{\mathrm{c},i-1}$ (or actuation delay D), demonstrating the delay-compensating property of our design.

3.5 Simulation Results

In this section, first, the performance of the actuation/communication delays-compensating controller (3.5) is demonstrated, followed by a comparison with the predictor-feedback CACC approach in [44], which does not achieve communication delay compensation. Moreover, to illustrate the efficiency of predictor-feedback CACC with integral action in more practical scenarios, we utilize real traffic data from NGSIM.

Note that the simulations are conducted in Matlab R2022b, where integrals in the predictor-based controller (3.7) are computed using the trapezoidal rule. Moreover, third-

order models for vehicles' dynamics, as described in (3.1)–(3.3), are implemented using the Euler method. These models are consistently applied throughout the simulations for both the proposed and conventional predictor-feedback CACC methods, ensuring a fair and direct comparison in Sections 3.5.1 and 3.5.2. Additionally, in Sections 3.5.1 and 3.5.2, a fixed time step of $T_s = 0.01$ is selected to align with the sampling time of control execution and measurements, see, e.g., [22], [23]. Furthermore, in Section 3.5.3, a fixed time step of $T_s = 0.1$ is used to match the sampling interval of the real traffic data that are employed, with the sampling time of measurements, and control execution used in the simulation investigations.

3.5.1 Predictor-Feedback CACC with Simultaneous Compensation of Actuator/Communication Delays

At first, we demonstrate the performance of the actuation/communication delays-compensating predictor-feedback CACC law. We consider a heterogeneous platoon of ten vehicles in order to make the numerical example more practical. For a heterogeneous platoon of ten vehicles with third-order dynamics given by (3.1)–(3.3), we consider a case in which $\tau_i = 0.1s$, $i = 1, 2, 6, 9$; $\tau_i = 0.2s$, $i = 0, 3, 5$; and $\tau_i = 0.25s$, $i = 4, 7, 8$. The desired time-headways are $h_{i,\text{des}} = 0.75$, $i = 3, 4, 7, 9$; $h_{i,\text{des}} = 0.9$, $i = 2, 5$; $h_{i,\text{des}} = 1.2$, $i = 1, 6, 8$. The actuation delay is set to $D = 0.7$ and communication delays are $D_{\text{c},i-1} = 0.1$, $i = 1, 4, 6$; $D_{\text{c},i-1} = 0.15$, $i = 5, 8$; $D_{\text{c},i-1} = 0.2$, $i = 3$; $D_{\text{c},i-1} = 0.25$, $i = 2, 9$; and $D_{\text{c},i-1} = 0.35$, $i = 7$. Following Remark 3.1, we assume that the communication delay is known. To address steady-state error, we employ in (3.5) time-headways $h_i = h_{\text{des},i} - D_{\text{c},i-1}$ (all h_i, $i = 1, 2, ..., 9$, satisfy the conditions in Theorem 3.1; see Figure 3.2) and choose $\sigma_{i_0} = -\int_{-D_{\text{c},i-1}}^{0} v_{i-1_0}(s)ds$ for all vehicles. Moreover, zero, steady-state spacing tracking errors are achieved as $\lim_{t\to+\infty} s_i(t) = h_{i,\text{des}}v^*$, $i = 1, 2, ..., N$ (see Remark 3.1). We choose control gains according to (3.83)–(3.85) with $p_i = \frac{-2.5}{h_i}$, $i = 1, 2, ..., 9$ which satisfy the conditions in Theorem 3.1. Moreover, we consider a scenario in which $a_{i-1}(s) = 0, s \in [-D_{\text{c},i-1}, 0]$ and $u_i(s) = 0$, $s \in [-D - D_{\text{c},i-1}, 0)$ for each vehicle i. While we set $v_{i_0} = 15\left(\frac{m}{s}\right)$, $i = 1, 2, ..., 9$ and $v_{\text{l}_0} = \frac{4v_{i_0}}{5} = 12\left(\frac{m}{s}\right)$; $v_{\text{l}}(s) = 12, s \in [-D_{\text{c},0}, 0]$ and $v_{i-1}(s) = 15, s \in [-D_{\text{c},i-1}, 0]$, $i = 2, ..., 9$; $s_{i_0} = h_{\text{des},i}v_{i_0} = h_{\text{des},i} \times 15\ m$, $i = 2, 3, ..., 9$, $s_{1_0} = 16\ m$. Furthermore, the leading vehicle performs both deceleration and acceleration maneuvers.

Note that, here, we consider a scenario in which the initial condition for the speed of the leading vehicle ($12\left(\frac{m}{s}\right)$) is smaller than the initial speed of vehicle no. 1 ($15\left(\frac{m}{s}\right)$), i.e., the vehicle immediately behind the leader; while their respective initial spacing is 16

m. Thus, this scenario may appear in cases in which a vehicle (taking the role of the leader) cuts in, in front of the platoon (e.g., as a result of lane-changing from an adjacent lane) at a lower speed and short distance; or when a vehicle in the platoon changes lane to avoid a slowly moving vehicle in front (that takes the role of the leader after the lane-changing maneuver). Such a realistic correspondence, between the practical scenario of a vehicle cutting in the platoon and the simulation test using initial conditions not at equilibrium (with the leading vehicle having lower initial speed than vehicle no. 1), has been also considered in, for example, [27] (Scenario 3 in Section 2.2). In addition, the sharp deceleration maneuver of the leading vehicle in the same scenario (at $t = 20\ s$) could be also considered as related to a practical scenario of a vehicle changing lane in front of the leading vehicle with lower speed, thus causing the leading vehicle to decelerate abruptly. Such a correspondence, between the practical scenario of a vehicle cutting-in in front of the platoon and the simulation scenario of a sharp deceleration maneuver of the leading vehicle, has been also considered in, for example, [65] (Scenario 1 in Section 4.1).

As depicted in Figure 3.3, the speed and acceleration responses to these maneuvers by the leading vehicle exhibit characteristics devoid of oscillations and overshoot. This desirable outcome is attributed to the obtained impulse response positivity and $\mathcal{L}_\infty$ string stability, respectively. These attributes are guaranteed for the corresponding transfer functions (3.86), subject to the condition (3.87). Furthermore, it is interesting to note that all states diverged with the nominal control law (3.4) in the presence of actuation/communication delays.

We note that if communication delays are not known exactly then we could still employ the choices $h_i = h_{i,\text{des}} - \hat{D}_{\text{c},i-1}$ and $\sigma_{i_0} = -\int_{-\hat{D}_{\text{c},i-1}}^{0} v_{i-1_0}(s)ds$, with an estimate $\hat{D}_{\text{c},i-1}$ of $D_{\text{c},i-1}$. It is anticipated that steady-state, spacing tracking errors would remain small. The only case in which steady-state spacing errors would be large is when $D_{\text{c},i-1}$ are both completely unknown and large which, in practice, may not be as realistic.

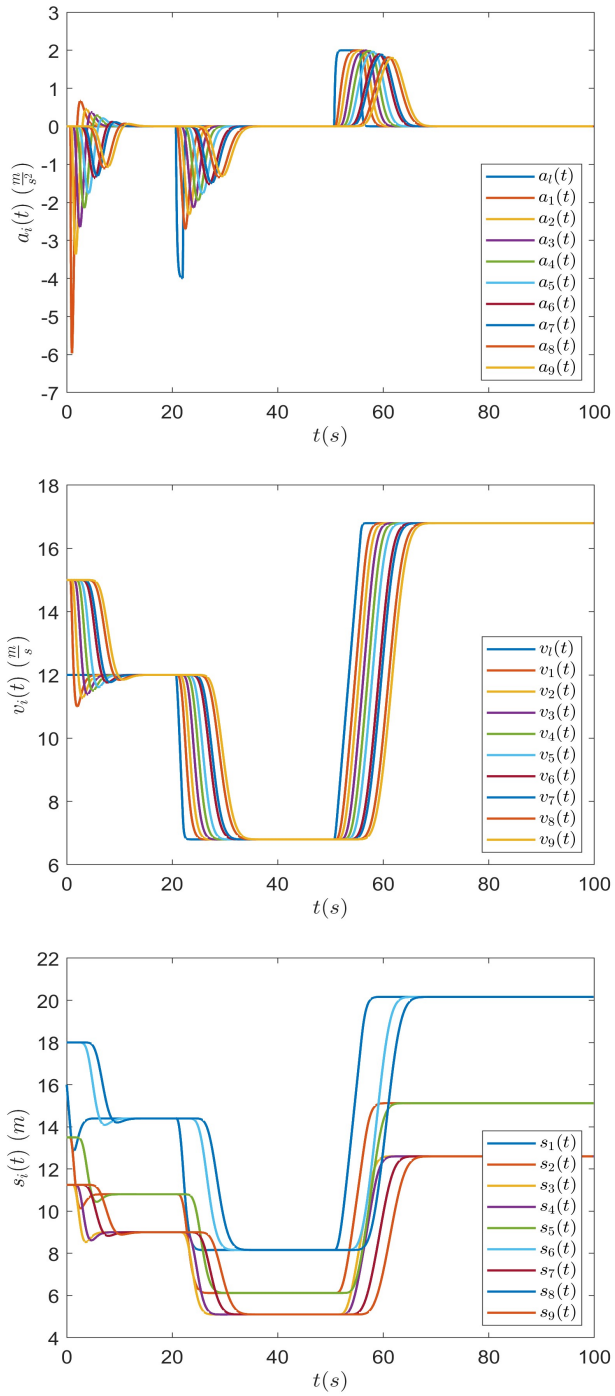

Figure 3.3: Acceleration (top), speed (middle), and spacing (bottom) of ten vehicles, with dynamics described by (3.1)–(3.3), where $D = 0.7$, $\tau_i = 0.1s$, $i = 1, 2, 6, 9$; $\tau_i = 0.2s$, $i = 0, 3, 5$; and $\tau_i = 0.25s$, $i = 4, 7, 8$, following a leader that performs an acceleration/deceleration maneuver, under the CACC laws (3.5), where $D_{\mathrm{c},i-1} = 0.1$, $i = 1, 4, 6$; $D_{\mathrm{c},i-1} = 0.15$, $i = 5, 8$; $D_{\mathrm{c},i-1} = 0.2$, $i = 3$; $D_{\mathrm{c},i-1} = 0.25$, $i = 2, 9$; and $D_{\mathrm{c},i-1} = 0.35$, $i = 7$. The desired time-headways are $h_{i,\mathrm{des}} = 0.75$, $i = 3, 4, 7, 9$; $h_{i,\mathrm{des}} = 0.9$, $i = 2, 5$; $h_{i,\mathrm{des}} = 1.2$, $i = 1, 6, 8$; while control parameters are chosen according to (3.83)–(3.85) with $p_i = \frac{-2.5}{h_i}$ and $h_i = h_{i,\mathrm{des}} - D_{\mathrm{c},i-1}$. Initial conditions are $v_{i_0} = 15\left(\frac{m}{s}\right)$, $i = 1, 2, ..., 9$, $v_{\mathrm{l}_0} = \frac{4v_{i_0}}{5} = 12\left(\frac{m}{s}\right)$; $s_{i_0} = h_{i,\mathrm{des}} v_{i_0} = h_{i,\mathrm{des}} \times 15\ m$, $i = 2, 3, ..., 9$, $s_{1_0} = 16\ m$; $\sigma_{i_0} = -\int_{-D_{\mathrm{c},i-1}}^{0} v_{i-1_0}(s)ds$ and $u_{i0} \equiv 0$, for $i = 1, 2, ..., 9$.

3.5.2 Predictor-Feedback without Compensation of Communication Delay

In Figure 3.4 we show the response of the heterogeneous platoon of ten vehicles under the predictor-feedback CACC law from [44] for system (3.1)–(3.3) that are given by

$$\bar{u}_i(t) = \frac{\tau_i \alpha_i}{h_i} \bar{q}_{i,1}(t) - \tau_i(\alpha_i + b_i)\bar{q}_{i,2}(t) + \tau_i b_i \bar{q}_{i,3}(t) + \tau_i c_i \bar{q}_{i,4}(t), \tag{3.88}$$

$$\bar{q}_i(t) = \mathrm{e}^{\Gamma_i D}\tilde{\bar{x}}_i(t) + \int_{t-D}^{t} \mathrm{e}^{\Gamma_i(t-\theta)} B_i \bar{u}_i(\theta)\, d\theta + \int_{t-D}^{t} \mathrm{e}^{\Gamma_i(t-\theta)} B_{1i} \bar{u}_{i-1,\mathrm{m}}(\theta)\, d\theta, \tag{3.89}$$

where

$$\bar{q}_i = \begin{bmatrix} \bar{q}_{i,1} \\ \bar{q}_{i,2} \\ \bar{q}_{i,3} \\ \bar{q}_{i,4} \\ \bar{q}_{i,5} \end{bmatrix}, \quad \tilde{\bar{x}}_i = \begin{bmatrix} s_i \\ v_i \\ v_{i-1} \\ a_i \\ a_{i-1,\mathrm{m}} \end{bmatrix}. \tag{3.90}$$

Control law (3.88) aims at only input delay compensation, but does not address communication delay. String stability under (3.88) is robust to the presence of small communication delay, as it is shown in [44]. We consider the scenario in which τ_i, D, and $D_{\mathrm{c},i-1}$ are the same with Section V-A and the desired time-headways are $h_i = 0.75$, $i = 3, 4, 7, 9$; $h_i = 0.9$, $i = 2, 5$; and $h_i = 1.2$, $i = 1, 6, 8$. We choose control gains according to (3.83)–(3.85) with $p_i = \frac{-2.5}{h_i}$, $i = 1, 2, ..., 9$, which satisfy the stability and string stability requirements when $D_{\mathrm{c},i-1} = 0$ (see Figure 1-top in [44]). Since we consider the same scenario with Section V-A we choose identical initial conditions for a_i, v_i, u_i; while we set the initial spacing for $i = 2, 3, ..., 9$ to the corresponding equilibria for this this case, namely, $s_{i_0} = h_i v_{i_0} = h_i \times 15\ m$, and set $s_{1_0} = 16\ m$. The respective responses are, in general, more oscillatory. In addition, the response of vehicle 7 is string unstable, for the given values of h_7 and $D_{\mathrm{c},6}$ (see Figure 3 in [44]), which results in overshoot in the respective response to leader's maneuvers.

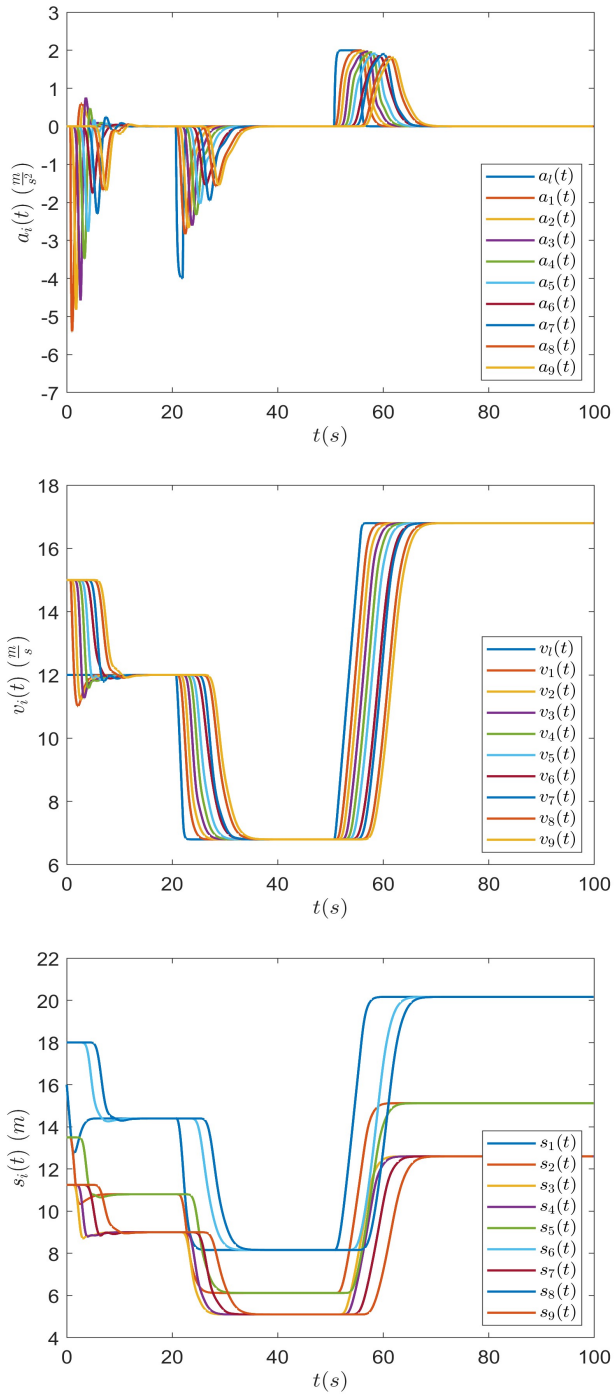

Figure 3.4: Acceleration (top), speed (middle), and spacing (bottom) of ten vehicles, with dynamics described by (3.1)–(3.3), where $D = 0.7$, $\tau_i = 0.1s$, $i = 1, 2, 6, 9$; $\tau_i = 0.2s$, $i = 0, 3, 5$; and $\tau_i = 0.25s$, $i = 4, 7, 8$, following a leader that performs an acceleration/deceleration maneuver, under the CACC laws in [44] (see also (3.88)–(3.90)), where $D_{c,i-1} = 0.1$, $i = 1, 4, 6$; $D_{c,i-1} = 0.15$, $i = 5, 8$; $D_{c,i-1} = 0.2$, $i = 3$; $D_{c,i-1} = 0.25$, $i = 2, 9$; and $D_{c,i-1} = 0.35$, $i = 7$. The desired time-headways are $h_i = 0.75$, $i = 3, 4, 7, 9$; $h_i = 0.9$, $i = 2, 5$; and $h_i = 1.2$, $i = 1, 6, 8$; while control parameters are chosen according to (3.83)–(3.85) with $p_i = \frac{-2.5}{h_i}$. Initial conditions are $v_{i_0} = 15\left(\frac{m}{s}\right)$, $i = 1, 2, ..., 9$, $v_{l_0} = \frac{4v_{i_0}}{5} = 12\left(\frac{m}{s}\right)$; $s_{i_0} = h_i v_{i_0} = h_i \times 15\ m$, $i = 2, 3, ..., 9$, $s_{1_0} = 16\ m$; and $u_{i_0} \equiv 0$, for $i = 1, 2, ..., 9$.

3.5.3 Validation with NGSIM Data

In Figure 3.5 we present the results of applying the predictor-feedback CACC law of Section V-A on NGSIM dataset. We extract reconstructed data from [37] to demonstrate the controller's performance in real maneuvering of the leading vehicle, considering that the leading vehicle's trajectory is taken from the real trajectory of vehicle no. 1601. This vehicle's trajectory is selected because it involves interesting dynamics with several acceleration/deceleration cycles. In fact, NGSIM data involve vehicles' trajectories that are taken from traffic in heavily congested conditions [37]. Indeed, from Fig. 5 (top and middle plots) it can be observed that the leading vehicle's (and thus, also the rest of the vehicles') trajectory features oscillations, as result of appearance of stop-and-go waves (evident in congested traffic flow); while its speed varies between around $15\left(\frac{m}{s}\right)$ and $4\left(\frac{m}{s}\right)$ (also a feature of congested traffic flow conditions).

We consider a heterogeneous platoon of five vehicles in order to make the numerical example more accessible and to more clearly illustrate the benefits of (3.5) in more practical scenarios. One difference from Section V-A is the predictor-feedback law for the first vehicle. Because we assume that the leading vehicle's dynamics satisfy $\dot{v}_{\rm l}(t) = u_{\rm l}(t-D)$ (and not the third-order system (3.1)–(3.3)) we have to modify slightly the predictor-feedback law for the first vehicle. In this case, for implementation of the predictor-feedback law, we set $u_{\rm l}(s)$, $s \geq 0$, using the practical command data, which are obtained from NGSIM dataset and we also set $u_{\rm l}(s) = 0$, for $s \in [-D - D_{\rm c,0}, 0)$. Furthermore $v_{\rm l}$ is computed from the model $\dot{v}_{\rm l}(t) = u_{\rm l}(t-D)$, where $u_{\rm l}(t) = a_{\rm l}(t)$, $t \geq 0$, and $a_{\rm l}(t)$ are the NGSIM values of acceleration. This scenario could correspond to a case of a leading vehicle that is connected/automated or only connected, in which the control input commands $u_{\rm l}(t)$ (desired acceleration) affect the vehicle with a delay D; while these commands are transmitted to the following vehicle with communication delay $D_{\rm c,0}$. We also note here that we do not validate the design in scenarios in which, for example, the leading vehicle's dynamics satisfy $\dot{v}_{\rm l}(t) = u_{\rm l}(t)$. The reason is that, because the leading vehicle's dynamics in such a case would not involve input delay, one would have to properly modify the predictor-feedback law for vehicle $i = 1$, for obtaining an implementable formula for the predictor state of $v_{\rm l}$. This could be done, for example, as in [36], assuming constant speed for the leader. We do not investigate this scenario here, because this would imply that we also validate the design in such type of model mismatches, rather than validating it only accounting for real, leading vehicle's trajectories, which is our current scope here.

In this scenario we consider a case in which $\tau_i = 0.1s$, $i = 1, 4$; $\tau_i = 0.2s$, $i = 0, 2$; and $\tau_i = 0.25s$, $i = 3$. The desired time-headways are $h_{i,\rm des} = 1.2$, $i = 1, 4$; $h_{i,\rm des} = 0.75$, $i = 2, 3$. The actuation delay is set to $D = 0.7$ and communication delays are $D_{{\rm c},i-1} =$

0.1, $i = 1, 3, 4$; $D_{\mathrm{c},i-1} = 0.2$, $i = 2$. Following a similar approach to Section V-A, we assume that the communication delay is known, so we employ in (3.5) time-headways $h_i = h_{\mathrm{des},i} - D_{\mathrm{c},i-1}$, $i = 1, 2, 3, 4$ and choose $\sigma_{i_0} = -\int_{-D_{\mathrm{c},i-1}}^{0} v_{i-1_0}(s)ds$ for all vehicles to address steady-state spacing error. Moreover, we choose control gains according to (3.83)–(3.85) with $p_i = \frac{-2.5}{h_i}$, $i = 1, 2, 3, 4$, which satisfy the conditions in Theorem 1. We set $a_i(s) = 0, s \in [-D_{\mathrm{c},i-1}, 0]$ and $u_i(s) = 0$, $s \in [-D - D_{\mathrm{c},i-1}, 0)$ for vehicles $i = 1, 2, 3, 4$. While we also set $v_{i_0} = 20\left(\frac{m}{s}\right)$, $i = 1, 2, 3, 4$ and $v_{1_0} = 14.9\left(\frac{m}{s}\right)$ (to match the initial speed of vehicle 1601 from NGSIM data); $v_1(s) = 14.9, s \in [-D_{\mathrm{c},0}, 0]$ and $v_{i-1}(s) = 20, s \in [-D_{\mathrm{c},i-1}, 0]$, $i = 2, 3, 4$; $s_{i_0} = h_{\mathrm{des},i} v_{i_0} = h_{\mathrm{des},i} \times 20\ m$, $i = 2, 3, 4$, $s_{1_0} = 22\ m$. Figure 3.5 illustrates that the performance of the predictor-feedback CACC law with integral action (3.5) is preserved even in more realistic traffic scenarios.

3.6 Chapter Conclusions and Related Publications

In the present chapter, we design a predictor-feedback CACC law with integral action, which achieves simultaneous actuation and communication delays compensation. We consider heterogeneous platoons with vehicles whose dynamics are described by a linear, third-order model with delayed actuation. The control design developed achieves string stability with respect to speed errors propagation, individual vehicle stability, and zero steady-state tracking errors. We provide constructive proof strategies that rely on a combination of an input-output approach and on deriving explicit solutions of the closed-loop systems. We demonstrate numerically the string stability conditions obtained and we provide simulation results for a platoon of ten vehicles, considering a realistic scenario of a vehicle cutting in the platoon and performing acceleration/deceleration maneuvers. We also validate the performance of the design developed in simulation, using real traffic data to describe the trajectory of the leading vehicle.

This chapter is an adaptation of material appearing in

A. Samii and N. Bekiaris-Liberis, "Simultaneous compensation of actuation and communication delays for heterogeneous platoons via predictor-feedback CACC with integral action," *IEEE Transactions on Intelligent Vehicles*, vol. 9, pp. 5618–5630, 2024.

A. Samii and N. Bekiaris-Liberis, "Simultaneous compensation of actuation and communication delays for heterogeneous platoons via predictor-feedback CACC with integral action," *European Control Conference*, Stockholm, 2024.

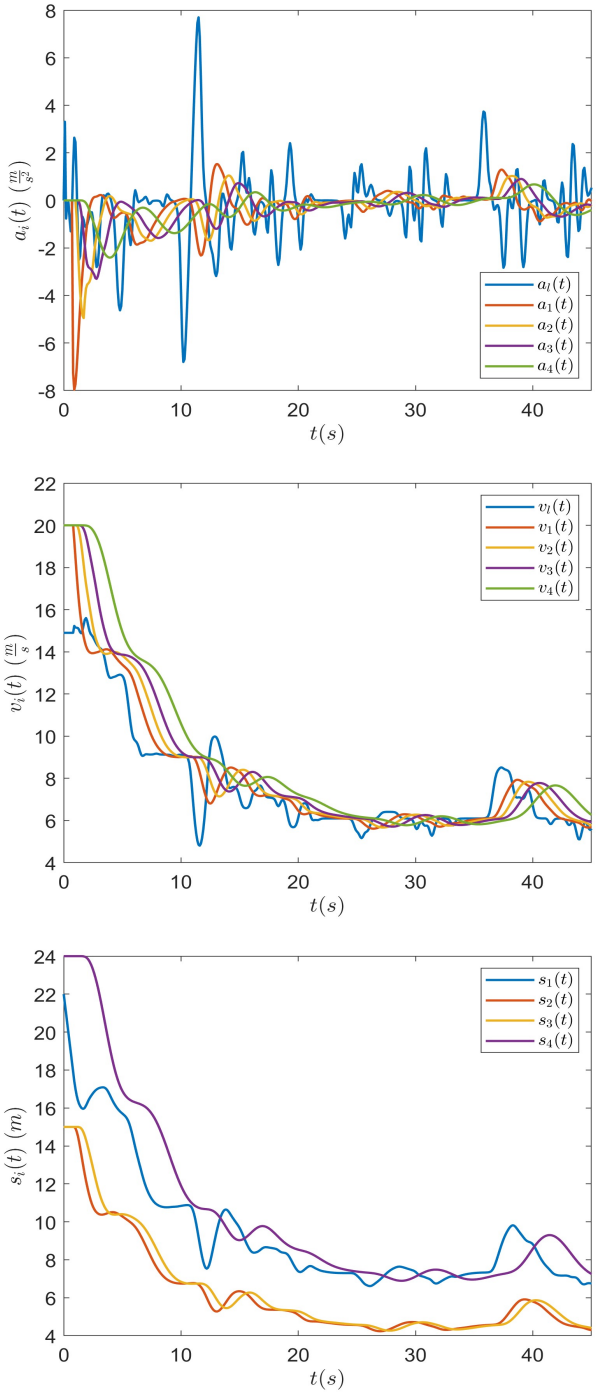

Figure 3.5: Acceleration (top), speed (middle), and spacing (bottom) of five vehicles, where $D = 0.7$, $\tau_i = 0.1s$, $i = 1, 4$; $\tau_i = 0.2s$, $i = 0, 2$; and $\tau_i = 0.25s$, $i = 3$, following a leader whose trajectory is obtained from the trajectory of vehicle no. 1601 in the NGSIM data, under the CACC laws (3.5), where $D_{c,i-1} = 0.1$, $i = 1, 3, 4$; $D_{c,i-1} = 0.2$, $i = 2$. The desired time-headways are $h_{i,\text{des}} = 1.2$, $i = 1, 4$; $h_{i,\text{des}} = 0.75$, $i = 2, 3$; while control parameters are chosen according to (3.83)–(3.85) with $p_i = \frac{-2.5}{h_i}$ and $h_i = h_{i,\text{des}} - D_{c,i-1}$, with $\sigma_{i_0} = -\int_{-D_{c,i-1}}^{0} v_{i-1_0}(s)ds$. Initial conditions are $v_{i_0} = 20\left(\frac{m}{s}\right)$, $i = 1, 2, 3, 4$, $v_{l_0} = 14.9\left(\frac{m}{s}\right)$; $s_{i_0} = h_{i,\text{des}} v_{i_0} = h_{i,\text{des}} \times 20\ m$, $i = 2, 3, 4$, $s_{1_0} = 22\ m$; and $u_{i0} \equiv 0$, for $i = 1, 2, 3, 4$.

Chapter 4

Numerical Investigation of Head-to-Tail String Stability and Performance of Predictor-Based ACC in a Mixed Traffic Scenario

We illustrate the performance of predictor-based adaptive cruise control (ACC) with integral action in a scenario of traffic consisting of both ACC-equipped and human-driven vehicles. We consider a linearized optimal velocity model (OVM) with input delay for human-driven vehicles, while for the ACC-equipped vehicle we consider linear, second-order dynamics with input delay. We demonstrate that a single ACC-equipped vehicle, located at the tail of the platoon, under the predictor-based ACC law, is capable of guaranteeing head-to-tail string stability, despite the presence of input delay and the string unstable behavior of the human-driven vehicles. We further analyze numerically the effect of the tuning parameters of the ACC law to three metrics quantifying performance in terms of fuel consumption, safety, and comfort, providing recommendations for their choice. The ACC law also guarantees individual vehicle stability and zero steady-state tracking errors, which is demonstrated in simulation, considering a platoon of four vehicles.

4.1 Chapter Organization

The outline of the chapter is as follows. Section 4.2 presents the model of mixed traffic platoons considered and the actuation delay-compensating predictor-based design with integral action. In Sections 4.3 and 4.4, we discuss stability, string stability, and head-to-

tail string stability of the platoon. In Section 4.5 we present numerical experiments for validation of the head-to-tail string stability guarantees. Simulation results along with numerical investigation of the performance of the platoon are presented in Section 4.6. In Section 4.7 we provide concluding remarks.

4.2 Predictor-Based ACC for Mixed Traffic

In this chapter, we consider the scenario of a heterogeneous platoon, as shown in Figure 4.1, in which the vehicles follow each other on a single line without overtaking. The traffic consists of human-driven vehicles and automated vehicles that are equipped with ACC system. The dynamics of the automated vehicles are governed by a linear, second-order model with delayed actuation, while the OVM is employed as a model for car-following dynamics of the human-driven vehicles. Automated vehicles can measure their own speed, as well as the relative speed and the spacing with respect to the preceding vehicle.

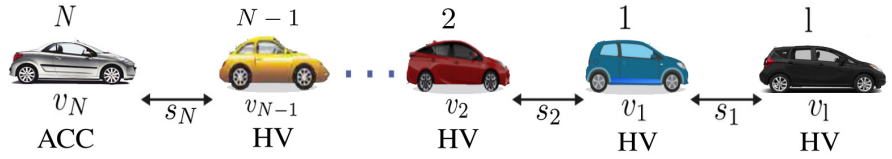

Figure 4.1: Platoon of $N + 1$ heterogeneous vehicles following each other on a single lane without overtaking. The platoon contains human-driven vehicles and an automated vehicle, equipped with an ACC system, at its tail.

4.2.1 Automated Vehicle Model and Nominal Delay-Free Control Design

Automated vehicle dynamics

The dynamics of the automated vehicle are modeled by the following second-order, linear system with actuator delay (see, e.g., [7], [20])

$$\dot{s}_N(t) = v_{N-1}(t) - v_N(t), \tag{4.1}$$

$$\dot{v}_N(t) = u_N(t - D), \tag{4.2}$$

where $s_N = x_{N-1} - x_N - l$ and x_N is the position of vehicle N, l is its length, v_N is vehicle speed, u_N is the individual vehicle's control variable, $D \geq 0$ is input delay, and $t \geq 0$ is time.

Nominal control design

Without input delay, the ACC laws with integral action are constructed as follows

$$u_N(t) = k_{1,N} s_N(t) + k_{2,N} \sigma_N(t) + k_{3,N} v_N(t), \tag{4.3}$$

$$\dot{\sigma}_N(t) = \frac{1}{h_N} s_N(t) - v_N(t), \tag{4.4}$$

where the control gains $k_{1,N}$, $k_{2,N}$, $k_{3,N}$ are yet to be chosen and $h_N > 0$ is desired time-headway.

4.2.2 Predictor-Based ACC Design with Actuator Delay

The predictor-based control laws with actuation delay compensation for system (4.1), (4.2) are given by

$$u_N(t) = k_{1,N} q_{1,N} + k_{2,N} q_{2,N} + k_{3,N} q_{3,N}, \tag{4.5}$$

$$q_N(t) = \mathrm{e}^{\Gamma_N D} x_N(t) + \int_{t-D}^{t} \mathrm{e}^{\Gamma_N (t-\theta)} B_N u_N(\theta) d\theta, \tag{4.6}$$

where

$$\Gamma_N = \begin{bmatrix} 0 & 0 & -1 \\ \frac{1}{h_N} & 0 & -1 \\ 0 & 0 & 0 \end{bmatrix}, x_N = \begin{bmatrix} s_N & \sigma_N & v_N \end{bmatrix}^{\mathrm{T}}, \tag{4.7}$$

$$B_N = \begin{bmatrix} 0 & 0 & 1 \end{bmatrix}^{\mathrm{T}}, q_N = \begin{bmatrix} q_{1,N} & q_{2,N} & q_{3,N} \end{bmatrix}^{T}. \tag{4.8}$$

One should notice that the control law (4.5) is suitable for autonomous operation since it employs only measurements of the current spacing s_N and speed v_N, as well as of the past D-second history of the control variable u_N, which are available to vehicle N using on-board sensors.

4.2.3 Human-Driven Vehicle Model

Here, we consider the linearized OVM for vehicles following human behavior (see, e.g., [20], [31])

$$\dot{s}_i(t) = v_{i-1}(t) - v_i(t), \tag{4.9}$$

$$\dot{v}_i(t) = u_i(t - D_h), \tag{4.10}$$

where

$$u_i(t) = \alpha_i \left(\frac{s_i(t)}{h_i} - v_i(t) \right) + b_i(v_{i-1}(t) - v_i(t)), \tag{4.11}$$

such that $\alpha_i > 0$, $b_i > 0$, and $D_h \geq 0$. Note the two feedback actions of human behavior in (4.11), namely a proportional action depending on the spacing error and a derivative action depending on the relative velocity. In addition, D_h represents time delay that encompasses the actuation delay of the vehicle's dynamics and the driver's reaction time.

4.3 Head-to-Tail String Stability of Mixed Traffic

In this section, we study the head-to-tail string stability of the platoon shown in Figure 4.1. The analysis is performed in the Laplace domain, deriving a transfer function associated with the responses of each vehicle of the platoon, starting from the leader, all the way through the ACC vehicle, see, e.g., [19]. With the transfer function $G_{i,i-1} = \frac{V_i}{V_{i-1}}$, we relate the speed errors of vehicle i and $i-1$. The transfer function between human-driven vehicle i and preceding human-driven vehicle $i-1$ is given by

$$G_{i,i-1}(s) = \frac{\left(b_i s + \frac{\alpha_i}{h_i}\right) \mathrm{e}^{-D_h s}}{s^2 + \left((\alpha_i + b_i)s + \frac{\alpha_i}{h_i}\right) \mathrm{e}^{-D_h s}}. \tag{4.12}$$

The transfer function between automated vehicle N and preceding human-driven vehicle $N-1$ is given by

$$G_{N,N-1}(s) = \frac{\left(\left(D + \frac{h_N k_{1,N}}{k_{2,N}}\right) s + 1\right) \mathrm{e}^{-sD}}{\frac{h_N}{k_{2,N}} s^3 - \frac{h_N k_{3,N}}{k_{2,N}} s^2 + \frac{h_N \left(k_{1,N} + k_{2,N}\right)}{k_{2,N}} s + 1}. \tag{4.13}$$

In that context, the overall speed response of the platoon from vehicle l to vehicle N gives the head-to-tail transfer function G_N as

$$G_N(s) = \prod_{i=1}^{N} G_{i,i-1}(s). \tag{4.14}$$

Transfer functions (4.12) and (4.13) are derived as follows. Taking Laplace transform of i-th vehicle's model (4.9), (4.10) we obtain

$$\begin{bmatrix} S_i(s) \\ V_i(s) \end{bmatrix} = \begin{bmatrix} -\frac{1}{s^2} \\ \frac{1}{s} \end{bmatrix} \mathrm{e}^{-sD_h} U_i(s) + \begin{bmatrix} \frac{1}{s} \\ 0 \end{bmatrix} V_{i-1}(s). \tag{4.15}$$

Using (4.11) we arrive at

$$U_i(s) = \alpha_i \left(\frac{S_i(s)}{h_i} - V_i(s) \right) + b_i(V_{i-1}(s) - V_i(s)). \tag{4.16}$$

Hence, substituting (4.16) in (4.15) we derive $\frac{V_i}{V_{i-1}}$, which gives (4.12). Furthermore, taking Laplace transform of the predictor states (4.6) we get

$$Q_N(s) = \mathrm{e}^{\Gamma_N D} X_N(s) + M_N(s) U_N(s), \tag{4.17}$$

where

$$M_N(s) = (sI_{3\times 3} - \Gamma_N)^{-1} \left(I_{3\times 3} - \mathrm{e}^{\Gamma_N D} \mathrm{e}^{-sD} \right) B_N. \tag{4.18}$$

Using (4.7), (4.8), and (4.18), we get

$$M_N(s) = \begin{bmatrix} M_{11,N}(s) & M_{21,N}(s) & M_{31,N}(s) \end{bmatrix}^{\mathrm{T}}, \tag{4.19}$$

where

$$M_{11,N}(s) = \frac{\left(\mathrm{e}^{-sD} - 1 \right)}{s^2} + \frac{D\mathrm{e}^{-sD}}{s}, \tag{4.20}$$

$$M_{21,N}(s) = \frac{(\mathrm{e}^{-sD} - 1)(h_N s + 1)}{h_N s^3} + \frac{D\mathrm{e}^{-sD}}{h_N s^2} + \frac{D\mathrm{e}^{-sD}(D + 2h_N)}{2h_N s}, \tag{4.21}$$

$$M_{31,N}(s) = -\frac{\mathrm{e}^{-Ds} - 1}{s}. \tag{4.22}$$

Using control laws (4.5), together with (4.17)–(4.22), we get

$$U_N(s) = \left(k_{1,N} + \frac{k_{2,N}}{h_N s} + \frac{k_{2,N} D}{h_N}\right) S_N(s) - \left(k_{1,N} D + \frac{k_{2,N}}{s} + \frac{k_{2,N} D(D + 2h_N)}{2h_N} - k_{3,N}\right) \times V_N(s) + g_N(s) U_N(s), \tag{4.23}$$

where

$$g_N(s) = k_{1,N} M_{11,N}(s) + k_{2,N} M_{21,N}(s) + k_{3,N} M_{31,N}(s). \tag{4.24}$$

Hence, using (4.1), (4.2), and (4.23) we arrive at (4.13).

4.4 Stability and String Stability

4.4.1 Automated Vehicles

Stability: From (4.13), we can derive that there exists choice of control parameters $k_{1,N}$, $k_{2,N}$, $k_{3,N}$ that leads to asymptotic stability. One can see this by matching the denominator of (4.13) with any desired third-order polynomial of the form $(T_{1,N}s + 1)(T_{2,N}s + 1)(T_{3,N}s + 1)$, where $T_{1,N} \geq T_{2,N} \geq T_{3,N} > 0$. The parameters $k_{1,N}$, $k_{2,N}$, $k_{3,N}$ can be chosen as

$$k_{1,N} = \frac{T_{1,N} + T_{2,N} + T_{3,N} - h_N}{T_{1,N} T_{2,N} T_{3,N}}, \tag{4.25}$$

$$k_{2,N} = \frac{h_N}{T_{1,N} T_{2,N} T_{3,N}}, \tag{4.26}$$

$$k_{3,N} = -\frac{T_{1,N} T_{2,N} + T_{1,N} T_{3,N} + T_{2,N} T_{3,N}}{T_{1,N} T_{2,N} T_{3,N}}. \tag{4.27}$$

String stability: String stability, with respect to transfer function (4.13), in $\mathcal{L}_p$, $p \in [1, +\infty]$, is established by properly selecting the parameters $T_{1,N}$, $T_{2,N}$, $T_{3,N}$. As inferred from [7], the validity of string stability is confirmed when the following conditions hold

$$D - h_N + T_{2,N} + T_{3,N} \leq 0, \tag{4.28}$$

$$D - h_N + T_{1,N} + T_{3,N} \geq 0. \tag{4.29}$$

Conditions (4.28), (4.29) can be satisfied by an appropriate choice of $T_{1,N} \geq T_{2,N} \geq T_{3,N} > 0$ when $D < h_N$. Note that string stability with respect to (4.13), is a necessary condition for head-to-tail string stability.

4.4.2 Human-Driven Vehicles

Stability: For transfer function (4.12) we choose the human behavior parameters as $\alpha_i = 0.12h_i$, $b_i = 0.4$, $h_i = 5/3$ (see, e.g., [31]) and $D_h = 0.8$ (see, e.g., [20]), which ensures stability of (4.12) [19].

String stability: For string stability a worst-case scenario is considered (see Figure 4.2), in the sense that each human-driven vehicle behaves in a string unstable manner and amplifies speed perturbations. In particular, $|G_{i,i-1}(j\omega)| > 1$, at some $\omega_1 > 0$, with maximum $|G_{i,i-1}(j\omega_1)| \approx 1.048$, for all i.

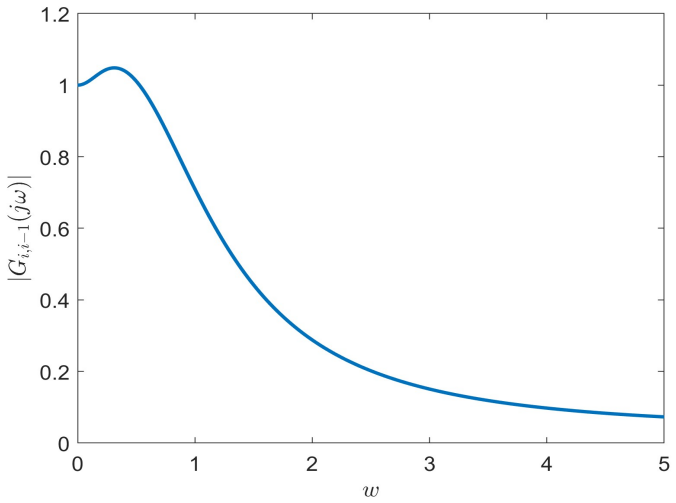

Figure 4.2: The norm $|G_{i,i-1}(j\omega)|$ of (4.12), which shows each human-driven vehicle string unstable behavior.

4.5 Numerical Investigation of Head-To-Tail String Stability

In this section, we numerically analyze the head-to-tail string stability properties of the closed-loop systems, using (4.14). We consider a mixed traffic platoon with one automated vehicle, as the last vehicle in the platoon, and three homogeneous human-driven vehicles, to make the numerical example more clear without distracting the reader with definitions of various numerical parameters. For the three human-driven vehicles with second-order dynamics given by (4.9)–(4.11), we consider the parameters that are described in Section 4.4.2; for the automated vehicle with second-order dynamics given by (4.1), (4.2),

under (4.5), (4.6) we consider a case in which $D = 0.4$, $h_3 = 4/3$. To numerically analyze the head-to-tail string stability properties of the closed-loop system, we illustrate the impact of the control parameters $T_{1,N}$, $T_{2,N}$, $T_{3,N}$. In the top plot of Figure 4.3, we show the values of $\sup_\omega |G_N(j\omega)|$, defined in (4.14), as a function of $0.2 \geq T_{2,N} > 0$ and $8 \geq T_{1,N} > 3$, with fixed $T_{3,N} = 0.1$. These choices are made to simplify the initial selec-

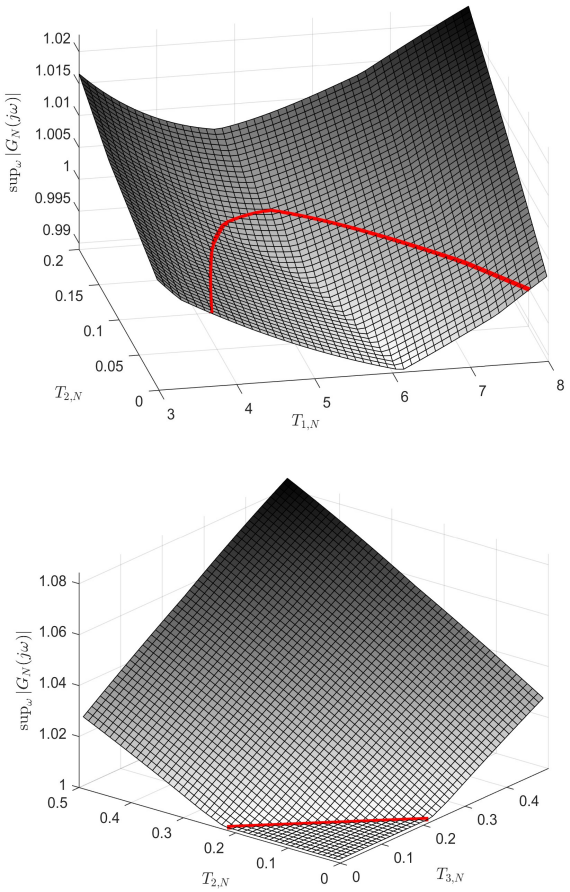

Figure 4.3: The values of function $\sup_\omega |G_N(j\omega)|$ corresponding to transfer function (4.14). Top: $\sup_\omega |G(j\omega)|$ as a function of $T_{2,N}$ and $T_{1,N}$, with fixed $T_{3,N} = 0.1$. Bottom: $\sup_\omega |G(j\omega)|$ as a function of $T_{3,N}$ and $T_{2,N}$, with fixed $T_{1,N} = 5$.

tion of control parameters, ensuring the satisfaction of (4.28), (4.29). The red line shows the distinction between head-to-tail string stability and instability. In the same manner, the bottom plot shows $\sup_\omega |G_N(j\omega)|$ as function of $0.5 \geq T_{3,N} > 0$, and $0.5 \geq T_{2,N} > 0$, with fixed $T_{1,N} = 5$, which corresponds to a value of $T_{1,N}$ that allows for larger variations of $T_{2,N}$, without violating head-to-tail string stability. Note that in the mentioned case, due to the homogeneity of the human-driven vehicles, increasing or decreasing the

number of human-driven vehicles deteriorates or improves head-to-tail string stability, respectively, which is consistent with the findings in [20].

4.6 Simulation and Optimal Choice of Controller Parameters

This section demonstrates numerically the performance of predictor-based ACC with integral action (4.5), in the scenario of mixed platoon of Section 4.5. We consider a case with human-driven parameters as in Section 4.4.2, along with the range of automated vehicle parameters indicated in Section 4.5. In the simulation investigation, we consider the initial conditions such that the platoon, apart from the leader, operates at equilibrium. That is, we consider a scenario in which $u_N(s) = 0$, $s \in [-D, 0]$, for the automated vehicle and $u_i(s) = 0$, $s \in [-D_{\rm h}, 0]$, $i = 1, 2, 3$, for the human-driven vehicles. In particular, we set $\sigma_{3_0} = -\frac{-v_N k_{2,N} D^2 - 2k_{1,N} D s_N + 2k_{1,N} s_N h_N + 2k_{3,N} s_N}{2h_N k_{2,N}}$ (so that $u_N(0) = 0$), $v_{i_0} = 21(\frac{m}{s})$ for $i = 1, 2, 3$ and $v_{l_0} = 18(\frac{m}{s})$; $s_{i_0} = h_i v_{i_0} = \frac{5}{3} \times 21\ (m)$ for $i = 1, 2$ and $s_N = \frac{4}{3} \times 21\ (m)$. Furthermore, $v_{\rm l}$ is computed from the model $\dot{v}_{\rm l}(t) = a_{\rm l}(t)$, $t \geq 0$, where $a_{\rm l}$ represents the acceleration of the leader, acting as exogenous input. The leading vehicle performs both deceleration at ($t = 20\ s$) and acceleration at ($t = 50\ s$) maneuvers. Subsequently, for the purposes of selecting control parameters $T_{1,N}$, $T_{2,N}$, $T_{3,N}$ and of performance evaluation we consider the following three practical indices (see, e.g., [2], [34], [51])
a) fuel consumption:

$$J_{\rm fuel} = \sum_{i=1}^{3} \int_0^T J_i \left(v_i(t), a_i(t) \right) \, dt, \tag{4.30}$$

$$J_i = \begin{cases} \beta_1 + \beta_2 R_{T_i} \left(v_i(t), a_i(t) \right) v_i(t) & \\ +\beta_3 v_i(t) a_i^2(t), & \text{if} \quad R_{T_i} > 0 \\ \beta_1, & \text{if} \quad R_{T_i} \leq 0, \end{cases} \tag{4.31}$$

$$R_{T_i} = \beta_4 + \beta_5 v_i^2(t) + \beta_6 a_i(t), \tag{4.32}$$

b) safety:

$$J_{\rm safety} = \sum_{i=1}^{3} \int_0^T \bar{J}_i \left(s_i(t), v_i(t), v_{i-1}(t) \right) \, dt, \tag{4.33}$$

$$\bar{J}_i = \begin{cases} \frac{2}{s_i(t)} \left(v_{i-1}(t) - v_i(t) \right)^2, & \text{if} \quad v_{i-1}(t) \leq v_i(t) \\ 0, & \text{otherwise} \end{cases}, \tag{4.34}$$

c) comfort:

$$J_{\text{comfort}} = \sum_{i=1}^{3} \int_0^T \dot{a}_i(t)^2 \, dt. \tag{4.35}$$

In this context, we set $T = 100$ s, and the parameters of (4.30)–(4.34) are shown in Table 4.1. Note that changing the values of control parameters only affects the defined costs for the ACC vehicle. For the human-driven vehicles, these changes do not have any effect on their costs. Therefore, the ACC vehicle costs determine the characteristics of the whole platoon costs.

Table 4.1: Parameters of Fuel Consumption and Safety Indices (4.30)–(4.34)

Parameter	β_1	β_2	β_3	β_4	β_5	β_6
Value	0.666	0.0717	0.0578	0.527	0.000948	1.68

In order to minimize the fuel consumption, safety, and comfort metrics of the platoon, we employ a numerical approach. More specifically, an exhaustive search is utilized to identify the optimal values of the control design parameters $k_{1,N}$, $k_{2,N}$, and $k_{3,N}$. In this direction, Figure 4.4 shows the three metrics as a function of $3 < T_{1,N} \leq 8$ and $0 < T_{2,N} \leq 0.2$, while keeping $T_{3,N}$ fixed at 0.1, i.e., within the specific ranges corresponding to the top plot of Figure 4.3, since our objective is to ensure head-to-tail string stability, while improving performance. Note that among control parameters, $T_{1,N}$ is the parameter corresponding to the dominant pole of (4.13). Consequently, changes in the value of $T_{1,N}$ have a significant impact on system performance. The top plot of Figure 4.4 illustrates that the optimal fuel consumption cost is observed when $T_{1,N}$ and $T_{2,N}$ are minimized, within the allowable range that guarantees head-to-tail string stability. Furthermore, the top plot of Figure 4.4 shows that increasing $T_{1,N}$ deteriorates fuel consumption. This observation is consistent with the fact that increasing $T_{1,N}$ leads to a decrease in rise time, corresponding to the transfer function (4.13) and parameters (4.30)–(4.35), which implies more aggressive response. The middle plot of Figure 4.4 indicates that the optimal value for safety cost is attained when $T_{1,N}$ is at its maximum value. This result is consistent with the observation that increasing $T_{1,N}$ reduces rise time, which implies that the automated vehicle can react more quickly to maneuvers of the preceding vehicle. The bottom plot of Figure 4.4 demonstrates the trade-off between improved comfort (for small $T_{1,N}$) and improved safety (for large $T_{1,N}$).

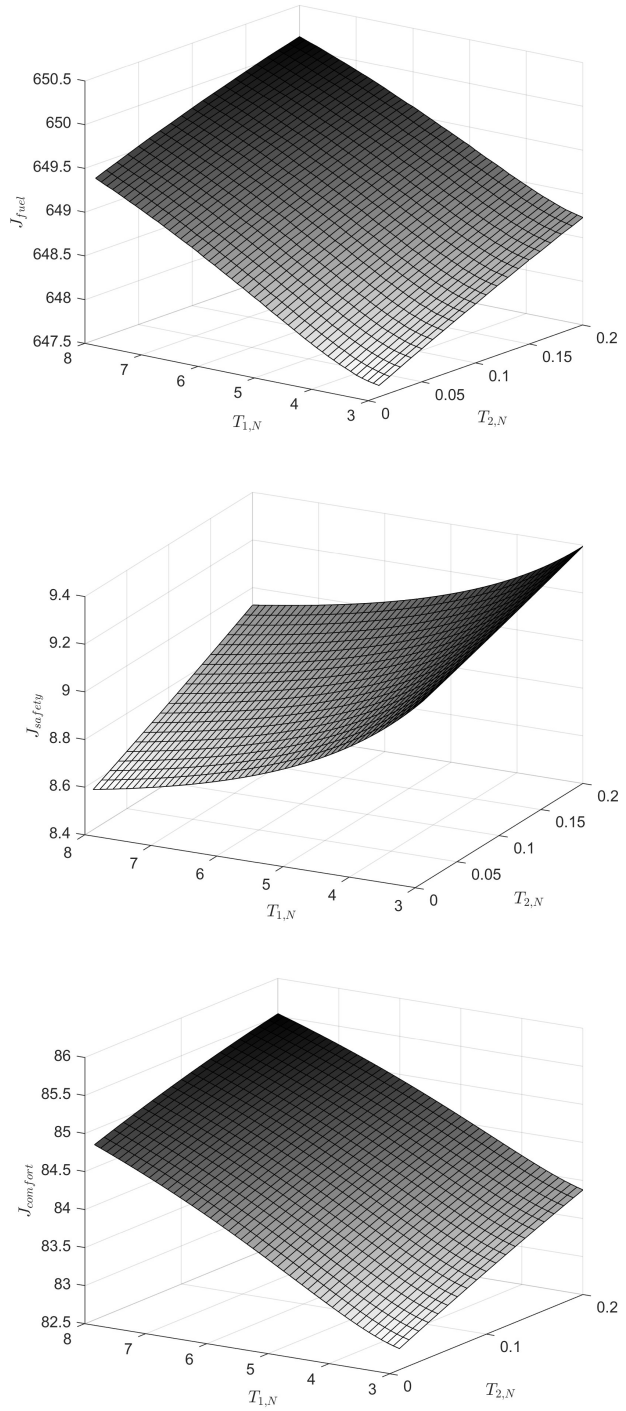

Figure 4.4: The values of the three metrics (4.30), (4.33), and (4.35) as function of $3 \leq T_{1,N} \leq 8$ and $0 < T_{2,N} \leq 0.2$, while keeping $T_{3,N}$ fixed at 0.1. Top: Fuel consumption cost. Middle: Safety cost. Bottom: Comfort cost.

In order to have optimal/allowable choice based on Figure 4.3 and Figure 4.4 we set $T_{1,N} = 5.2$, $T_{2,N} = 0.1$, and $T_{3,N} = 0.1$. We choose the middle value for $T_{1,N}$ within the allowable range (see Figure 4.3) to effectively balance all associated costs. Figure 4.5 illustrates that the selected control parameters for the tail vehicle equipped with an ACC system maintains head-to-tail string stability. However, three human-driven vehicles exhibit string unstable behavior within the platoon.

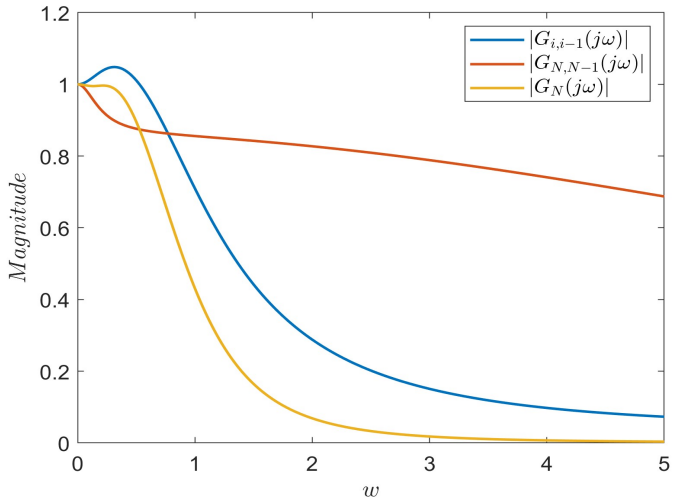

Figure 4.5: Norms $|G_{i,i-1}(j\omega)|$ of (4.12), $|G_{N,N-1}(j\omega)|$ of (4.13), and $|G_N(j\omega)|$ of (4.14).

In Figure 4.6 we show the respective responses of vehicles 1 and 2, which are string unstable (see Figure 4.2), together with the response of vehicle 3, equipped with an ACC system, which maintains string stability. The respective response from the leader to the ACC vehicle exhibits overshoot, although $\mathcal{L}_2$ head-to-tail string stability is preserved (see Figure 4.5).

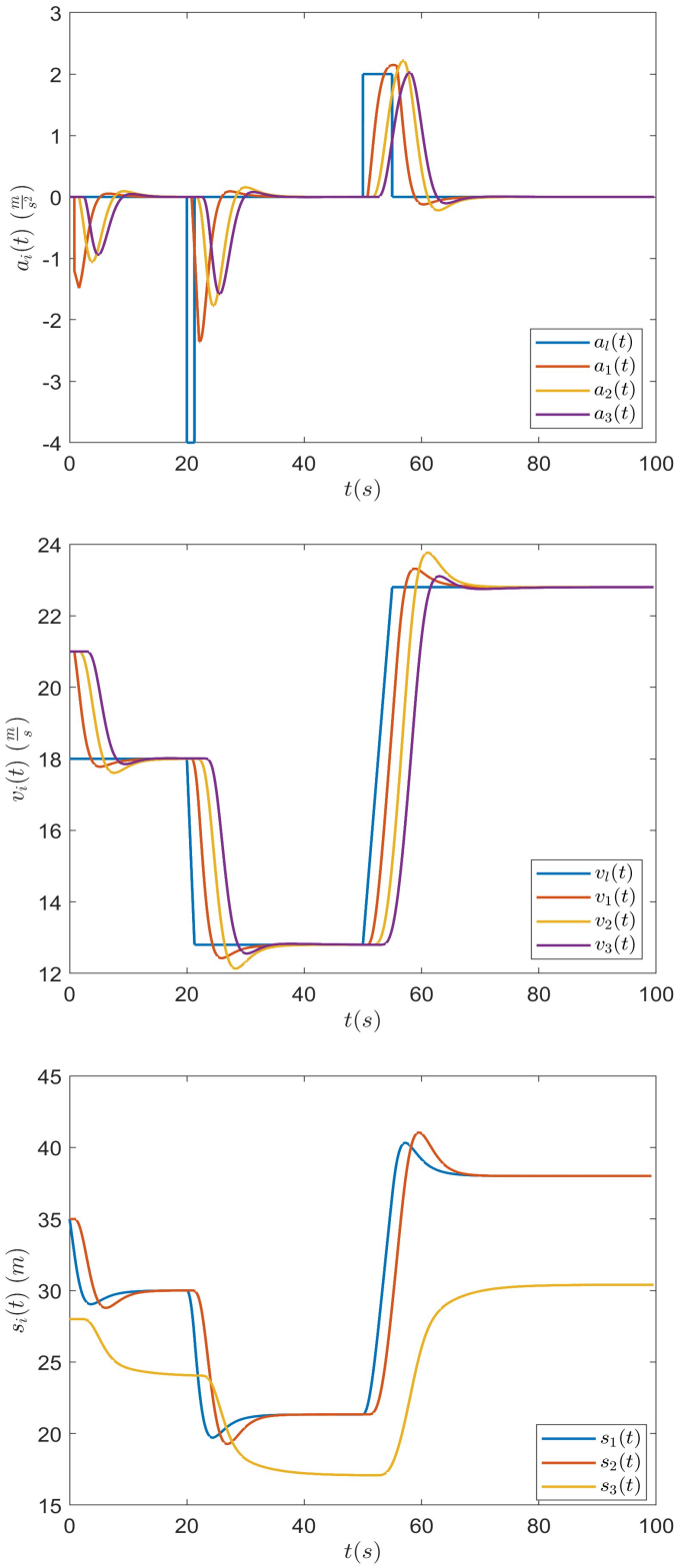

Figure 4.6: Acceleration (top), speed (middle), and spacing (bottom) of three vehicles, following a leader that performs a deceleration/acceleration maneuver. Vehicles 1 and 2 are human-driven, while vehicle 3 is equipped with ACC. The initial conditions and model/controller parameters are given in Sections 4.4–4.6.

4.7 Chapter Conclusions and Related Publications

In the present chapter, we demonstrated the performance of predictor-based ACC in a mixed traffic scenario consisting of both ACC-equipped and human-driven vehicles. We considered a linearized OVM with input delay for human-driven vehicles, while for the ACC-equipped vehicle we considered linear, second-order dynamics with input delay. We numerically showed that a single ACC-equipped vehicle located at the tail of the platoon is able to guarantee head-to-tail string stability even in the presence of string unstable human-driven vehicles. We also presented thorough numerical analysis of the impact of the tuning parameters of the ACC law on three metrics quantifying performance in terms of fuel consumption, safety, and comfort. Moreover, simulation results, considering a platoon of four vehicles, utilized to validate both head-to-tail string stability and an efficient choice provided for the controller's parameters.

This chapter is an adaptation of material appearing in

A. Samii, P. Karafotis, and N. Bekiaris-Liberis, "Numerical investigation of head-to-tail string stability and performance of predictor-based ACC in a mixed traffic scenario," *Mediterranean Conference on Control and Automation*, Chania, Greece, 2024.

Chapter 5

Predictor-Based CACC Design for Heterogeneous Vehicles with Distinct Input Delays

We develop a predictor-based cooperative adaptive cruise control (CACC) design for platoons with heterogeneous vehicles, whose dynamics are described by a third-order linear system subject to actuators delays, which are *distinct* for each individual vehicle. The design achieves individual vehicle stability, string stability, and zero, steady-state speed/spacing tracking errors, relying on a nominal, constant time headway (CTH)-type CACC design that achieves these specifications when all actuators' delays are zero. This is achieved owing to the delay-compensating mechanism, of the CACC law introduced, for long delays and despite the fact that each vehicle's dynamics are subject to different input delays, which makes the available predictor-feedback CACC designs inapplicable. The proofs of individual vehicle stability, string stability, and regulation rely on employment of an input-output approach on the frequency domain. We present consistent simulation results, including an example in which we employ real traffic data for the trajectory of the leading vehicle and an example via which we compare the performance of our design with the existing, predictor-feedback CACC and predictor-based ACC laws. In addition, we study numerically the robustness properties with respect to string stability of our predictor-based CACC design to (uncertain) communication delays. Thus, our numerical results validate the performance of the design in realistic scenarios and as compared with related, existing control laws.

5.1 Chapter Organization

The outline of the chapter is as follows. Section 5.2 presents the model of heterogeneous platoons considered and the actuation delay-compensating predictor-based design. In Section 5.3, we state our main result, which is vehicle stability and string stability under the CACC law developed. In Section 5.4 we present numerical results for validation of the theoretical guarantees. Simulation results are presented in Section 5.5, including an example with real traffic data and comparisons with related, existing control laws. In Section 5.6 we study robustness of string stability of our predictor-based CACC design to communication delays, and in Section 5.7 we provide concluding remarks.

5.2 Predictor-Based CACC for Heterogeneous Platoons with Distinct Actuator Delays

5.2.1 Vehicle Model and Nominal Delay-Free Design

a) Vehicle dynamics: We consider a heterogeneous string of vehicles (see Figure 5.1) each one modeled by the following third-order, linear system with distinct actuator delays that describes vehicle dynamics (see, e.g., [44], [57], [58])

$$\dot{s}_i(t) = v_{i-1}(t) - v_i(t), \tag{5.1}$$

$$\dot{v}_i(t) = a_i(t), \tag{5.2}$$

$$\dot{a}_i(t) = -\frac{1}{\tau_i}a_i(t) + \frac{1}{\tau_i}u_i(t - D_i), \tag{5.3}$$

where $D_i \geq 0$, $i = 1, ..., N$, are input delays, and $t \geq 0$ is time.

b) Available measurements: For the platoons considered here the measurements available to the ego vehicle i are its own spacing s_i, speed v_i, acceleration a_i, and control input u_i, as well as the speed of the preceding vehicle v_{i-1}. It is possible to obtain this information through on-board sensors. Furthermore, the control input of the preceding vehicle, as well as its acceleration and speed (typically not required) are also available and are denoted by u_{i-1}, a_{i-1}, and v_{i-1} respectively. These measurements are transmitted from the preceding vehicle, through V2V communication, see, e.g., [30, 47, 56].

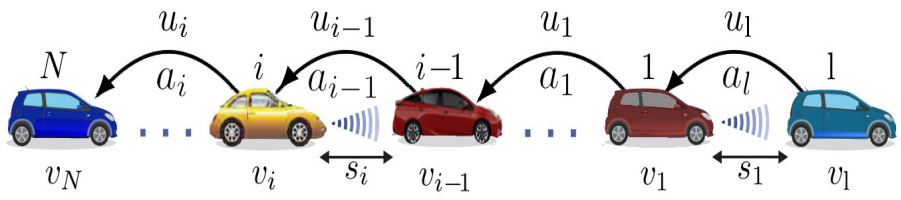

Figure 5.1: Platoon of $N+1$ heterogeneous vehicles following each other in a single lane without overtaking. The dynamics of each vehicle $i = 1, ..., N$ are governed by system (5.1)–(5.3). Each vehicle can measure its own speed, the relative speed with the preceding vehicle, and the spacing with respect to the preceding vehicle. The control input and acceleration of each vehicle is communicated to the following vehicle via V2V communication.

c) Nominal control design: Without input delay, the following control strategy is constructed (see, e.g., [1, 11])

$$u_i(t) = \tau_i \alpha_i \left(\frac{s_i(t)}{h_i} - v_i(t) \right) + \tau_i b_i (v_{i-1}(t) - v_i(t)) + \tau_i c_i \left(a_{i-1}(t) - a_i(t) \right), \tag{5.4}$$

where $\alpha_i > 0$, $b_i > 0$, and $c_i > 0$ are design parameters, and $h_i > 0$ is time-headway.

5.2.2 Predictor-Based Control Design for Compensation of Distinct Actuation Delays

The predictor-based control laws for system (5.1)–(5.3) are given by

$$u_i(t) = \frac{\tau_i \alpha_i}{h_i} q_{i,1}(t) - \tau_i(\alpha_i + b_i) q_{i,2}(t) + \tau_i b_i q_{i,3}(t) + \tau_i c_i \left(q_{i,5}(t) - q_{i,4}(t) \right), \tag{5.5}$$

$$q_i(t) = \mathrm{e}^{\Gamma_i D_i} \bar{x}_i(t) + \int_{t-D_i}^{t} \mathrm{e}^{\Gamma_i (t-\theta)} B_i u_i(\theta)\, d\theta + \int_{t-D_{i-1}}^{t} \mathrm{e}^{\Gamma_i (t+D_i-\theta-D_{i-1})} B_{1i} u_{i-1}(\theta)\, d\theta, \tag{5.6}$$

where

$$q_i = \begin{bmatrix} q_{i,1} & q_{i,2} & q_{i,3} & q_{i,4} & q_{i,5} \end{bmatrix}^{\mathrm{T}}, \quad \bar{x}_i = \begin{bmatrix} s_i & v_i & v_{i-1} & a_i & a_{i-1} \end{bmatrix}^{\mathrm{T}}, \tag{5.7}$$

$$B_i = \begin{bmatrix} 0 & 0 & 0 & \frac{1}{\tau_i} & 0 \end{bmatrix}^{\mathrm{T}}, B_{1i} = \begin{bmatrix} 0 & 0 & 0 & 0 & \frac{1}{\tau_{i-1}} \end{bmatrix}^{\mathrm{T}}, \tag{5.8}$$

$$\Gamma_i = \begin{bmatrix} 0 & -1 & 1 & 0 & 0 \\ 0 & 0 & 0 & 1 & 0 \\ 0 & 0 & 0 & 0 & 1 \\ 0 & 0 & 0 & -\frac{1}{\tau_i} & 0 \\ 0 & 0 & 0 & 0 & -\frac{1}{\tau_{i-1}} \end{bmatrix}. \tag{5.9}$$

The feedback law (5.5) is the predictor-based version of (5.4), which relies on the design for general linear systems from [53] (see also [3]).

5.3 String Stability Despite Distinct Actuation Delays

To state our main result we need to first define the following functions

$$\begin{aligned}\beta_i =& \left(c_i + \frac{1}{\tau_i}\right)^2 - 2(\alpha_i + b_i) - \left(\frac{\alpha_i}{h_i}\tau_{i-1}\left(D_i - D_{i-1}\right) + b_i\tau_{i-1} - \frac{\alpha_i}{h_i}\tau_{i-1}^2\right. \\ &\left. + \mathrm{e}^{-\frac{(D_i - D_{i-1})}{\tau_{i-1}}}\left(\frac{\alpha_i}{h_i}\tau_{i-1}^2 - b_i\tau_{i-1} + c_i\right)\right)^2, \end{aligned} \tag{5.10}$$

$$\begin{aligned}\gamma_i =& (\alpha_i + b_i)^2 - \left(\left(D_i - D_{i-1}\right)\frac{\alpha_i}{h_i} + b_i\right)^2 - \frac{2\alpha_i}{h_i}\left(\frac{1}{\tau_i} + c_i - \left(\frac{\alpha_i}{h_i}\tau_{i-1}\left(D_i - D_{i-1}\right)\right.\right. \\ &\left.\left. + b_i\tau_{i-1} - \frac{\alpha_i}{h_i}\tau_{i-1}^2 + \mathrm{e}^{-\frac{(D_i - D_{i-1})}{\tau_{i-1}}}\left(\frac{\alpha_i}{h_i}\tau_{i-1}^2 - b_i\tau_{i-1} + c_i\right)\right)\right). \end{aligned} \tag{5.11}$$

Theorem 5.1: Consider a platoon of vehicles with heterogeneous dynamics modeled by (5.1)–(5.3), under control laws (5.5) with (5.6)–(5.9). For any $D_i \geq 0$, $i = 1, ..., N$, the platoon is $\mathcal{L}_2$ string stable with respect to speed errors propagation provided that the following conditions hold for $i = 1, ..., N$:

$$\frac{1}{\tau_i} + c_i > 0, \tag{5.12}$$

$$\left(\frac{1}{\tau_i} + c_i\right)(\alpha_i + b_i) - \frac{\alpha_i}{h_i} > 0, \tag{5.13}$$

along with

$$4\gamma_i - \beta_i^2 > 0, \tag{5.14}$$

or

$$4\gamma_i - \beta_i^2 \leq 0, \tag{5.15}$$

with

$$\beta_i \geq 0 \quad \text{and} \quad \gamma_i \geq 0. \tag{5.16}$$

Furthermore, for a constant leading vehicle's speed, zero, steady-state, spacing and speed tracking errors are achieved.

Remark 5.1: The first two conditions of Theorem 5.1 come from the Routh-Hurwitz criterion and they are a prerequisite for string stability of the platoon. While the remaining two conditions are derived from the string stability criterion with respect to speed errors propagation.

Proof of Theorem 5.1: In order to study stability and string stability of speed errors propagation, we first compute the transfer functions

$$G_i(s) = \frac{V_i(s)}{V_{i-1}(s)}, \quad i = 1, ..., N, \tag{5.17}$$

viewing as input the preceding vehicle's speed and as output the current vehicle's speed. Taking Laplace transform of the predictor states (5.6) we get

$$Q_i(s) = \mathrm{e}^{\Gamma_i D_i}\bar{X}_i(s) + M_{1,i}(s)U_i(s) + M_{2,i}(s)U_{i-1}(s), \tag{5.18}$$

where

$$M_{1,i}(s) = (sI_{5\times5} - \Gamma_i)^{-1}\left(I_{5\times5} - \mathrm{e}^{\Gamma_i D_i}\mathrm{e}^{-sD_i}\right)B_i, \tag{5.19}$$

$$M_{2,i}(s) = (sI_{5\times5} - \Gamma_i)^{-1}\left(I_{5\times5} - \mathrm{e}^{\Gamma_i D_{i-1}}\mathrm{e}^{-sD_{i-1}}\right)\mathrm{e}^{\Gamma_i(D_i - D_{i-1})}B_{1i}. \tag{5.20}$$

Using (5.8), (5.9), (5.19), and (5.20) we get

$$(sI_{5\times5} - \Gamma_i)^{-1} = \frac{1}{s^2}\begin{bmatrix} s & -1 & 1 & -\frac{\tau_i}{s\tau_i+1} & -\frac{\tau_{i-1}}{s\tau_{i-1}+1} \\ 0 & s & 0 & \frac{s\tau_i}{s\tau_i+1} & 0 \\ 0 & 0 & s & 0 & \frac{s\tau_{i-1}}{s\tau_{i-1}+1} \\ 0 & 0 & 0 & \frac{s^2\tau_i}{s\tau_i+1} & 0 \\ 0 & 0 & 0 & 0 & \frac{s^2\tau_{i-1}}{s\tau_{i-1}+1} \end{bmatrix}, \tag{5.21}$$

and

$$M_{1,i}(s) = \begin{bmatrix} M_{11,i}(s) & M_{21,i}(s) & 0 & M_{41,i}(s) & 0 \end{bmatrix}^{\mathrm{T}}, \tag{5.22}$$

$$M_{2,i}(s) = \begin{bmatrix} m_{11,i}(s) & 0 & m_{31,i}(s) & 0 & m_{51,i}(s) \end{bmatrix}^{\mathrm{T}}, \tag{5.23}$$

where

$$M_{11,i}(s) = \frac{\mathrm{e}^{-sD_i}\left(\tau_i - \tau_i e^{\frac{-D_i}{\tau_i}}\right)}{s^2\tau_i} + \frac{\mathrm{e}^{-sD_i}\left(\tau_i^2 \mathrm{e}^{\frac{-D_i}{\tau_i}} + D_i\tau_i - \tau_i^2\right)}{s\tau_i} + \frac{\tau_i\left(\mathrm{e}^{-\frac{D_i}{\tau_i}}\mathrm{e}^{-sD_i} - 1\right)}{s^2\tau_i(s\tau_i+1)}, \tag{5.24}$$

$$M_{21,i}(s) = -\frac{\mathrm{e}^{-sD_i}(\tau_i - \tau_i \mathrm{e}^{\frac{-D_i}{\tau_i}})}{s\tau_i} - \frac{\tau_i\left(\mathrm{e}^{\frac{-D_i}{\tau_i}}\mathrm{e}^{-sD_i} - 1\right)}{s\tau_i(s\tau_i+1)}, \tag{5.25}$$

$$M_{41,i}(s) = -\frac{\mathrm{e}^{\frac{-D_i}{\tau_i}}\mathrm{e}^{-sD_i} - 1}{s\tau_i + 1}, \tag{5.26}$$

$$\begin{aligned} m_{11,i}(s) = &-\left(\frac{\mathrm{e}^{-sD_{i-1}} - 1}{s^2\tau_{i-1}} + \frac{D_{i-1}\mathrm{e}^{-sD_{i-1}}}{s\tau_{i-1}}\right) s\left(\tau_{i-1} - \tau_{i-1}\mathrm{e}^{\frac{-(D_i - D_{i-1})}{\tau_{i-1}}}\right) - \mathrm{e}^{\frac{-(D_i-D_{i-1})}{\tau_{i-1}}} \\ &\times \left(\frac{\mathrm{e}^{-sD_{i-1}}\left(\tau_{i-1} - \tau_{i-1}\mathrm{e}^{\frac{-D_{i-1}}{\tau_{i-1}}}\right)}{s^2\tau_{i-1}} + \frac{\mathrm{e}^{-sD_{i-1}}\left(\tau_{i-1}^2\mathrm{e}^{\frac{-D_{i-1}}{\tau_{i-1}}} + D_{i-1}\tau_{i-1} - \tau_{i-1}^2\right)}{s\tau_{i-1}}\right. \\ &\left. + \frac{\tau_{i-1}\left(\mathrm{e}^{-sD_{i-1}}\mathrm{e}^{-\frac{D_{i-1}}{\tau_{i-1}}} - 1\right)}{s^2\left(s\tau_{i-1}+1\right)}\right) - \frac{\left(\mathrm{e}^{-sD_{i-1}} - 1\right)}{s\tau_{i-1}} \\ &\times \left(\tau_{i-1}^2\mathrm{e}^{\frac{-(D_i-D_{i-1})}{\tau_{i-1}}} + D_i\tau_{i-1} - D_{i-1}\tau_{i-1} - \tau_{i-1}^2\right), \end{aligned} \tag{5.27}$$

$$\begin{aligned} m_{31,i}(s) = &-\frac{\left(\mathrm{e}^{-sD_{i-1}} - 1\right)\left(\tau_{i-1} - \tau_{i-1}\mathrm{e}^{\frac{-(D_i-D_{i-1})}{\tau_{i-1}}}\right)}{s\tau_{i-1}} - \mathrm{e}^{\frac{-(D_i-D_{i-1})}{\tau_{i-1}}} \\ &\times \left(\frac{\mathrm{e}^{-sD_{i-1}}\left(\tau_{i-1} - \tau_{i-1}\mathrm{e}^{\frac{-D_{i-1}}{\tau_{i-1}}}\right)}{s\tau_{i-1}} + \frac{\tau_{i-1}\left(\mathrm{e}^{\frac{-D_{i-1}}{\tau_{i-1}}}\mathrm{e}^{-sD_{i-1}} - 1\right)}{s\tau_{i-1}(s\tau_{i-1}+1)}\right), \end{aligned} \tag{5.28}$$

$$m_{51,i}(s) = -\frac{\mathrm{e}^{-\frac{D_i-D_{i-1}}{\tau_{i-1}}}\left(\mathrm{e}^{\frac{-D_{i-1}(s\tau_{i-1}+1)}{\tau_{i-1}}} - 1\right)}{s\tau_{i-1}+1}. \tag{5.29}$$

Using the i-th vehicle's model (5.1)–(5.3) we obtain

$$\begin{bmatrix} S_i(s) \\ V_i(s) \\ A_i(s) \end{bmatrix} = \left(sI_{3\times 3} - \hat{\Gamma}_i\right)^{-1} \left(\begin{bmatrix} 0 \\ 0 \\ \frac{1}{\tau_i} \end{bmatrix} \mathrm{e}^{-sD_i} U_i(s) + \begin{bmatrix} 1 \\ 0 \\ 0 \end{bmatrix} V_{i-1}(s) \right), \tag{5.30}$$

where

$$\hat{\Gamma}_i = \begin{bmatrix} 0 & -1 & 0 \\ 0 & 0 & 1 \\ 0 & 0 & -\frac{1}{\tau_i} \end{bmatrix}, \tag{5.31}$$

and hence,

$$\begin{bmatrix} S_i(s) \\ V_i(s) \\ A_i(s) \end{bmatrix} = \begin{bmatrix} -\frac{1}{s^2(s\tau_i+1)} \\ \frac{1}{s(s\tau_i+1)} \\ \frac{1}{s\tau_i+1} \end{bmatrix} \mathrm{e}^{-sD_i} U_i(s) + \begin{bmatrix} \frac{1}{s} \\ 0 \\ 0 \end{bmatrix} V_{i-1}(s). \tag{5.32}$$

Using control laws (5.5), together with (5.18)–(5.29), we get

$$\begin{aligned} U_i(s) = {} & \frac{\tau_i\alpha_i}{h_i} S_i(s) - \left(\tau_i(\alpha_i+b_i) + \frac{D_i\tau_i\alpha_i}{h_i}\right) V_i(s) + \left(\tau_i b_i + \frac{D_i\tau_i\alpha_i}{h_i}\right) V_{i-1}(s) \\ & + \left(-\tau_i c_i \mathrm{e}^{\frac{-D_i}{\tau_i}} - \tau_i(\alpha_i+b_i)\left(\tau_i - \tau_i \mathrm{e}^{\frac{-D_i}{\tau_i}}\right) - \frac{\tau_i\alpha_i}{h_i}\left(\tau_i^2 \mathrm{e}^{\frac{-D_i}{\tau_i}} + D_i\tau_i - \tau_i^2\right)\right) A_i(s) \\ & + \left(\tau_i c_i \mathrm{e}^{\frac{-D_i}{\tau_i}} + \tau_i b_i\left(\tau_{i-1} - \tau_{i-1}\mathrm{e}^{\frac{-D_i}{\tau_{i-1}}}\right) + \frac{\tau_i\alpha_i}{h_i}\left(\tau_{i-1}^2 \mathrm{e}^{\frac{-D_i}{\tau_{i-1}}} + D_i\tau_{i-1} - \tau_{i-1}^2\right)\right) A_{i-1}(s) \\ & + g_{1,i}(s)U_i(s) + g_{2,i}(s)U_{i-1}(s), \end{aligned} \tag{5.33}$$

where

$$g_{1,i}(s) = \frac{\tau_i\alpha_i}{h_i} M_{11,i}(s) - \tau_i(\alpha_i+b_i)M_{21,i}(s) - \tau_i c_i M_{41,i}(s), \tag{5.34}$$

$$g_{2,i}(s) = \frac{\tau_i\alpha_i}{h_i} m_{11,i}(s) + \tau_i b_i m_{31,i}(s) + \tau_i c_i m_{51,i}(s). \tag{5.35}$$

Hence, substituting (5.32) in (5.33) we derive $\frac{U_i}{U_{i-1}}$, which, after multiplying it by $\frac{\mathrm{e}^{-D_i s}(s\tau_{i-1}+1)}{\mathrm{e}^{-D_{i-1}s}(s\tau_i+1)}$, gives

$$G_i(s) = \frac{\delta_i(s)}{s^3 + \left(\frac{1}{\tau_i} + c_i\right)s^2 + (\alpha_i+b_i)s + \frac{\alpha_i}{h_i}}, \tag{5.36}$$

where

$$\delta_i(s) = \mathrm{e}^{-(D_i-D_{i-1})s}\left(\left(\frac{\alpha_i}{h_i}\tau_{i-1}\left(D_i-D_{i-1}\right)+b_i\tau_{i-1}-\frac{\alpha_i}{h_i}\tau_{i-1}^2 + \mathrm{e}^{-\frac{(D_i-D_{i-1})}{\tau_{i-1}}}\left(\frac{\alpha_i}{h_i}\tau_{i-1}^2-b_i\tau_{i-1}+c_i\right)\right)s^2+\left(\left(D_i-D_{i-1}\right)\frac{\alpha_i}{h_i}+b_i\right)s+\frac{\alpha_i}{h_i}\right).^{1} \tag{5.37}$$

String stability in $\mathcal{L}_2$ is guaranteed when $|G_i(j\omega)| \leq 1$, for all $\omega \geq 0$. The condition is satisfied for $\omega = 0$ since $|G_i(0)| = 1$. Moreover, from (5.36) we have

$$G_i(j\omega) = \frac{f_{1,i}(\omega)+jf_{2,i}(\omega)}{f_{3,i}(\omega)+jf_{4,i}(\omega)}\mathrm{e}^{-(D_i-D_{i-1})j\omega}, \tag{5.38}$$

$$f_{1,i}(\omega) = \frac{\alpha_i}{h_i}-\left(\frac{\alpha_i}{h_i}\tau_{i-1}\left(D_i-D_{i-1}\right)+b_i\tau_{i-1}-\frac{\alpha_i}{h_i}\tau_{i-1}^2 + \mathrm{e}^{-\frac{(D_i-D_{i-1})}{\tau_{i-1}}}\left(\frac{\alpha_i}{h_i}\tau_{i-1}^2-b_i\tau_{i-1}+c_i\right)\right)\omega^2, \tag{5.39}$$

$$f_{2,i}(\omega) = \left(\left(D_i-D_{i-1}\right)\frac{\alpha_i}{h_i}+b_i\right)\omega, \tag{5.40}$$

$$f_{3,i}(\omega) = -\omega^2\left(\mathrm{c}_i+\frac{1}{\tau_i}\right)+\frac{\alpha_i}{h_i}, \tag{5.41}$$

$$f_{4,i}(\omega) = \omega(\alpha_i+b_i)-\omega^3. \tag{5.42}$$

By using the fact that $\sup_\omega |\mathrm{e}^{-(D_i-D_{i-1})j\omega}| = 1$, the condition for string stability becomes $f_{1,i}(\omega)^2+f_{2,i}(\omega)^2 < f_{3,i}(\omega)^2+f_{4,i}(\omega)^2$, $\omega > 0$, $i = 1, ..., N$, and hence, after straightforward computations, we get the following condition, which has to hold for all $\omega > 0$ and $i = 1, ..., N$,

$$\omega^6+\omega^4\beta_i+\omega^2\gamma_i > 0, \tag{5.43}$$

where β_i and γ_i are defined in (5.10) and (5.11), respectively. Using $z = \omega^2$ in relation (5.43), we obtain

$$z^2+z\beta_i+\gamma_i > 0. \tag{5.44}$$

The relation (5.44) (that is a second-order polynomial in z) holds for all $\omega > 0$, under condition (5.14) or under conditions (5.15), (5.16), from Theorem 5.1.

[1]The appearance of the non-casual term $e^{sD_{i-1}}$ is reasonably expected. This arises because the integral term (5.6) depends on u_{i-1}, including values of u_{i-1} up to the current time t. Consequently, the control input u_i reacts immediately to changes in u_{i-1}. However, v_{i-1} reacts to changes in u_{i-1} after a delay of D_{i-1}, thus, essentially, u_i involves a prediction of v_{i-1}, which leads to the appearance of this term.

Using (5.36), we deduce (as $G_i(0) = 1$) that $\lim_{t\to+\infty} v_i(t) = \lim_{t\to+\infty} v_{i-1}(t) = v_{\rm ss}$, for a constant leader's speed $v_{\rm ss}$. Moreover, with $V_0 = \frac{v_{\rm ss}}{s}$ we have from (5.1) and (5.17)

$$\lim_{s\to 0} sS_1(s) = \lim_{s\to 0} v_{\rm ss}\left(\frac{1-G_1(s)}{s}\right). \tag{5.45}$$

Thus, as $G_1(0) = 1$[2] we have

$$\lim_{s\to 0} sS_1(s) = -\lim_{s\to 0} v_{\rm ss} G_1'(s). \tag{5.46}$$

Since $\lim_{s\to 0} G_1'(s) = -h_1$ and $\lim_{s\to 0} sV_1(s) = \lim_{t\to+\infty} v_1(t) = v_{\rm ss}$, the steady-state spacing error is calculated as

$$\lim_{t\to+\infty} (s_1(t) - h_1 v_1(t)) = \lim_{s\to 0} s(S_1(s) - h_1 V_1(s)) = 0. \tag{5.47}$$

Proceeding in the exact same manner and using $\lim_{t\to\infty} v_i(t) = v_{\rm ss}$, $i = 1, ..., N$, we complete the proof. □

5.4 Numerical Illustration of String Stability

In this section, we numerically analyze the $\mathcal{L}_2$ string stability properties of the closed-loop system concerning the propagation of speed errors. The transfer function $G_i = \frac{V_i}{V_{i-1}}$, which corresponds to the closed-loop systems described by equations (5.1)–(5.3), (5.5)–(5.9) is given in (5.36). Figure 5.2 depicts $\sup_\omega |G_i(j\omega)|$ as a function of $D_i - D_{i-1}$ and h_i for choices of Table 5.1. In Figure 5.2, the region between the red lines indicates where $\mathcal{L}_2$ string stability holds. As evident from Figure 5.2, increasing h_i allows larger differences in actuation delays.

Table 5.1: The parameters employed for numerical illustration of string stability with respect to speed errors.

Parameter	Value
τ_i	0.3 s
τ_{i-1}	0.25 s
α_i	15
b_i	5
c_i	1

[2]In fact, the transfer function $\frac{1-G_1(s)}{s}$ features a zero-pole cancellation at $s = 0$, which implies that its poles are all on the left half-plane.

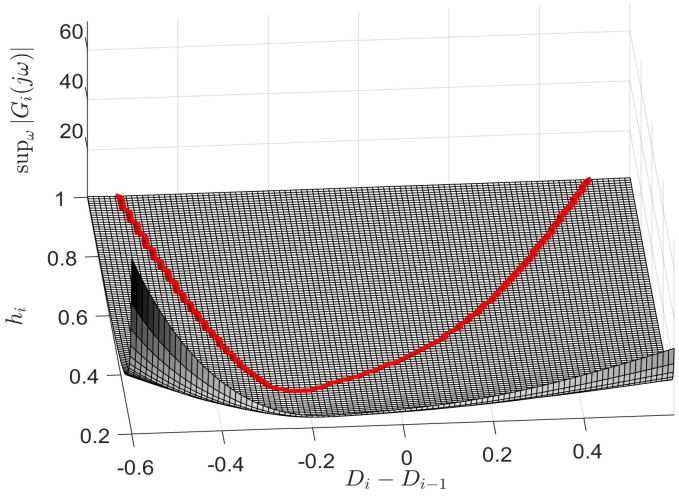

Figure 5.2: The values of function $\sup_\omega |G_i(j\omega)|$ corresponding to (5.36), for different values of $D_i - D_{i-1}$ and h_i with choices of Table 5.1.

Such a condition on the actuation delays' differences[3] may be explained as follows. In view of (5.6) one can observe that the ego vehicle's controller is coupled with the control input of the preceding vehicle. From the viewpoint of disturbance attenuation, for disturbances propagating upstream in the platoon, it may not be beneficial the ego vehicle's controller to react much slower or much faster than the preceding vehicle's controller; while the allowable magnitude of such timing difference may depend on the desired/equilibrium inter-vehicle distance. This is reasonably expected for the case in which the ego vehicle reacts much slower than the preceding vehicle (to a disturbance propagating upstream). When the ego vehicle's dynamics react too fast, based on the prediction the ego vehicle's controller makes for the preceding vehicle's dynamics, this perhaps may also not be beneficial, as the preceding vehicle's dynamics would be affected by its own control input much later. This type of control input signals (and measurements) "synchronization" has been reported to be beneficial for string stability also in, e.g., [44], [64], [62].

Performing an exhaustive search for identifying suitable control gains to achieve string (and individual vehicle) stability is challenging due to the large number of parameters involved, as outlined in (5.14)–(5.16). In discussing how a choice of parameters may ensure string stability, we consider a case satisfying (5.14). The shaded area in Figure 5.3 indicates where $4\gamma_i - \beta_i^2$ is positive, given $h_i = 0.8$, $D_i - D_{i-1} = 0.3$, $\tau_i = 0.25$, $\tau_{i-1} = 0.2$,

[3]Note that the values themselves of each individual delay are not necessarily restricted. Note also that such a condition on the delays' differences is a result of the fact that (5.6) does not correspond to the exact predictor states.

and $\alpha_i = 15$. Furthermore, for (b_i,c_i) in the shaded region in Figure 5.3, conditions (5.12) and (5.13), which ensure individual vehicle stability, also hold.

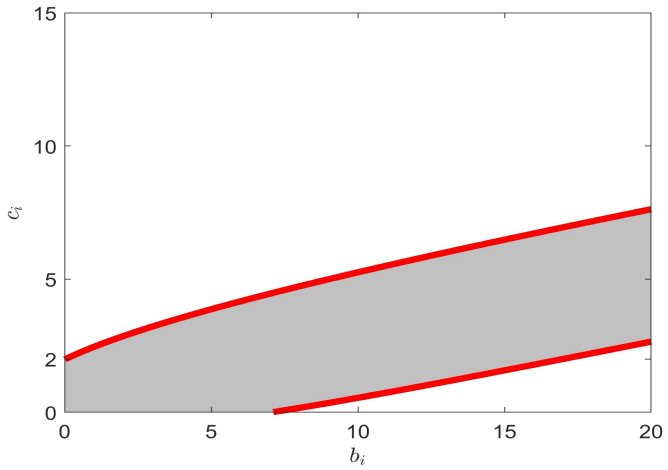

Figure 5.3: The shaded area indicates where (5.14) holds, and thus, string stability holds. The other parameters are $h_i = 0.8$, $D_i - D_{i-1} = 0.3$, $\tau_i = 0.25$, $\tau_{i-1} = 0.2$, and $\alpha_i = 15$.

5.5 Simulation Results

In this section, the performance of the delay-compensating CACC design (5.5) is demonstrated, followed by a comparison with the predictor-feedback CACC approach in [8] and with the predictor-based ACC design from [9]. Moreover, to illustrate the efficiency of the control design developed here in more practical scenarios, we utilize real traffic data from OpenACC dataset [33].

The simulation testbed employed in this chapter is identical to the one described in the second paragraph of Section 3.5.

Moreover, we configure the desired time headways based on two considerations: first, in order to be close to real-world parameters (see, e.g., [21], [19], [33], [57]), and second, to ensure they fall well within the region enclosed by the red line in Figure 5.2, which adds a degree of robustness to string stability.

5.5.1 Predictor-Based CACC Design

We consider a heterogeneous platoon of seven vehicles in order to make the numerical example more practical. For a heterogeneous platoon of seven vehicles with third-order dynamics given by (5.1)–(5.3), we consider a case in which τ_i, time-headways h_i, and

actuation delays D_i, are set according to Table 5.2. We choose control gains α_i, b_i, and c_i for $i = 1, 2, ..., 6$ according to Table 5.1, which guarantee $\mathcal{L}_2$ string stability according to Figure 5.2. Moreover, we consider a scenario in which $a_i(0) = 0$ and $u_i(s) = 0$, $s \in [-D_i, 0)$, for each vehicle i. While we set $v_{i_0} = 15 \left(\frac{m}{s}\right)$, $i = 1, 2, ..., 6$ and $v_{l_0} = 13 \left(\frac{m}{s}\right)$; $s_{i_0} = h_i v_{i_0} = h_i \times 15\ m$, $i = 2, 3, ..., 6$, $s_{1_0} = 11\ m$. The respective responses are shown in Figure 5.4. We observe that there is no overshoot in the responses, due to deceleration or acceleration maneuvers performed by the leader, because the responses are string stable. This is further illustrated in Figure 5.6 that shows functions $\|\delta_i\|_{2,t} = \sqrt{\int_0^t \delta_i(s)^2 ds}$, where $\delta_i = s_i - h_i v_i$, which implies that $\mathcal{L}_2$ string stability with respect to spacing errors is also achieved[4]. Moreover, with respect to Figure 5.5, for a constant leading vehicle's speed, zero, steady-state spacing errors are achieved.

Table 5.2: The parameters employed for the simulation results presented in Sections 5.5.1 and 5.5.2.

Parameters / Vehicle No.	τ_i	h_i	D_i
0	0.3 s	–	0.2 s
1	0.2 s	0.8 s	0.4 s
2	0.25 s	0.8 s	0.7 s
3	0.25 s	0.9 s	0.6 s
4	0.2 s	0.9 s	0.4 s
5	0.25 s	1 s	0.6 s
6	0.18 s	1 s	0.5 s

[4]We illustrate in simulation that string stability with respect to spacing errors also holds. However, to analytically (or even numerically) study string stability with respect to spacing errors is quite challenging, while certain conditions obtained may not be realistic both from a theoretical and practical viewpoint. For example, the transfer functions that correspond to spacing errors may incorporate an additional pole on which individual vehicle stability depends, which appears as imposing a redundant individual vehicle stability condition (due to the particular input-output relation); while the respective string stability conditions may involve the dynamics of two preceding vehicles that does not allow studying and guaranteeing string stability of pairs of vehicles, which may be a suitable index of platoon performance.

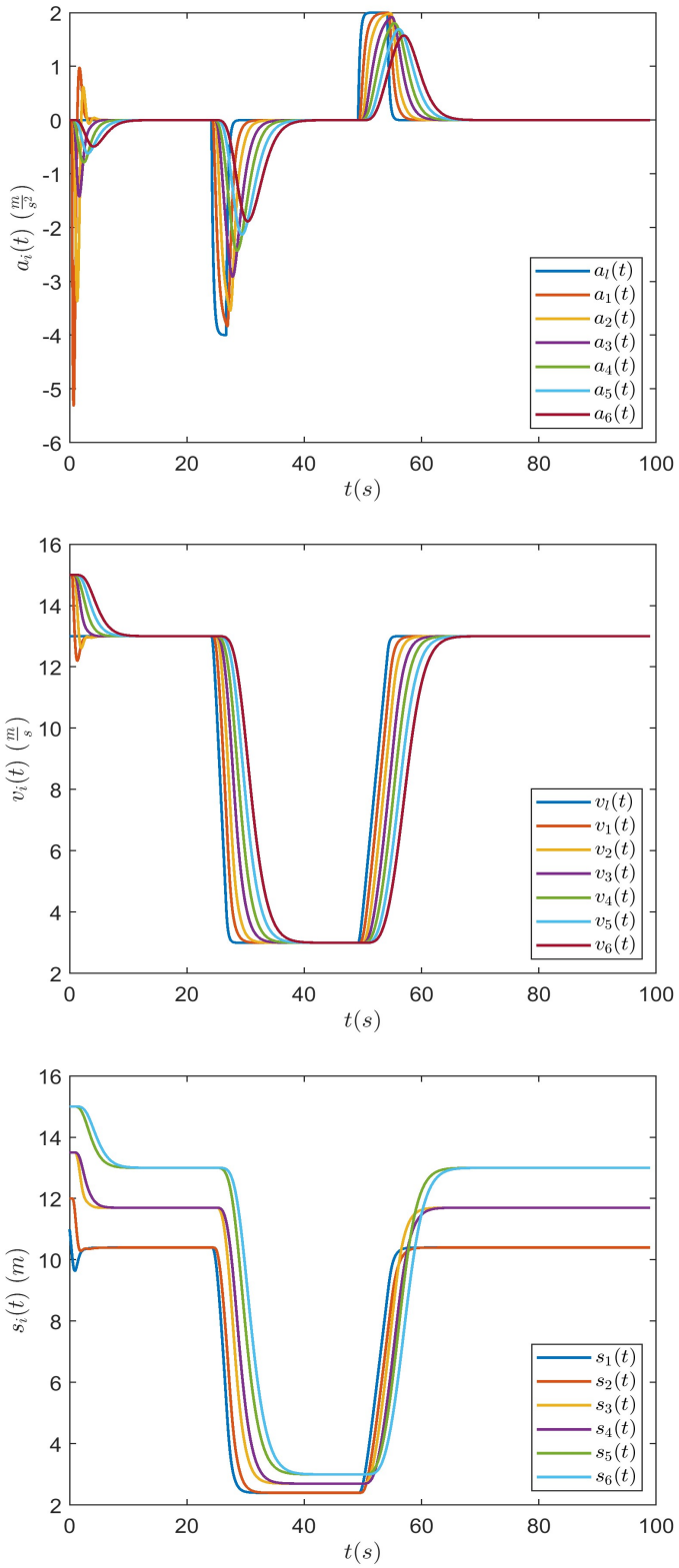

Figure 5.4: Acceleration (top), speed (middle), and spacing (bottom) of seven vehicles, with dynamics described by (5.1)–(5.3), under the predictor-based control laws (5.5), (5.6), where the selected parameters and control gains are shown in Table 5.2 and Table 5.1, respectively. Initial conditions are $v_{i_0} = 15\left(\frac{m}{s}\right)$, $i = 1, 2, ..., 6$, $v_{l_0} = 13\left(\frac{m}{s}\right)$; $s_{i_0} = h_i v_{i_0} = h_i \times 15\ m$, $i = 2, 3, ..., 6$, $s_{1_0} = 11\ m$; and $u_{i0} \equiv 0$, for $i = 1, 2, ..., 6$.

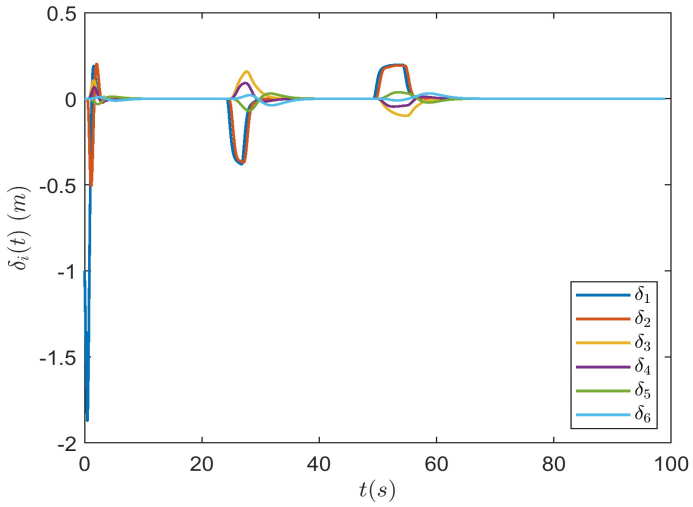

Figure 5.5: Spacing errors $\delta_i(t) = s_i(t) - h_i v_i(t)$, $i = 1, 2, 3, 4, 5, 6$, corresponding to the responses of Figure 5.4.

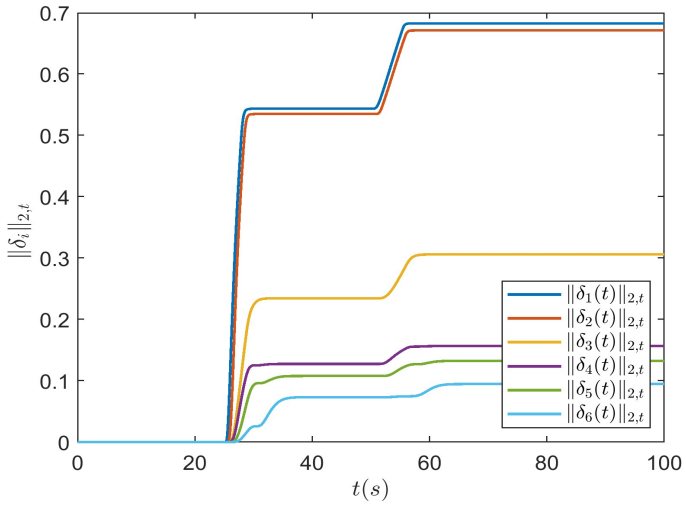

Figure 5.6: Norms $\|\delta_i\|_{2,t} = \sqrt{\int_0^t \delta_i(s)^2 ds}$ corresponding to Figure 5.4's scenario.

5.5.2 Predictor-Feedback Control Design

In Figure 5.7 we show the response of the heterogeneous platoon of seven vehicles under the predictor-feedback CACC law from [8] for system (5.1)–(5.3). These control laws do not address distinct input delays. We implemented the predictor-feedback controller assuming identical input delays $D = D_i = 0.7$ for all vehicles, despite each one having a different actuation delay in the actual model (5.3). We consider the scenario in which τ_i, D_i (for the model only), and h_i are the same with Section 5.5.1. We choose control gains α_i, b_i, and c_i according to Table 5.1. Since we consider the same scenario with Section 5.5.1 we choose identical initial conditions for a_i, v_i, u_i; while we set the initial spacing for $i = 2, 3, ..., 6$ to the corresponding equilibria for this case, namely, $s_{i_0} = h_i v_{i_0} = h_i \times 15\ m$, and set $s_{1_0} = 11\ m$. Regarding Figure 5.8, the predictor-feedback control design achieves zero steady-state spacing errors for a constant leading vehicle's speed. However, the respective responses are generally more oscillatory and $\mathcal{L}_2$ string stability, with respect to spacing errors, does not hold with the predictor-feedback CACC law, as it is indicated in Figure 5.9. In principle, the predictor-feedback design from [8], which assumes identical input delays for all vehicles, would still be string stable when the differences $|D_i - D_{i-1}|$ are small, but not for larger values of $|D_i - D_{i-1}|$.

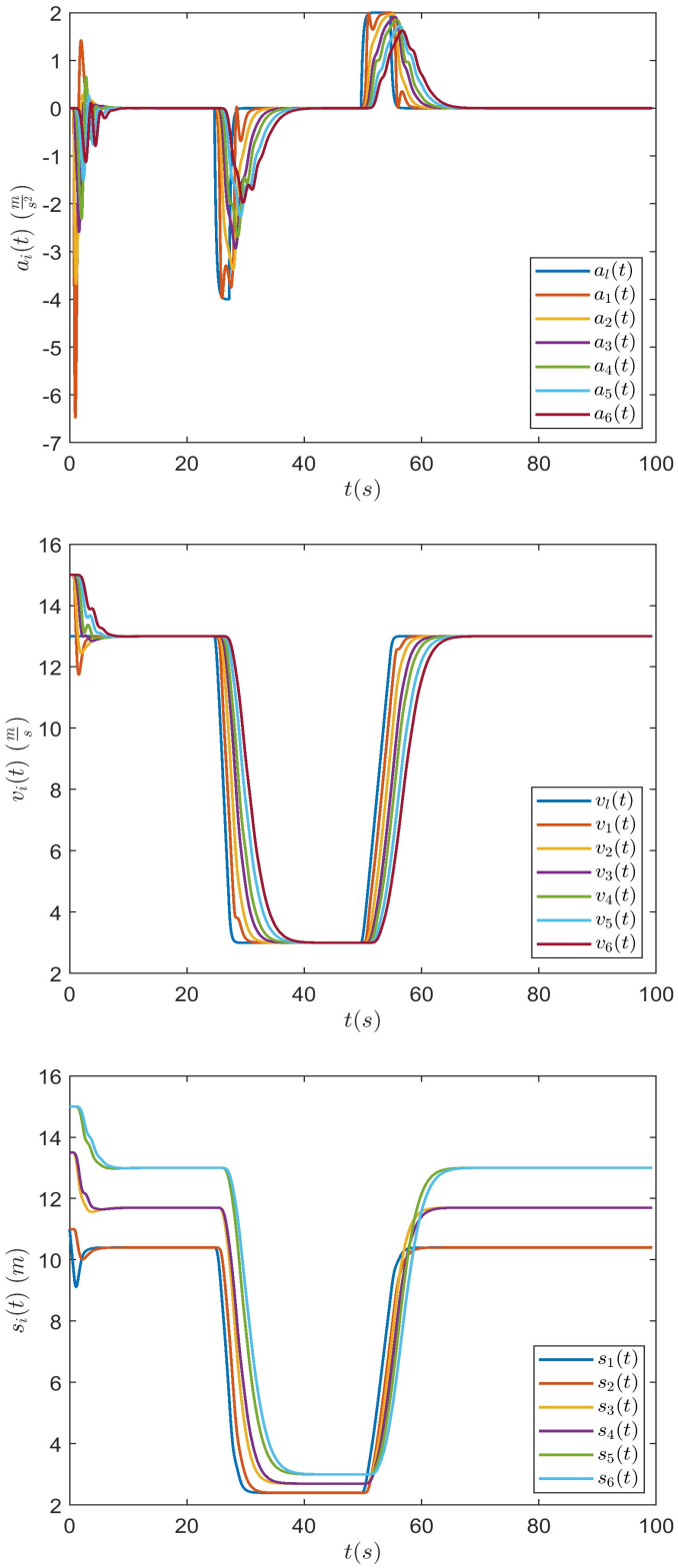

Figure 5.7: Acceleration (top), speed (middle), and spacing (bottom) of seven vehicles, with dynamics described by (5.1)–(5.3), under the predictor-feedback control laws from [8], where the selected parameters and control gains are shown in Table 5.2 and Table 5.1, respectively. Initial conditions are $v_{i_0} = 15\left(\frac{m}{s}\right)$, $i = 1, 2, ..., 6$, $v_{l_0} = 13\left(\frac{m}{s}\right)$; $s_{i_0} = h_i v_{i_0} = h_i \times 15\ m$, $i = 2, 3, ..., 6$, $s_{1_0} = 11\ m$; and $u_{i0} \equiv 0$, for $i = 1, 2, ..., 6$.

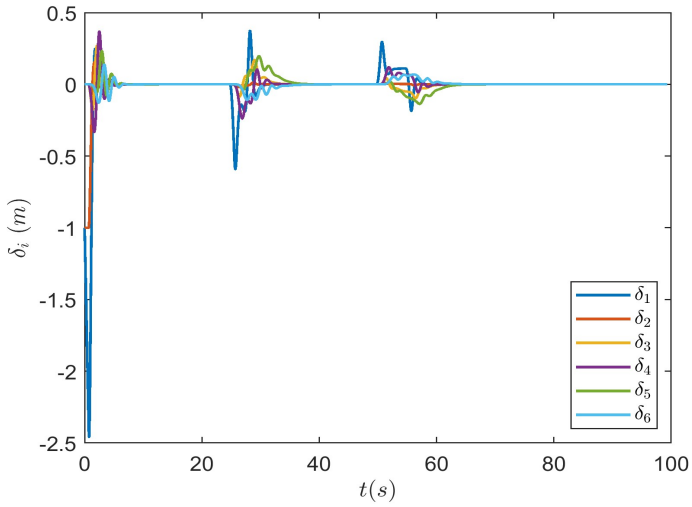

Figure 5.8: Spacing errors $\delta_i(t) = s_i(t) - h_i v_i(t)$, $i = 1, 2, 3, 4, 5, 6$, corresponding to the responses of Figure 5.7.

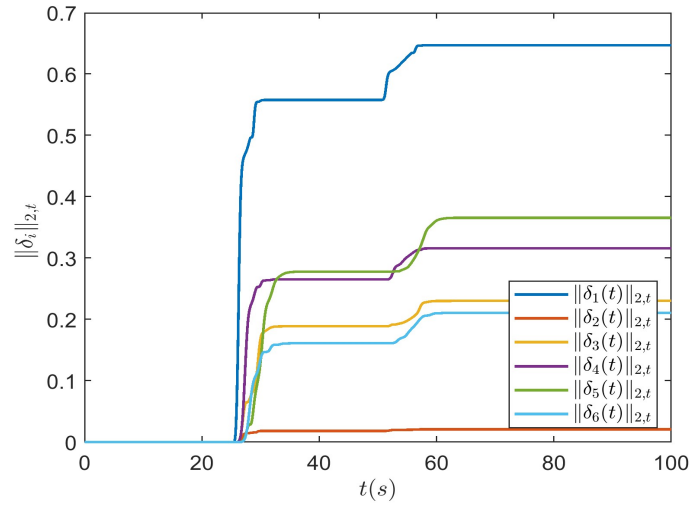

Figure 5.9: Norms $\|\delta_i\|_{2,t} = \sqrt{\int_0^t \delta_i(s)^2 ds}$ corresponding to Figure 5.7's scenario.

5.5.3 Predictor-Based CACC Design Validation with the OpenACC Dataset

In Figure 5.10 we present the results of applying the predictor-based CACC law of Section 5.5.1 to OpenACC dataset. We extract reconstructed data from [33] to demonstrate the controller's performance in real maneuvers of the leading vehicle, considering that the

leading vehicle's trajectory is taken from the real trajectory of vehicle no. 2 in AstaZero platoon 2. This vehicle's trajectory is selected because it involves interesting dynamics with several acceleration/deceleration cycles.

We consider a heterogeneous platoon of four vehicles in order to make the numerical example more accessible and to more clearly illustrate the benefits of (5.5) in more practical scenarios. One difference from Section 5.5.1 is the predictor-based law for the first vehicle. Because we assume that the leading vehicle's dynamics satisfy $\dot{v}_{\mathrm{l}}(t) = a_{\mathrm{l}}(t)$ (and not the third-order system (5.1)–(5.3)) we have to modify slightly the predictor-based control law for the first vehicle. In this case, for implementation of the predictor-based law, because only velocity data are available from the OpenACC dataset, we obtain $a_l(t)$ by numerically computing $\dot{v}_l(t)$.

In the present scenario we consider a case in which τ_i, time-headways h_i, and actuation delays D_i are set according to Table 5.3. Moreover, we choose control gains α_i, b_i, c_i according to Table 5.1. We set $a_i(0) = 0$ and $u_i(s) = 0$, $s \in [-D_i, 0)$ for vehicles $i = 1, 2, 3$. While we also set $v_{i_0} = 20\left(\frac{m}{s}\right)$, $i = 1, 2, 3$ and $v_{\mathrm{l}_0} = 19.3\left(\frac{m}{s}\right)$ (to match with the initial speed of vehicle no. 2 in AstaZero platoon 2 from the OpenACC dataset); $s_{i_0} = h_i v_{i_0} = h_i \times 20\ m$, $i = 2, 3$, $s_{1_0} = 13.5\ m$. Figures 5.10–5.12 illustrate that the performance of the predictor-based CACC law (5.5) is preserved even in more realistic traffic scenarios.

Table 5.3: The parameters employed for the simulation results in Section 5.5.3.

Parameters / Vehicle No.	τ_i	h_i	D_i
0	–	–	–
1	0.2 s	0.7 s	0.4 s
2	0.3 s	0.8 s	0.7 s
3	0.25 s	0.6 s	0.5 s

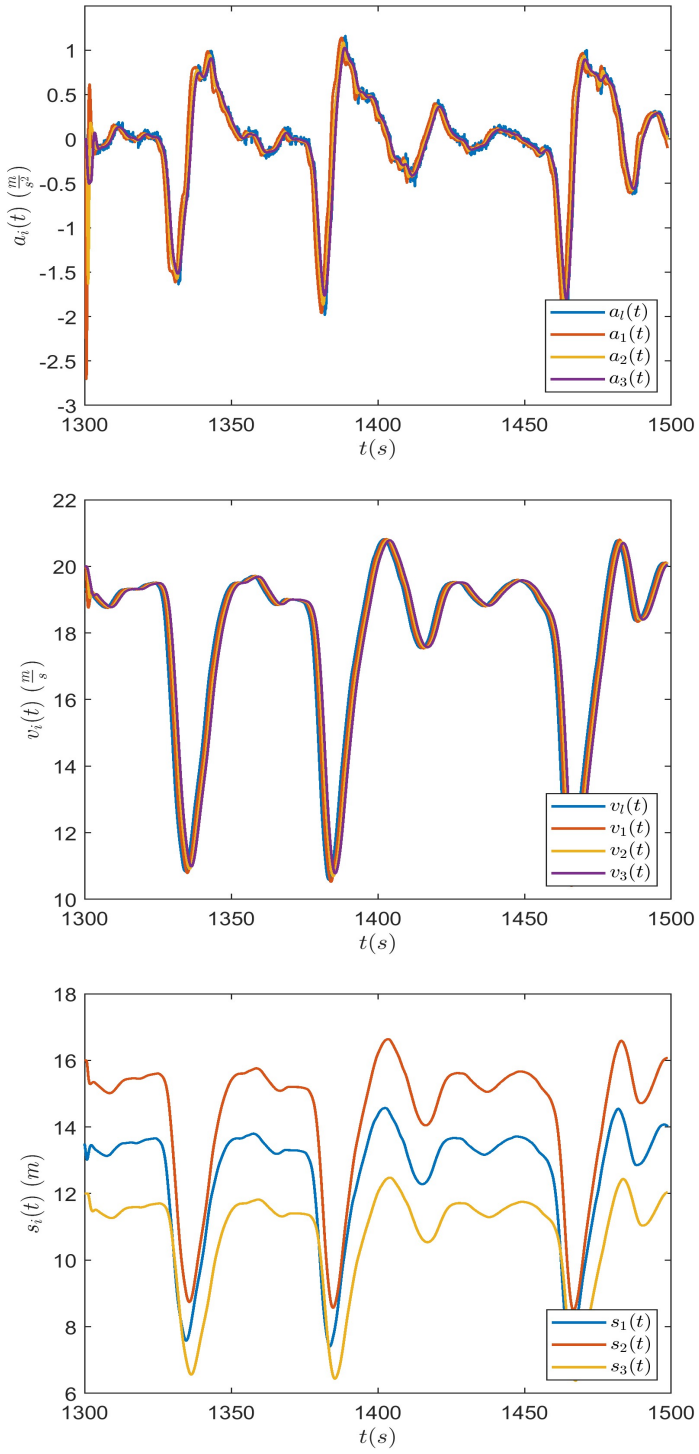

Figure 5.10: Acceleration (top), speed (middle), and spacing (bottom) of three vehicles, with dynamics described by (5.1)–(5.3), under the predictor-based control laws (5.5), (5.6), where the selected parameters and control gains are shown in Table 5.3 and Table 5.1 respectively. The speed (and acceleration) of the leading vehicle is taken from vehicle no. 2 in AstaZero platoon 2 in [33]. Initial conditions are $v_{i_0} = 20\left(\frac{m}{s}\right)$, $i = 1, 2, 3$, $v_{l_0} = 19.3\left(\frac{m}{s}\right)$; $s_{i_0} = h_i v_{i_0} = h_i \times 20\ m$, $i = 2, 3$, $s_{1_0} = 13.5\ m$.

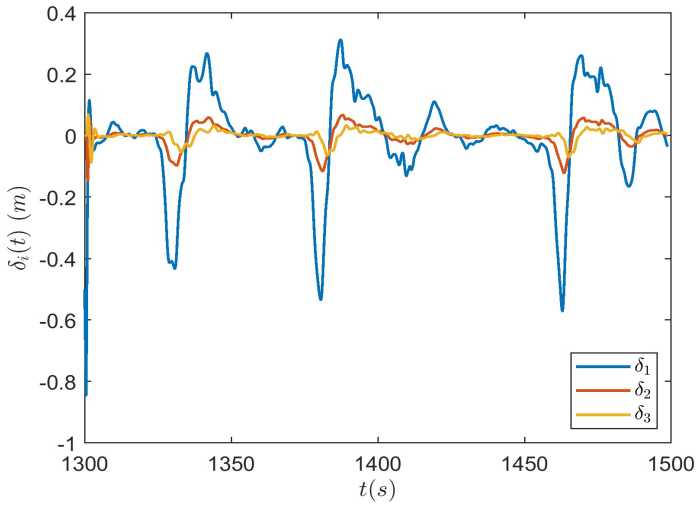

Figure 5.11: Spacing errors $\delta_i(t) = s_i(t) - h_i v_i(t)$, $i = 1, 2, 3$, corresponding to the responses of Figure 5.10.

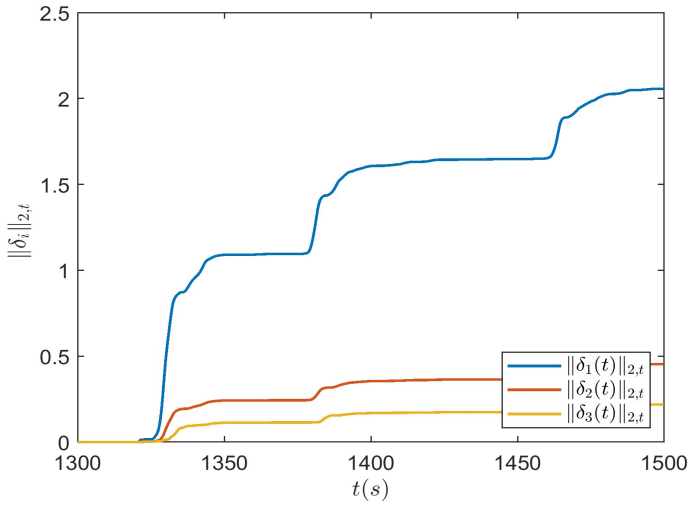

Figure 5.12: Norms $\|\delta_i\|_{2,t} = \sqrt{\int_0^t \delta_i(s)^2 ds}$ corresponding to Figure 5.10's scenario.

5.5.4 Predictor-Based ACC Design

Finally, we also present, inspired by [9], a predictor-based version of controller (5.4) omitting the terms v_{i-1} and a_{i-1}, in order to be able to construct a predictor-based ACC

law. This gives the following controller

$$u_{i,\mathrm{ACC}}(t) = K_{1,i}\tilde{q}_{i,1}(t) + K_{2,i}\tilde{q}_{i,2}(t) + K_{3,i}\tilde{q}_{i,3}(t) - \tau_i c_i \tilde{q}_{i,4}(t), \tag{5.48}$$

$$\tilde{q}_i(t) = \mathrm{e}^{\tilde{\Gamma}_i D_i}\tilde{x}_i(t) + \int_{t-D_i}^{t} \mathrm{e}^{\tilde{\Gamma}_i(t-\theta)}\tilde{B}_i u_i(\theta)\, d\theta, \tag{5.49}$$

where

$$\tilde{q}_i = \begin{bmatrix} \tilde{q}_{i,1} \\ \tilde{q}_{i,2} \\ \tilde{q}_{i,3} \\ \tilde{q}_{i,4} \end{bmatrix}, \quad \tilde{x}_i = \begin{bmatrix} s_i \\ \sigma_i \\ v_i \\ a_i \end{bmatrix}, \tag{5.50}$$

$$\tilde{\Gamma}_i = \begin{bmatrix} 0 & 0 & -1 & 0 \\ \frac{1}{h_i} & 0 & -1 & 0 \\ 0 & 0 & 0 & 1 \\ 0 & 0 & 0 & -\frac{1}{\tau_i} \end{bmatrix}, \quad \tilde{B}_i = \begin{bmatrix} 0 \\ 0 \\ 0 \\ \frac{1}{\tau_i} \end{bmatrix}, \tag{5.51}$$

and

$$\dot{\sigma}_i(t) = \frac{s_i(t)}{h_i} - v_i(t). \tag{5.52}$$

We choose our parameters according to Table 5.3, with control gains set as $K_{1,i} = 20$, $K_{2,i} = 40$, $K_{3,i} = -20$, and $c_i = 5$ for $i = 2, ..., 6$. For the first vehicle, however, we set $K_{1,1} = 15$, $K_{2,1} = 25$, $K_{3,1} = -20$, and $c_1 = 5$ to prevent large initial transients in acceleration response. Moreover, we consider a scenario in which $a_i(0) = 0$ and $u_i(s) = 0$, $s \in [-D_i, 0)$, for each vehicle i. While we set $v_{i_0} = 15\left(\frac{m}{s}\right)$, $i = 1, 2, ..., 6$ and $v_{1_0} = 13\left(\frac{m}{s}\right)$; $\sigma_{i_0} = 0$, $i = 2, ..., 6$, $\sigma_{1_0} = 1$; $s_{i_0} = h_i v_{i_0} = h_i \times 15\ m$, $i = 2, 3, ..., 6$, $s_{1_0} = 11\ m$. The respective responses are shown in Figure 5.13. Figure 5.13 demonstrates that, despite the ACC laws (5.50)-–(5.52) maintaining vehicle stability, string stability cannot be achieved. In particular, vehicles 4–6 are string stable, but vehicles 1–3 are not. The reason is that the string stability conditions from [9] can be satisfied for vehicles 4–6 with small enough control gains that result in realistic values of acceleration/deceleration (in response to non-equilibrium initial conditions), because the time headways for vehicles 4–6 are sufficiently larger than the respective actuation delays and the respective initial conditions deviations from equilibrium are not large (as it is the case with vehicle no. 1, which imposes choosing smaller control gains that, however, cannot guarantee string stability).

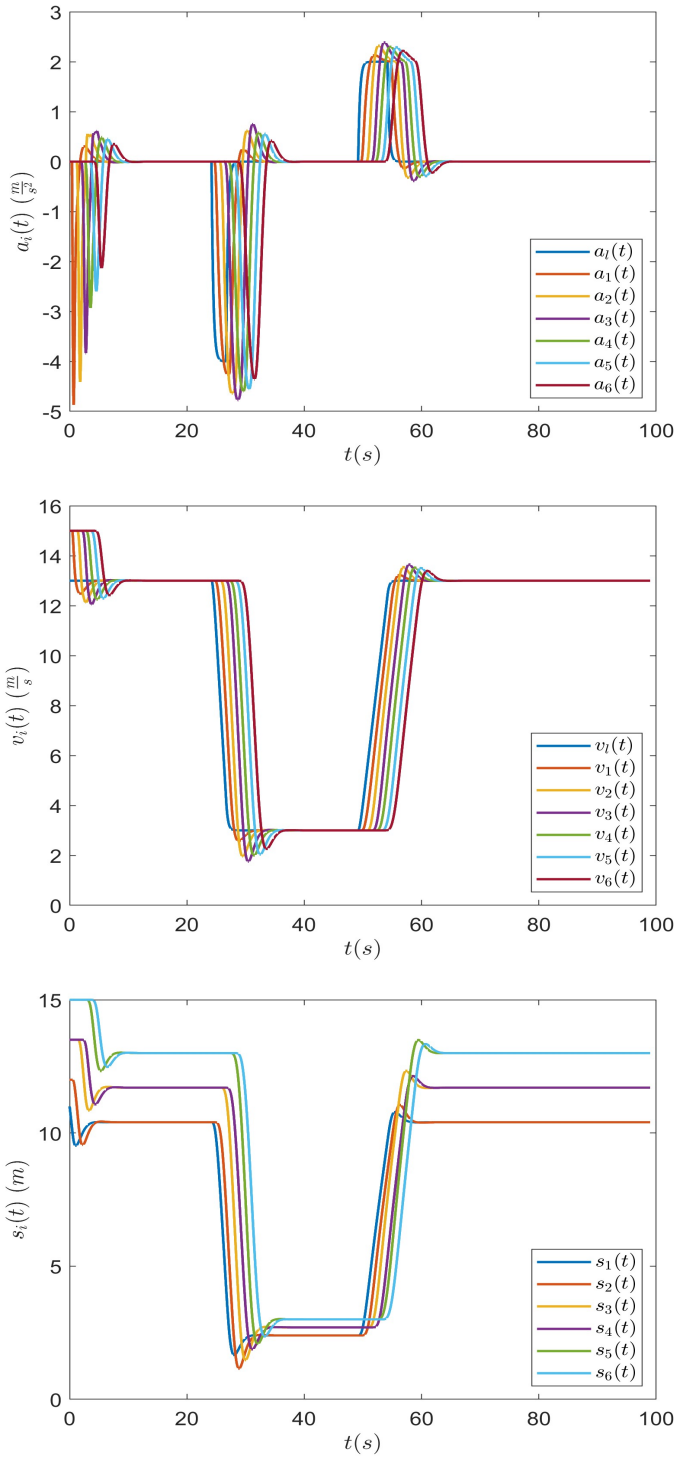

Figure 5.13: Acceleration (top), speed (middle), and spacing (bottom) of seven vehicles, with dynamics described by (5.1)–(5.3), under the predictor-based ACC laws (5.50)–(5.52), where we select our parameters according to Table 5.3, with control gains set as $K_{1,i} = 20$, $K_{2,i} = 40$, $K_{3,i} = -20$, and $c_i = 5$ for $i = 2, ..., 6$. For the first vehicle we set $K_{1,1} = 15$, $K_{2,1} = 25$, $K_{3,1} = -20$, and $c_1 = 5$. Initial conditions are $v_{i_0} = 15\left(\frac{m}{s}\right)$, $i = 1, 2, ..., 6$, $v_{l_0} = 13\left(\frac{m}{s}\right)$; $\sigma_{i_0} = 0$, $i = 2, ..., 6$, $\sigma_{1_0} = 1$; $s_{i_0} = h_i v_{i_0} = h_i \times 15\ m$, $i = 2, 3, ..., 6$, $s_{1_0} = 11\ m$; and $u_{i0} \equiv 0$, for $i = 1, 2, ..., 6$.

The predictor-based ACC law (5.50)—(5.52) neither involves a predictor of the states v_{i-1} and a_{i-1} nor a mechanism to address distinct input delays, and thus, its performance (at least without advanced modifications) is not as efficient as the performance under predictor-based laws of CACC type.

5.6 Robustness of String Stability of Predictor-Based CACC for Distinct Input Delays to Distinct Communication Delays

In this section, we examine the robustness of string stability of the predictor-based CACC law, which is designed to compensate for actuator delays, in the presence of communication delays. As discussed in Section 5.2, the transmitted information, u_{i-1} and a_{i-1}, is obtained from the preceding vehicle via V2V communication, which may be subject to communication delays. They are denoted by $u_{i-1,\mathrm{m}}$ and $a_{i-1,\mathrm{m}}$, respectively, which are defined as $a_{i-1,\mathrm{m}}(t) = a_{i-1}(t - D_{\mathrm{c,i-1}})$ and $u_{i-1,\mathrm{m}}(\theta) = u_{i-1}(\theta - D_{\mathrm{c,i-1}}), \theta \in [t - D, t]$, respectively, where $D_{\mathrm{c,i-1}} \geq 0$, $i = 1, ..., N$, are communication delays.

The predictor-based control laws, under communication delay, for system (5.1)–(5.3) are given by

$$\bar{u}_i(t) = \frac{\tau_i \alpha_i}{h_i} \bar{q}_{i,1}(t) - \tau_i(\alpha_i + b_i)\bar{q}_{i,2}(t) + \tau_i b_i \bar{q}_{i,3}(t) + \tau_i c_i \left(\bar{q}_{i,5}(t) - \bar{q}_{i,4}(t)\right), \tag{5.53}$$

$$\bar{q}_i(t) = \mathrm{e}^{\Gamma_i D_i}\hat{x}_i(t) + \int_{t-D_i}^{t} \mathrm{e}^{\Gamma_i(t-\theta)} B_i u_i(\theta)\, d\theta + \int_{t-D_{i-1}}^{t} \mathrm{e}^{\Gamma_i(t+D_i-\theta-D_{i-1})} B_{1i} u_{i-1,\mathrm{m}}(\theta)\, d\theta, \tag{5.54}$$

where

$$\bar{q}_i = \begin{bmatrix} \bar{q}_{i,1} \\ \bar{q}_{i,2} \\ \bar{q}_{i,3} \\ \bar{q}_{i,4} \\ \bar{q}_{i,5} \end{bmatrix}, \quad \hat{x}_i = \begin{bmatrix} s_i \\ v_i \\ v_{i-1} \\ a_i \\ a_{i-1,\mathrm{m}} \end{bmatrix}. \tag{5.55}$$

The corresponding transfer functions bar $\bar{G}_i$ are derived as follows.

By applying (5.53)–(5.55) and following the same steps outlined in the proof of Theorem 5.1, we get

$$\bar{G}_i(s) = \frac{\bar{\delta}_i(s)}{s^3 + \left(\frac{1}{\tau_i} + c_i\right) s^2 + (\alpha_i + b_i)s + \frac{\alpha_i}{h_i}}, \tag{5.56}$$

where

$$\begin{aligned}\bar{\delta}_i(s) =& \mathrm{e}^{-(D_i - D_{i-1} + D_{\mathrm{c},i-1})s} \Bigg(\Bigg(\frac{\alpha_i}{h_i}\tau_{i-1}\left(D_i - D_{i-1}\right) + b_i\tau_{i-1} - \frac{\alpha_i}{h_i}\tau_{i-1}^2 \\ &+ \mathrm{e}^{-\frac{(D_i - D_{i-1})}{\tau_{i-1}}} \left(\frac{\alpha_i}{h_i}\tau_{i-1}^2 - b_i\tau_{i-1} + c_i \right) \Bigg) s^2 + \Bigg(\left(D_i - D_{i-1}\right) \frac{\alpha_i}{h_i} \\ &+ D_i \frac{\alpha_i}{h_i} \left(\mathrm{e}^{(D_{\mathrm{c},i-1} - D_{i-1})s} - \mathrm{e}^{-D_{i-1}s} \right) + b_i \left(\mathrm{e}^{(D_{\mathrm{c},i-1} - D_{i-1})s} - \mathrm{e}^{-D_{i-1}s} + 1 \right) \Bigg) s \\ &+ \frac{\alpha_i}{h_i} \left(\mathrm{e}^{(D_{\mathrm{c},i-1} - D_{i-1})s} - \mathrm{e}^{-D_{i-1}s} + 1 \right) \Bigg). \end{aligned} \tag{5.57}$$

5.6.1 Numerical Illustration of String Stability

In this section, we numerically analyze the $\mathcal{L}_2$ string stability properties of the closed-loop system, which concern the propagation of speed errors. The transfer function $\bar{G}_i = \frac{V_i}{V_{i-1}}$, which corresponds to the closed-loop systems described by equations (5.1)–(5.3), (5.53)–(5.55) is given in (5.56). Figure 5.14 depicts $\sup_\omega |\bar{G}_i(j\omega)|$ as a function of $D_{\mathrm{c},i-1}$ and h_i for the choice of parameters shown in Table 5.4. In Figure 5.14, the region between the red lines indicates where $\mathcal{L}_2$ string stability holds. As shown in Figure 5.14, a decrease in $D_{\mathrm{c},i-1}$ allows for smaller values of the time headway. We note that communication delay does not affect vehicle stability (as it is evident from the denominator in (5.56)), since it affects only the measurements of the preceding vehicle's states.

Table 5.4: The parameters employed for numerical illustration of string stability under communication delays.

Parameter	Value
τ_i	0.3 s
τ_{i-1}	0.25 s
α_i	15
b_i	5
c_i	1
D_i	0.6 s
D_{i-1}	0.5 s

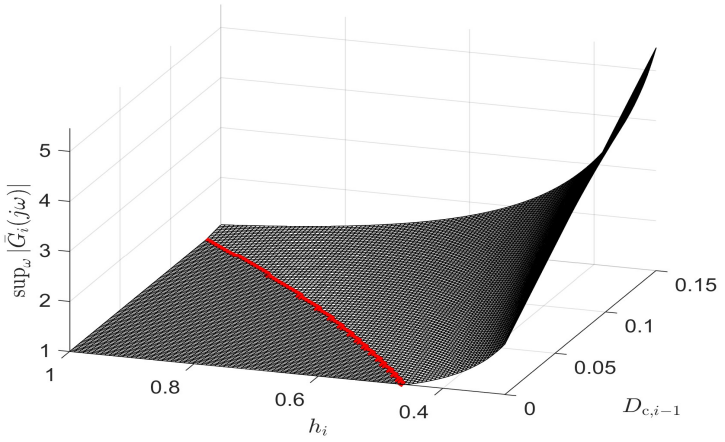

Figure 5.14: The values of function $\sup_\omega |\bar{G}_i(j\omega)|$ corresponding to (5.56), for different values of communication delays and time headways, with parameters' choice of Table 5.4.

5.6.2 Simulation Results

In Figure 5.15 we show the response of the heterogeneous platoon of seven vehicles under the predictor-based CACC law (5.53)–(5.55) for system (5.1)–(5.3). We consider a case in which τ_i, time-headways h_i, $D_{\mathrm{c},i-1}$, and actuation delays D_i, are set according to Table 5.5. We choose control gains α_i, b_i, and c_i for $i = 1, 2, ..., 6$ according to Table 5.4, which guarantee $\mathcal{L}_2$ string stability according to Figure 5.14. Since we consider the same scenario with Section 5.5.1 we choose identical initial conditions for a_i, v_i, u_i; while we set the initial spacing for $i = 2, 3, ..., 6$ to the corresponding equilibria for this case, namely, $s_{i_0} = h_i v_{i_0} = h_i \times 15\ m$, and set $s_{1_0} = 11\ m$. As Figure 5.15 shows, even though acceleration/speed responses exhibit oscillations and potentially larger overshoots in the response due to non-equilibrium initial conditions as compared with the responses in Figure 5.4, $\mathcal{L}_2$ string stability is maintained. This string stability robustness property of predictor-based CACC to communication delays is consistent with the results in [44].

Table 5.5: The parameters employed for the simulation results in Section 5.6.

Parameters / Vehicle No.	τ_i	h_i	D_i	$D_{\mathrm{c},i-1}$
0	0.3 s	–	0.2 s	–
1	0.2 s	0.8 s	0.4 s	0.07 s
2	0.25 s	0.8 s	0.7 s	0.04 s
3	0.25 s	0.9 s	0.6 s	0.12 s
4	0.2 s	0.9 s	0.4 s	0.14 s
5	0.25 s	1 s	0.6 s	0.09 s
6	0.18 s	1 s	0.5 s	0.11 s

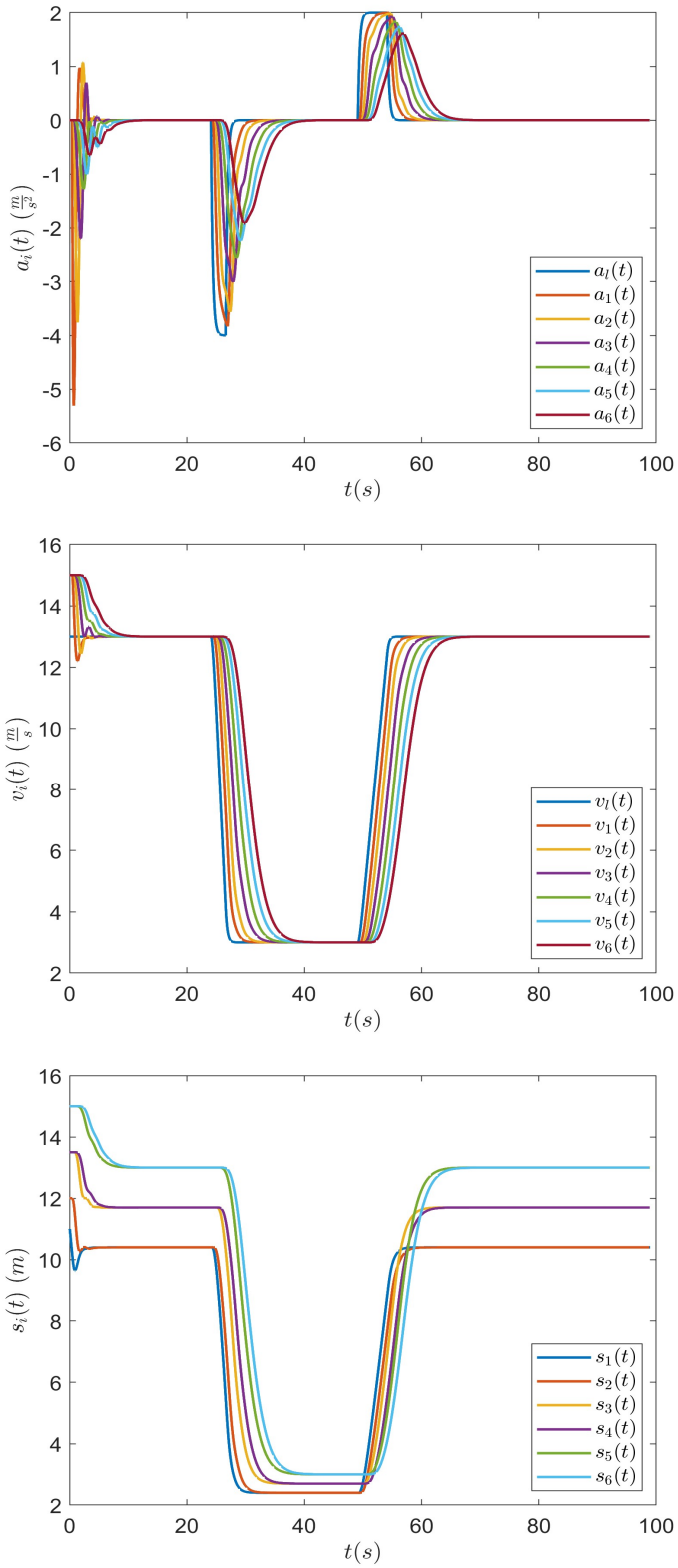

Figure 5.15: Acceleration (top), speed (middle), and spacing (bottom) of seven vehicles, with dynamics described by (5.1)–(5.3), under the predictor-based CACC laws (5.53), (5.54), where the selected parameters and control gains are shown in Table 5.5 and Table 5.4, respectively. Initial conditions are $v_{i_0} = 15\left(\frac{m}{s}\right)$, $i = 1, 2, ..., 6$, $v_{l_0} = 13\left(\frac{m}{s}\right)$; $s_{i_0} = h_i v_{i_0} = h_i \times 15\ m$, $i = 2, 3, ..., 6$, $s_{1_0} = 11\ m$; and $u_{i0} \equiv 0$, for $i = 1, 2, ..., 6$.

5.7 Chapter Conclusions and Related Publications

In the present chapter, we design a predictor-based CACC law, which achieves compensation of long actuation delays, for heterogeneous platoons with vehicles whose dynamics are subject to distinct actuator delays. The control design that we develop achieves string stability with respect to speed errors propagation, individual vehicle stability, and zero, steady-state speed/spacing tracking errors. We provide constructive proof strategies that rely on an input-output approach. We numerically demonstrate the string stability conditions obtained and provide simulation results for a platoon of seven vehicles, including comparisons with related, existing ACC/CACC laws. The simulation results include a realistic scenario of a vehicle cutting-in in front of the platoon and subsequently performing acceleration/deceleration maneuvers. We also validate the performance of the design developed in simulation using real traffic data to describe the trajectory of the leading vehicle. In addition, we study numerically the robustness of string stability of our predictor-based CACC design to communication delays.

This chapter is an adaptation of material appearing in

A. Samii and N. Bekiaris-Liberis, "Predictor-based CACC design for heterogeneous vehicles with distinct input delays," *IEEE Open Journal of Intelligent Transportation Systems*, vol. 5, pp. 783–796, 2024.

A. Samii and N. Bekiaris-Liberis, "Compensation of distinct actuator delays for heterogeneous vehicular platoons via predictor-based CACC," *European Control Conference*, Thessaloniki, 2025.

Chapter 6

Exact Predictor-Feedback CACC of Heterogeneous Vehicular Platoons With Distinct Actuation Delays

We develop a predictor-feedback cooperative adaptive cruise control (CACC) design for platoons with heterogeneous vehicles, each featuring a different input delay. Complete input delay compensation is achieved as the control laws for each vehicle rely on construction of exact predictor states over a prediction horizon equal to the respective input delay. Such construction of the predictor states is enabled through V2V (vehicle-to-vehicle) or V2X (vehicle-to-everything) communication, which allows the ego vehicle to receive the state (including the actuator state) and model/control information from a certain number of vehicles ahead of it (specifically, from all consecutive vehicles ahead that feature a smaller delay and from the first vehicle ahead that features a larger delay). The design guarantees individual vehicle stability, $\mathcal{L}_2$ string stability, and speed/spacing regulation, which is established capitalizing on the exact input delay compensation property of the design. We illustrate the design in simulation through a numerical example, including a comparison with an alternative predictor-based CACC scheme, which cannot guarantee string stability for large differences in the delay values among different vehicles. We also present consistent simulation results for even more practically realistic scenarios, in which we employ real traffic data for the trajectory of the leading vehicle, obtained from both the OpenACC and NGSIM datasets, as well as we account for communication delays and parameter uncertainties.

6.1 Chapter Organization

The outline of the chapter is as follows. Section 6.2 presents the model of heterogeneous platoons considered and the actuation delay-compensating, predictor-feedback design. In Section 6.3, we state our main result, which is vehicle stability and string stability under the CACC law developed. In Section 6.4 we present a specific example for illustration of the design introduced in Section 6.3. Simulation results are presented in Section 6.5, including comparison with a related, existing control law, as well as testings with real traffic data and in the presence of parameter uncertainties and communication delays. In Section 6.6 we provide concluding remarks.

6.2 Exact Predictor-Feedback CACC for Heterogeneous Platoons with Distinct Delays

6.2.1 Vehicle Model and Nominal Delay-Free Design

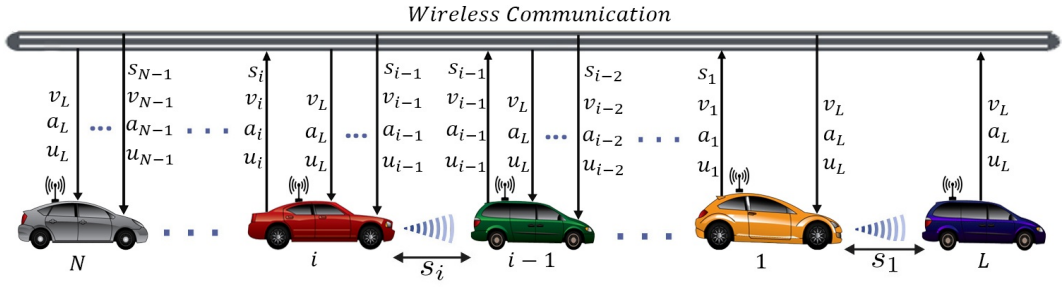

Figure 6.1: Platoon of $N+1$ heterogeneous vehicles following each other in a single lane without overtaking. The dynamics of each vehicle $i = 1, ..., N$ are governed by system (6.1)–(6.3). Each vehicle can measure its own speed/acceleration, the relative speed with the preceding vehicle, and the spacing with respect to the preceding vehicle. Moreover, the control input, acceleration, spacing, and velocity of each vehicle is communicated to all following vehicles via V2V or V2X communication.

a) Vehicle dynamics: We consider a heterogeneous string of vehicles (see Figure 6.1) each one modeled by the following third-order, linear system with distinct actuator delays

that describes vehicle dynamics (see, e.g., [1], [22], [41], [45], [57], [58])

$$\dot{s}_i(t) = v_{i-1}(t) - v_i(t), \tag{6.1}$$

$$\dot{v}_i(t) = a_i(t), \tag{6.2}$$

$$\dot{a}_i(t) = -\frac{1}{\tau_i}a_i(t) + \frac{1}{\tau_i}u_i(t - D_i), \tag{6.3}$$

where $D_i \geq 0$ are input delays, and $t \geq 0$ is time.

b) Available measurements/information: For the platoon considered here the measurements available to the ego vehicle i are its own spacing s_i, speed v_i, acceleration a_i, and control input u_i, as well as the speed of the preceding vehicle v_{i-1}. It is possible to obtain this information through on-board sensors. Furthermore, control inputs of all preceding vehicles, as well as their own acceleration, spacing, and speed are also available to vehicle i. These measurements are transmitted from the preceding vehicles, through V2V or V2X communication ([40], [66]). The delay/lag and control parameter values of all preceding vehicles are also available to the ego vehicle via V2V/V2X communication.

c) Nominal control design: Without input delay, the following control strategy is constructed (see, e.g., [1], [11])

$$u_i(t) = \tau_i\alpha_i\left(\frac{s_i(t)}{h_i} - v_i(t)\right) + \tau_i b_i(v_{i-1}(t) - v_i(t)) + \tau_i c_i\left(a_{i-1}(t) - a_i(t)\right), \tag{6.4}$$

where $\alpha_i > 0$, $b_i > 0$, and $c_i > 0$ are design parameters, and $h_i > 0$ is a desired time-headway. In the delay-free case, design (6.4) achieves the desired time-headways and regulation of speed/accelerations, as well as string stability, under certain conditions on the control parameters (see, e.g., [1], [53]).

6.2.2 Exact Predictor-Feedback CACC for Distinct Delays

The CACC design we develop here is inspired by the general design in [6]. In particular, each control input i employs the D_i time units ahead predictors of the states involved in (6.4). These predictor states are constructed following the recursive procedure from [6], in which one starts from constructing the predictor state corresponding to the smallest delay, and subsequently using the dynamics of this predictor state to compute the predictor state corresponding to the input with the second smallest delay. This procedure continues recursively until the predictor state corresponding to the largest delay is computed. In the present case, this procedure is followed for constructing the control input of each

vehicle i. In Figure 6.2, we present a block diagram that illustrates how each ego vehicle constructs each own controller, as well as which information is needed.

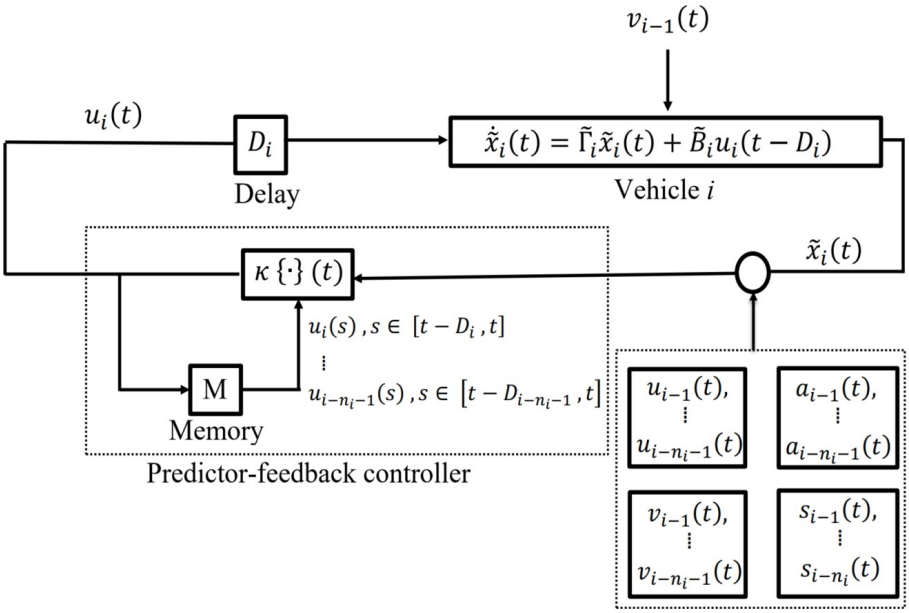

Figure 6.2: Block diagram of the predictor-feedback control design. The operator $\kappa\{\cdot\}$ defines the predictor-feedback law of each ego vehicle that utilizes the available past actuation commands of the ego vehicle and preceding vehicles. Moreover, the right dashed box illustrates all the needed information from the preceding vehicles, which is obtained via onboard sensors and V2V or V2X communication systems.

The predictor-feedback control laws for system (6.1)–(6.3) with

- $D_{i-1} \geq D_i > 0$ are given by

$$u_i(t) = \frac{\tau_i \alpha_i}{h_i} q_{i,1}(t) - \tau_i(\alpha_i + b_i) q_{i,2}(t) + \tau_i b_i q_{i,3}(t) + \tau_i c_i \left(q_{i,5}(t) - q_{i,4}(t)\right), \tag{6.5}$$

$$q_i(t) = \mathrm{e}^{\Gamma_i D_i} x_i(t) + \int_{t-D_i}^{t} \mathrm{e}^{\Gamma_i (t-\theta)} B_i u_i(\theta)\, d\theta + \int_{t-D_{i-1}}^{t-D_{i-1,i}} \mathrm{e}^{\Gamma_i (t-\theta-D_{i-1,i})} B_{1i} u_{i-1}(\theta)\, d\theta, \tag{6.6}$$

where $D_{i-1,i} = D_{i-1} - D_i$ and

$$q_i = \begin{bmatrix} q_{i,1} & q_{i,2} & q_{i,3} & q_{i,4} & q_{i,5} \end{bmatrix}^{\mathrm{T}}, \tag{6.7}$$

$$x_i = \begin{bmatrix} s_i & v_i & v_{i-1} & a_i & a_{i-1} \end{bmatrix}^{\mathrm{T}}, \tag{6.8}$$

$$B_i = \begin{bmatrix} 0 & 0 & 0 & \frac{1}{\tau_i} & 0 \end{bmatrix}^{\mathrm{T}}, \tag{6.9}$$

$$B_{1i} = \begin{bmatrix} 0 & 0 & 0 & 0 & \frac{1}{\tau_{i-1}} \end{bmatrix}^{\mathrm{T}}, \tag{6.10}$$

$$\Gamma_i = \begin{bmatrix} 0 & -1 & 1 & 0 & 0 \\ 0 & 0 & 0 & 1 & 0 \\ 0 & 0 & 0 & 0 & 1 \\ 0 & 0 & 0 & -\frac{1}{\tau_i} & 0 \\ 0 & 0 & 0 & 0 & -\frac{1}{\tau_{i-1}} \end{bmatrix}, \tag{6.11}$$

- $D_i > D_{i-1} > ... > D_{i-n_i}$ and $D_i \leq D_{i-n_i-1}$ are given by [1]

$$u_i(t) = \frac{\tau_i \alpha_i}{h_i} q^i_{i,s_i}(t) - \tau_i(\alpha_i + b_i) q^i_{i,v_i}(t) + \tau_i b_i q^i_{i,v_{i-1}}(t) + \tau_i c_i \left(q^i_{i,a_{i-1}}(t) - q^i_{i,a_i}(t) \right), \tag{6.12}$$

$$q_i^{i-n_i}(t) = \mathrm{e}^{\Gamma_i^{i-n_i} D_{i-n_i}} \bar{x}_i(t) + \int_{t-D_{i-n_i}}^{t} \mathrm{e}^{\Gamma_i^{i-n_i}(t-\theta)} \sum_{m=i-n_i-1}^{i} B_i^m u_m(\theta - D_{m,i-n_i}) d\theta, \tag{6.13}$$

$$\begin{aligned} q_i^{i-n_i+1}(t) =& \mathrm{e}^{\Gamma_i^{i-n_i+1} D_{i-n_i+1,i-n_i}} q_i^{i-n_i}(t) + \int_{t-D_{i-n_i+1,i-n_i}}^{t} \mathrm{e}^{\Gamma_i^{i-n_i+1}(t-\theta)} \\ & \times \left(\sum_{m=i-n_i+1}^{i} B_i^m u_m(\theta - D_{m,i-n_i+1}) + B_i^{i-n_i-1} u_{i-n_i-1}(\theta - D_{i-n_i-1,i-n_i+1}) \right) d\theta, \end{aligned} \tag{6.14}$$

$$\vdots$$

$$q_i^i(t) = \mathrm{e}^{\Gamma_i^i D_{i,i-1}} q_i^{i-1}(t) + \int_{t-D_{i,i-1}}^{t} \mathrm{e}^{\Gamma_i^i(t-\theta)} \left(B_i^i u_i(\theta) + B_i^{i-n_i-1} u_{i-n_i-1}(\theta - D_{i-n_i-1,i}) \right) d\theta, \tag{6.15}$$

[1] We note that each $q_i^{i-n_i+1}$ denotes the predictor state, D_{i-n_i+1} time units in the future, of $\bar{x}_i$.

$$q_i^{i-n_i+m_i} = \begin{bmatrix} q_{i,s_i}^{i-n_i+m_i} \\ q_{i,s_{i-1}}^{i-n_i+m_i} \\ \vdots \\ q_{i,s_{i-n_i}}^{i-n_i+m_i} \\ q_{i,v_i}^{i-n_i+m_i} \\ q_{i,v_{i-1}}^{i-n_i+m_i} \\ \vdots \\ q_{i,v_{i-n_i-1}}^{i-n_i+m_i} \\ q_{i,a_i}^{i-n_i+m_i} \\ q_{i,a_{i-1}}^{i-n_i+m_i} \\ \vdots \\ q_{i,a_{i-n_i-1}}^{i-n_i+m_i} \end{bmatrix}, \quad \bar{x}_i = \begin{bmatrix} s_i \\ s_{i-1} \\ \vdots \\ s_{i-n_i} \\ v_i \\ v_{i-1} \\ \vdots \\ v_{i-n_i-1} \\ a_i \\ a_{i-1} \\ \vdots \\ a_{i-n_i-1} \end{bmatrix}, \tag{6.16}$$

for $m_i = 0, ..., n_i$, where

$$\Gamma_i^{i-n_i} = \left[\begin{array}{c|c|c} \mathbf{0}_{(n_i+1)\times(n_i+1)} & M_{i,1_{(n_i+1)\times(n_i+2)}}^{i-n_i} & \mathbf{0}_{(n_i+1)\times(n_i+2)} \\ \hline \mathbf{0}_{(n_i+2)\times(n_i+1)} & \mathbf{0}_{(n_i+2)\times(n_i+2)} & M_{i,2_{(n_i+2)\times(n_i+2)}}^{i-n_i} \\ \hline \mathbf{0}_{(n_i+2)\times(n_i+1)} & \mathbf{0}_{(n_i+2)\times(n_i+2)} & M_{i,3_{(n_i+2)\times(n_i+2)}}^{i-n_i} \end{array}\right], \tag{6.17}$$

with

$$\begin{aligned} M_{i,1_{(n_i+1)\times(n_i+2)}}^{i-n_i} &= \begin{bmatrix} -1 & 1 & 0 & ... & 0 \\ & \ddots & \ddots & \ddots & \\ 0 & 0 & ... & -1 & 1 \end{bmatrix}, \\ M_{i,2_{(n_i+2)\times(n_i+2)}}^{i-n_i} &= \mathbb{I}_{(n_i+2)\times(n_i+2)}, \\ M_{i,3_{(n_i+2)\times(n_i+2)}}^{i-n_i} &= \begin{bmatrix} -\frac{1}{\tau_i} & 0 & ... & 0 \\ & \ddots & \ddots & \\ 0 & ... & 0 & -\frac{1}{\tau_{i-n_i-1}} \end{bmatrix}, \end{aligned} \tag{6.18}$$

and for $m_i = 0, ..., n_i$,

$$\Gamma_i^{i-n_i+m_i} = \Gamma_i^{i-n_i} + \sum_{j=0}^{m_i-1} B_i^{i-n_i+j} K_i^{i-n_i+j^{\mathrm{T}}}, \tag{6.19}$$

where

$$B_i^{i-n_i+m_i} = \begin{bmatrix} \mathbf{0}_{3n_i-m_i+3} \\ \frac{1}{\tau_{i-n_i+m_i}} \\ \mathbf{0}_{m_i+1} \end{bmatrix}, \quad B_i^i = \begin{bmatrix} \mathbf{0}_{2n_i+3} \\ \frac{1}{\tau_i} \\ \mathbf{0}_{n_i+1} \end{bmatrix}, \tag{6.20}$$

$$K_i^{i-n_i+m_i} = \begin{bmatrix} \mathbf{0}_{n_i-m_i} \\ \frac{\tau_{i-n_i+m_i}\alpha_{i-n_i+m_i}}{h_{i-n_i+m_i}} \\ \mathbf{0}_{m_i} \\ \mathbf{0}_{n_i-m_i} \\ -\tau_{i-n_i+m_i}(\alpha_{i-n_i+m_i} + b_{i-n_i+m_i}) \\ \tau_{i-n_i+m_i}b_{i-n_i+m_i} \\ \mathbf{0}_{m_i} \\ \mathbf{0}_{n_i-m_i} \\ -\tau_{i-n_i+m_i}c_{i-n_i+m_i} \\ \tau_{i-n_i+m_i}c_{i-n_i+m_i} \\ \mathbf{0}_{m_i} \end{bmatrix}, \tag{6.21}$$

- $D_i > D_{i-1} > ... > D_0$ are given by (6.12)–(6.21), where $n_i = i - 1$. In this case, it is necessary for the leader to provide its intentions, i.e., its future input values, $u_0(\theta), \theta \in [t, t + D_i - D_0]$ for each vehicle i, which are viewed as a reference trajectory. This information can be obtained through a combination of V2V and V2X communication. The ability to predict the future behavior of vehicles in practice, is discussed in [36], [40], [52], [54] and it enables the generation of real-time, onboard predictions. Such methods rely on traffic forecasting based on collection of data from a certain number of vehicles ahead via V2V or V2X communication and utilization of various models to predict future maneuvers [52], [54].

6.3 String Stability Despite Distinct Actuation Delays

The velocity is chosen here to perform the string stability analysis, as this is more relevant than spacing errors in the scope of traffic flow performance analysis [50]. Particularly, in heterogeneous platoons with varying time headways h_i, such a definition of string stability

may lead to misleading conclusions regarding platoon performance, as the respective string stability property for each pair of vehicles (that is a desirable property for traffic flow as well) may depend on the controller's parameters of the preceding vehicle, which is not the case here, according to (6.30), when considering string stability in pairs of vehicles with respect to speed errors propagation.

Theorem 6.1: Consider a platoon of vehicles with heterogeneous dynamics modeled by (6.1)–(6.3), under control laws (6.5) with (6.6)–(6.11), or (6.12) with (6.13)–(6.20). For any $D_i \geq 0$, $h_i > 0$, $i = 1, ..., N$, each individual vehicular system is stable and the platoon is $\mathcal{L}_2$ string stable with respect to speed errors propagation provided that the following conditions hold for $i = 1, ..., N$:

$$\frac{1}{\tau_i} + c_i > 0, \tag{6.22}$$

$$\left(\frac{1}{\tau_i} + c_i\right)(\alpha_i + b_i) - \frac{\alpha_i}{h_i} > 0, \tag{6.23}$$

along with

$$\frac{2c_i}{\tau_i} + \frac{1}{\tau_i^2} - 2(\alpha_i + b_i) > 0, \tag{6.24}$$

$$\alpha_i^2 + 2\alpha_i b_i - \frac{2\alpha_i}{h_i \tau_i} > 0, \tag{6.25}$$

or

$$\left(\frac{2c_i}{\tau_i} + \frac{1}{\tau_i^2} - 2(\alpha_i + b_i)\right)^2 - 4\left(\alpha_i^2 + 2\alpha_i b_i - \frac{2\alpha_i}{h_i \tau_i}\right) < 0, \tag{6.26}$$

$$\frac{2c_i}{\tau_i} + \frac{1}{\tau_i^2} - 2(\alpha_i + b_i) < 0. \tag{6.27}$$

Moreover, for a constant leader's speed, zero steady-state spacing and speed tracking errors are achieved.

Remark 6.1: The first two conditions of Theorem 6.1 come from the Routh-Hurwitz criterion and they are a prerequisite for string stability of the platoon. While the remaining two sets of conditions are derived from the string stability criterion in speed error propagation. Feasibility of simultaneous satisfaction of the conditions in Theorem 6.1 is explained noting, for example, that, since b_i and c_i are positive, the first four conditions can be satisfied with a proper, potentially large, choice of α_i, b_i, and c_i. Moreover, a detailed numerical analysis on the selection of control parameters is presented in Figure 6.3. In particular, the region within the red line in Figure 6.3 shows where string stability and

individual stability hold, for transfer function (6.30) with $\tau_1 = 0.18$, $h_1 = 0.7$, and $c_1 = 1$, for different values of α_1 and b_1.

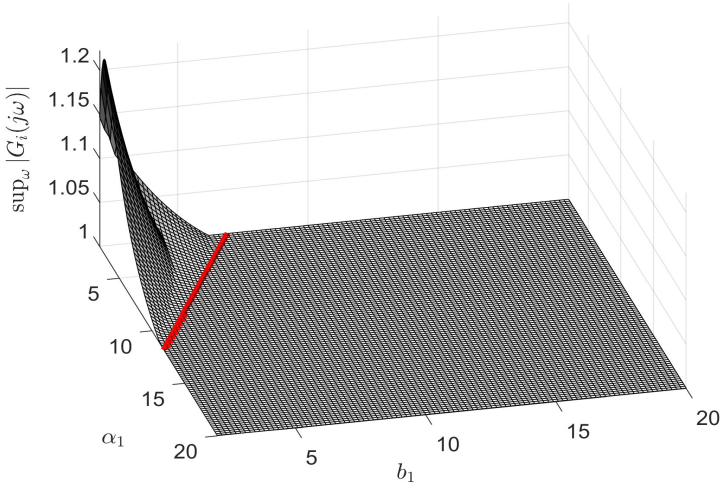

Figure 6.3: The values of function $\sup_\omega |G_i(j\omega)|$ corresponding to (6.30), for different values of α_1 and b_1.

Proof of Theorem 6.1: In order to study stability and string stability of speed errors propagation, we first compute the transfer functions

$$G_i(s) = \frac{V_i(s)}{V_{i-1}(s)}, \tag{6.28}$$

viewing as input the preceding vehicle's speed and as output the current vehicle's speed. Using the delay-compensating property of exact predictor-feedback, namely that $u_i(t) = \tau_i\alpha_i\left(\frac{s_i(t+D_i)}{h_i} - v_i(t+D_i)\right) + \tau_i b_i(v_{i-1}(t+D_i) - v_i(t+D_i)) + \tau_i c_i\left(a_{i-1}(t+D_i) - a_i(t+D_i)\right)$, we have that for $t \geq D_i$ (note that, due to linearity of systems (6.1)–(6.3) and controllers (6.5), no finite escape time phenomenon can appear for $t < D_i$), we recover the nominal closed-loop systems, and thus, it holds that

$$\begin{bmatrix} \dot{s}_i(t) \\ \dot{v}_i(t) \\ \dot{a}_i(t) \end{bmatrix} = \begin{bmatrix} 0 & -1 & 0 \\ 0 & 0 & 1 \\ \frac{a_i}{h_i} & -(a_i + b_i) & -c_i - \frac{1}{\tau_i} \end{bmatrix} \begin{bmatrix} s_i(t) \\ v_i(t) \\ a_i(t) \end{bmatrix} + \begin{bmatrix} 1 \\ 0 \\ b_i \end{bmatrix} v_{i-1}(t) + \begin{bmatrix} 0 \\ 0 \\ c_i \end{bmatrix} a_{i-1}(t). \tag{6.29}$$

Taking Laplace transform of (6.29), after straightforward computations we get

$$G_i(s) = \frac{c_i s^2 + b_i s + \frac{\alpha_i}{h_i}}{s^3 + \left(\frac{1}{\tau_i} + c_i\right) s^2 + (\alpha_i + b_i)\, s + \frac{\alpha_i}{h_i}}. \tag{6.30}$$

Thus, the poles of G_i are on the left half plane under the conditions of Theorem 6.1. String stability in $\mathcal{L}_2$ is guaranteed when $|G_i(j\omega)| \leq 1$, for all $\omega \geq 0$. The condition is satisfied for $\omega = 0$ since $|G_i(0)| = 1$. Moreover, from (6.30) we have

$$G_i(j\omega) = \frac{f_{1,i}(\omega) + jf_{2,i}(\omega)}{f_{3,i}(\omega) + jf_{4,i}(\omega)}, \tag{6.31}$$

$$f_{1,i}(\omega) = -c_i\omega^2 + \frac{\alpha_i}{h_i}, \tag{6.32}$$

$$f_{2,i}(\omega) = b_i\omega, \tag{6.33}$$

$$f_{3,i}(\omega) = -\omega^2\left(\mathrm{c}_i + \frac{1}{\tau_i}\right) + \frac{\alpha_i}{h_i}, \tag{6.34}$$

$$f_{4,i}(\omega) = \omega(\alpha_i + b_i) - \omega^3. \tag{6.35}$$

By using (6.31)–(6.35), the condition for string stability becomes $f_{1,i}(\omega)^2 + f_{2,i}(\omega)^2 < f_{3,i}(\omega)^2 + f_{4,i}(\omega)^2$, $\omega > 0$, for all i, and then we get the following condition that has to hold for all $\omega > 0$ and i

$$\omega^4 + \omega^2 f_{5,i} + f_{6,i} > 0, \tag{6.36}$$

where

$$f_{5,i} = \frac{2c_i}{\tau_i} + \frac{1}{\tau_i^2} - 2(\alpha_i + b_i), \tag{6.37}$$

$$f_{6,i} = \alpha_i^2 + 2\alpha_i b_i - \frac{2\alpha_i}{h_i\tau_i}. \tag{6.38}$$

Using $z = \omega^2$ in relation (6.36), we obtain

$$z^2 + f_{5,i}z + f_{6,i} > 0. \tag{6.39}$$

The relation (6.39) (that is a second-order polynomial in z) holds for all $\omega > 0$, under the conditions on the parameters a_i, b_i, c_i, τ_i, h_i of Theorem 6.1. To see this note that (6.36) holds either when $f_{5,i}$ and $f_{6,i}$ are positive, or when the discriminant of (6.39) is negative, which leads to the mutually exclusive string stability conditions in Theorem 6.1. □

6.4 Illustrative Example

To help the reader better understand the structure/formulae of the exact predictor-feedback CACC design from Section 6.2 we specialize here the design to two cases for

a platoon of three vehicles. We consider the first case of Section 6.2.2 for vehicle 1 with $D_1 \leq D_0$, and the second case of Section 6.2.2 for vehicle 2 with $D_2 > D_1$, $D_2 \leq D_0$ that correspond to $n_2 = 1$ and $m_2 = 0, 1$, which gives the designs

$$u_1(t) = \frac{\tau_1 \alpha_1}{h_1} q_{1,1}(t) - \tau_1(\alpha_1 + b_1) q_{1,2}(t) + \tau_1 b_1 q_{1,3}(t) + \tau_1 c_1 \left(q_{1,4}(t) - q_{1,5}(t)\right), \tag{6.40}$$

with

$$q_1(t) = \mathrm{e}^{\Gamma_1 D_1} x_1(t) + \int_{t-D_1}^{t} \mathrm{e}^{\Gamma_1 (t-\theta)} B_1 u_1(\theta) d\theta + \int_{t-D_0}^{t-D_{0,1}} \mathrm{e}^{\Gamma_1 (t-\theta-D_{0,1})} B_{11} u_0(\theta) d\theta, \tag{6.41}$$

$$q_1 = \begin{bmatrix} q_{1,1} & q_{1,2} & q_{1,3} & q_{1,4} & q_{1,5} \end{bmatrix}^{\mathrm{T}}, \tag{6.42}$$

$$x_1 = \begin{bmatrix} s_1 & v_1 & v_0 & a_1 & a_0 \end{bmatrix}^{\mathrm{T}}, \tag{6.43}$$

$$B_1 = \begin{bmatrix} 0 & 0 & 0 & \frac{1}{\tau_1} & 0 \end{bmatrix}^{\mathrm{T}}, \quad B_{11} = \begin{bmatrix} 0 & 0 & 0 & 0 & \frac{1}{\tau_0} \end{bmatrix}^{\mathrm{T}}, \tag{6.44}$$

$$\Gamma_1 = \begin{bmatrix} 0 & -1 & 1 & 0 & 0 \\ 0 & 0 & 0 & 1 & 0 \\ 0 & 0 & 0 & 0 & 1 \\ 0 & 0 & 0 & -\frac{1}{\tau_1} & 0 \\ 0 & 0 & 0 & 0 & -\frac{1}{\tau_0}, \end{bmatrix}, \tag{6.45}$$

and

$$u_2(t) = \frac{\tau_2 \alpha_2}{h_2} q^2_{2,s_2}(t) - \tau_2(\alpha_2 + b_2) q^2_{2,v_2}(t) + \tau_2 b_2 q^2_{2,v_1}(t) + \tau_2 c_2 \left(q^2_{2,a_1}(t) - q^2_{2,a_2}(t)\right), \tag{6.46}$$

with

$$q_2^1(t) = \mathrm{e}^{\Gamma_2^1 D_1} \bar{x}_2(t) + \int_{t-D_1}^{t} \mathrm{e}^{\Gamma_2^1 (t-\theta)} \sum_{m=0}^{2} B_2^m u_m(\theta - D_{m,1}) d\theta, \tag{6.47}$$

$$q_2^2(t) = \mathrm{e}^{\Gamma_2^2 D_{2,1}} q_2^1(t) + \int_{t-D_{2,1}}^{t} \mathrm{e}^{\Gamma_2^2 (t-\theta)} \left(B_2^2 u_2(\theta) + B_2^0 u_0(\theta - D_{0,2})\right) d\theta, \tag{6.48}$$

$$q_2^2 = \begin{bmatrix} q^2_{2,s_2} & q^2_{2,s_1} & q^2_{2,v_2} & q^2_{2,v_1} & q^2_{2,v_0} & q^2_{2,a_2} & q^2_{2,a_1} & q^2_{2,a_0} \end{bmatrix}, \tag{6.49}$$

$$q_2^1 = \begin{bmatrix} q^1_{2,s_2} & q^1_{2,s_1} & q^1_{2,v_2} & q^1_{2,v_1} & q^1_{2,v_0} & q^1_{2,a_2} & q^1_{2,a_1} & q^1_{2,a_0} \end{bmatrix}, \tag{6.50}$$

$$\bar{x}_2 = \begin{bmatrix} s_2 & s_1 & v_2 & v_1 & v_0 & a_2 & a_1 & a_0 \end{bmatrix}, \tag{6.51}$$

where

$$\Gamma_2^1 = \left[\begin{array}{c|c|c} \mathbf{0}_{2\times 2} & M_{2,1}^1 & \mathbf{0}_{2\times 3} \\ \hline \mathbf{0}_{3\times 2} & \mathbf{0}_{3\times 3} & M_{2,2}^1 \\ \hline \mathbf{0}_{3\times 2} & \mathbf{0}_{3\times 3} & M_{2,3}^1 \end{array}\right], \tag{6.52}$$

$$M_{2,1}^1 = \begin{bmatrix} -1 & 1 & 0 \\ 0 & -1 & 1 \end{bmatrix}, \quad M_{2,2}^1 = \begin{bmatrix} 1 & 0 & 0 \\ 0 & 1 & 0 \\ 0 & 0 & 1 \end{bmatrix}, \tag{6.53}$$

$$M_{2,3}^1 = \begin{bmatrix} -\frac{1}{\tau_2} & 0 & 0 \\ 0 & -\frac{1}{\tau_1} & 0 \\ 0 & 0 & -\frac{1}{\tau_0} \end{bmatrix}, \tag{6.54}$$

$$B_2^0 = \begin{bmatrix} 0 & 0 & 0 & 0 & 0 & 0 & 0 & \frac{1}{\tau_0} \end{bmatrix}^{\mathrm{T}}, \tag{6.55}$$

$$B_2^1 = \begin{bmatrix} 0 & 0 & 0 & 0 & 0 & 0 & \frac{1}{\tau_1} & 0 \end{bmatrix}^{\mathrm{T}}, \tag{6.56}$$

$$B_2^2 = \begin{bmatrix} 0 & 0 & 0 & 0 & 0 & \frac{1}{\tau_2} & 0 & 0 \end{bmatrix}^{\mathrm{T}}, \tag{6.57}$$

and

$$\Gamma_2^2 = \Gamma_2^1 + B_2^1 K_2^{1^{\mathrm{T}}}, \tag{6.58}$$

where

$$K_2^{1^{\mathrm{T}}} = \begin{bmatrix} 0 & \frac{\tau_1\alpha_1}{h_1} & 0 & -\tau_1(\alpha_1 + b_1) & \tau_1 b_1 & 0 & -\tau_1 c_1 & \tau_1 c_1 \end{bmatrix}. \tag{6.59}$$

Next, we consider a scenario with $D_2 > D_1 > D_0$, $n_2 = 1$, $m_2 = 0, 1$, $n_1 = 0$, and $m_1 = 0$. We specialize the design from the third case of Section 6.2.2, which, essentially, is the design (6.40)–(6.59), but with additionally utilizing the leader's intentions. Specifically, $D_2 - D_1$ and $D_1 - D_0$ time units ahead intentions are used for vehicles 2 and 1, respectively. In order to help the reader to better understand the construction of the exact predictor-feedback CACC laws we review next the main premises for their derivation from [6].

We review here the basic ideas of predictor-feedback for multi-input systems with distinct input delays from [6], for a platoon with one leader and two following vehicles with dynamics described by (6.1)–(6.3). The main idea is to replace the states x_i and $\bar{x}_i$ (defined in (6.8) and (6.16), respectively), in the nominal CACC laws (6.4), by their predictors over a D_i-time-unit horizon, namely signals $x_i(t + D_i)$ and $\bar{x}_i(t + D_i)$, respectively. For vehicle 1, with $D_1 \leq D_0$ that corresponds to the first case of Section 6.2.2, we have for

the dynamics of $q_1(\theta) = x_1(\theta + D_1)$ that

$$\frac{dq_1(\theta)}{d\theta} = \Gamma_1 q_1(\theta) + B_1 u_1(\theta) + B_{11} u_0(\theta - D_{0,1}), \theta \in [t - D_1, t]. \tag{6.60}$$

For vehicle 2, with $D_2 > D_1$, $D_2 \leq D_0$ that corresponds to the second case of Section 6.2.2 with $n_2 = 1$ and $m_2 = 0, 1$, the dynamics of $q_2^1(\theta) = \bar{x}_2(\theta + D_1)$ and $q_2^2(\theta) = \bar{x}_2(\theta + D_2)$ can be written as

$$\frac{dq_2^1(\theta)}{d\theta} = \Gamma_2^1 q_2^1(\theta) + \sum_{i=0}^{2} B_2^i u_i(\theta - D_{i,1}), \quad \theta \in [t - D_1, t], \tag{6.61}$$

$$\frac{dq_2^2(\theta)}{d\theta} = \left(\Gamma_2^1 + B_2^1 K_2^{1^T}\right) q_2^2(\theta) + B_2^0 u_0(\theta - D_{0,2}) + B_2^2 u_2(\theta), \theta \in [t - D_{2,1}, t], \tag{6.62}$$

where in (6.62) the term $B_2^1 K_2^{1^{\mathrm{T}}}$ comes from employment of relation $u_1(\theta + D_{2,1}) = K_2^{1^{\mathrm{T}}} q_2^1(\theta + D_{2,1}) = K_2^{1^{\mathrm{T}}} \bar{x}_2(\theta + D_2) = K_2^{1^{\mathrm{T}}} q_2^2(\theta), \theta \geq -D_{2,1}$. The predictor-feedback laws then are derived by integrating the resulting ODEs in θ given in (6.60)–(6.62) for initial conditions $q_1(t - D_1) = x_1(t)$, $q_2^1(t - D_1) = \bar{x}_1(t)$, and $q_2^2(t - D_{2,1}) = q_2^1(t)$.

6.5 Simulation Results

In this section, the performance of the delay-compensating CACC design from Section 6.2.2 is demonstrated, followed by a comparison with the predictor-based CACC approach in [53]. We further validate performance using real traffic data taken from [33] and [37].

Note that implementation of the proposed controllers requires only past values of control inputs, which can be stored in the vehicle's on-board CPU. The control signal is then computed through an inner product operation, reducing the computational burden. In this study, third-order models for vehicles' dynamics, as described in (6.1)–(6.3), are implemented using the Euler method. Moreover, integrals in the predictor-feedback controller are computed using the trapezoidal rule. The rest of the simulation parameters are identical to those from Chapter 3.5.

6.5.1 Exact Predictor-Feedback CACC Design with Leader's Intention

We consider a heterogeneous platoon of eight vehicles with third-order dynamics given by (6.1)–(6.3). We consider a case in which $\tau_0 = 0.25$, $\tau_1 = 0.18$, $\tau_2 = 0.17$, $\tau_3 = 0.2$, $\tau_4 = 0.16$, $\tau_5 = 0.17$, $\tau_6 = 0.2$, $\tau_7 = 0.16$; the desired time-headways are $h_1 = 0.7$, $h_2 = 0.6$, $h_3 = 0.6$, $h_4 = 0.7$, $h_5 = 0.8$, $h_6 = 0.8$, $h_7 = 0.8$; actuation delays are

$D_0 = 0$, $D_1 = 0.3$, $D_2 = 0.6$, $D_3 = 0.7$, $D_4 = 1.0$, $D_5 = 0.8$, $D_6 = 0.5$, $D_7 = 0.3$. In addition, to make the scenario more realistic, we incorporate communication delays in the transmission of information from each vehicle i to the following vehicles with values $D_{0,\mathrm{c}} = 0.01$, $D_{1,\mathrm{c}} = 0.03$, $D_{2,\mathrm{c}} = 0.02$, $D_{3,\mathrm{c}} = 0.04$, $D_{4,\mathrm{c}} = 0.02$, $D_{5,\mathrm{c}} = 0.01$, and $D_{6,\mathrm{c}} = 0.03$, which are based on experimentally validated data [22], [23]. We choose control gains $\alpha_i = 15$, $b_i = 5$, and $c_i = 1$ for $i = 1, 2, 3, 4, 5, 6, 7$. Initial conditions are $v_{i_0} = 15\left(\frac{m}{s}\right)$, $i = 1, 2, 3, 4, 5, 6, 7$, $v_{0_0} = 13\left(\frac{m}{s}\right)$; $s_{i_0} = h_i v_{i_0}\ m$, $i = 1, 2, 3, 4, 5, 6, 7$; $a_{i_0} = 0$, and $u_{i_0} \equiv 0$, for $i = 1, 2, 3, 4, 5, 6, 7$. The first five vehicles, as discussed in the third case of Section 6.2.2, require knowledge of the leader's intention for control implementation. This information could be transmitted to all following vehicles, for example, via a V2X communication setup, see, e.g., [52]. In particular, each following vehicle utilizes the $D_{i,0}$-horizon ahead values of the leader's control input for its computations. The last three vehicles in the platoon correspond to the configuration described in the first case of Section 6.2.2, which requires information only from the immediately preceding vehicle. Figure 6.4 demonstrates the effectiveness, due to deceleration or acceleration maneuvers performed by the leader, of the predictor-feedback CACC law under distinct actuation and communication delays, maintaining $\mathcal{L}_2$ string stability. As shown in Figure 6.5, by utilizing the leader vehicle's intentions to implement each control law, vehicles 1, 2, 3, 4 responds $D_{i,0}$ time units earlier than the onset of the leader's maneuver. In particular, vehicle 2 responds earlier than vehicle 1, even if vehicle 1 is immediately behind the leader.

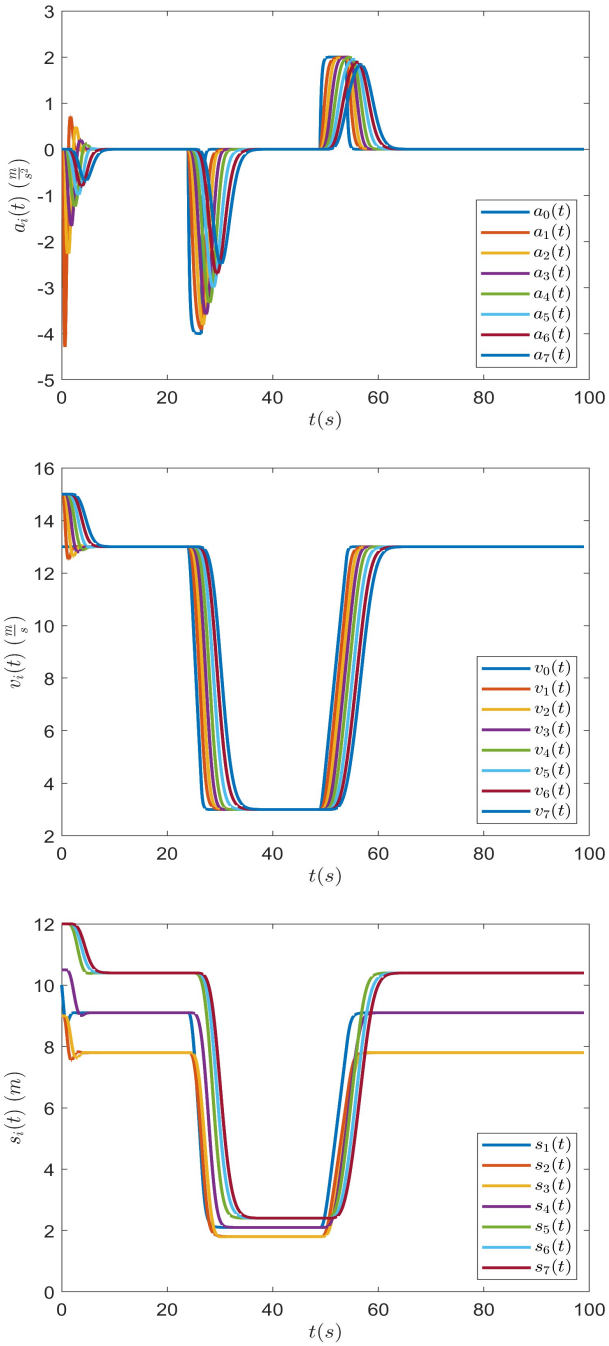

Figure 6.4: Acceleration (top), speed (middle), and spacing (bottom) of seven vehicles following a leader, with dynamics described by (6.1)–(6.3), under the predictor-feedback control laws from Section 6.2.2 in which $\tau_0 = 0.25$, $\tau_1 = 0.18$, $\tau_2 = 0.17$, $\tau_3 = 0.2$, $\tau_4 = 0.16$, $\tau_5 = 0.17$, $\tau_6 = 0.2$, $\tau_7 = 0.16$; the desired time-headways are $h_1 = 0.7$, $h_2 = 0.6$, $h_3 = 0.6$, $h_4 = 0.7$, $h_5 = 0.8$, $h_6 = 0.8$, $h_7 = 0.8$; actuation delays are $D_0 = 0$, $D_1 = 0.3$, $D_2 = 0.6$, $D_3 = 0.7$, $D_4 = 1.0$, $D_5 = 0.8$, $D_6 = 0.5$, $D_7 = 0.3$; and communication delays are $D_{0,\mathrm{c}} = 0.01$, $D_{1,\mathrm{c}} = 0.03$, $D_{2,\mathrm{c}} = 0.02$, $D_{3,\mathrm{c}} = 0.04$, $D_{4,\mathrm{c}} = 0.02$, $D_{5,\mathrm{c}} = 0.01$, $D_{6,\mathrm{c}} = 0.03$. We choose control gains $\alpha_i = 15$, $b_i = 5$, and $c_i = 1$ for $i = 1, 2, 3, 4, 5, 6, 7$. Initial conditions are $v_{i_0} = 15\left(\frac{m}{s}\right)$, $i = 1, 2, 3, 4, 5, 6, 7$, $v_{0_0} = 13\left(\frac{m}{s}\right)$; $s_{i_0} = h_i v_{i_0}\ m$, $i = 1, 2, 3, 4, 5, 6, 7$; $a_{i_0} = 0$, and $u_{i_0} \equiv 0$, for $i = 1, 2, 3, 4, 5, 6, 7$.

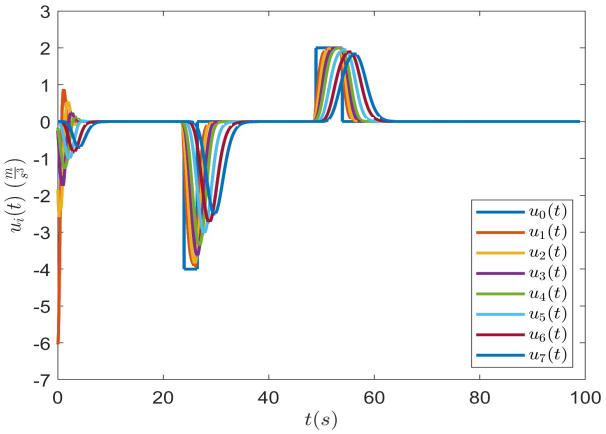

Figure 6.5: Control inputs corresponding to the scenario of Fig. 6.4.

6.5.2 Predictor-Based CACC Design

In Figure 6.6 we show the response of the heterogeneous platoon of three vehicles under the predictor-based CACC law from [53] for system (6.1)–(6.3). We consider the scenario in which τ_i, D_i, h_i, and control gains α_i, b_i, c_i are the same with Section 6.5.1. As evident in Figure 6.6, string stability is not maintained in this scenario (neither of vehicles 1, 2 responses are string stable) and the respective responses exhibit oscillations. This is due to the large differences in delay values among each pair of vehicles, making it impossible to find control gains for the control design from [53] that satisfy the string stability conditions for the scenario in Section 6.5.1.

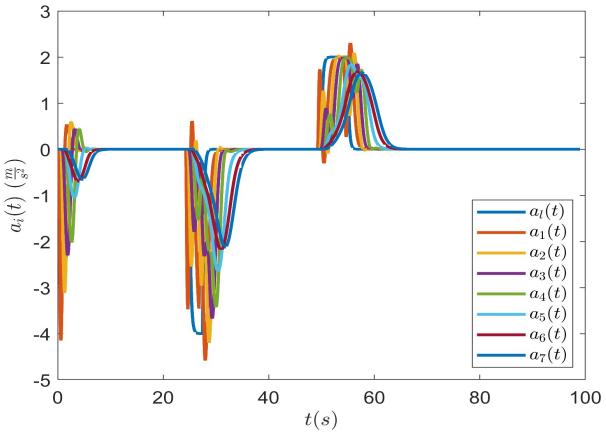

Figure 6.6: Acceleration of seven vehicles following a leader, with dynamics described by (6.1)–(6.3), under the predictor-based control laws in [53]. Control/model parameters and initial conditions are as in Figure 4.3.

6.5.3 Robustness of String Stability of Predictor-Feedback CACC to Parameters Mismatches

The next scenario considers uncertainty in the actuation delays and time constants, in order to further assess the robustness of string stability under the proposed predictor-feedback CACC design. We adopt the same parameters as in Figure 6.4, representing the actual characteristics of the vehicles in the platoon. However, discrepancies in the control design parameters (available to the designers) are introduced, reflecting the imperfect reception of information by the ego vehicle. In this case, we consider $\tau_{0,\mathrm{r}} = 0.24$, $\tau_{1,\mathrm{r}} = 0.2$, $\tau_{2,\mathrm{r}} = 0.15$, $\tau_{3,\mathrm{r}} = 0.19$, $\tau_{4,\mathrm{r}} = 0.17$, $\tau_{5,\mathrm{r}} = 0.16$, $\tau_{6,\mathrm{r}} = 0.18$, $\tau_{7,\mathrm{r}} = 0.17$; actuation delays are $D_{0,\mathrm{r}} = 1.0$, $D_{1,\mathrm{r}} = 0.25$, $D_{2,\mathrm{r}} = 0.55$, $D_{3,\mathrm{r}} = 0.60$, $D_{4,\mathrm{r}} = 0.93$, $D_{5,\mathrm{r}} = 0.77$, $D_{6,\mathrm{r}} = 0.46$, $D_{7,\mathrm{r}} = 0.28$. The respective responses are shown in Figure 6.7. The results indicate that, although small parameter mismatches introduce oscillations, both stability and string stability are preserved, as evidenced by the absence of overshoot in the velocity responses.

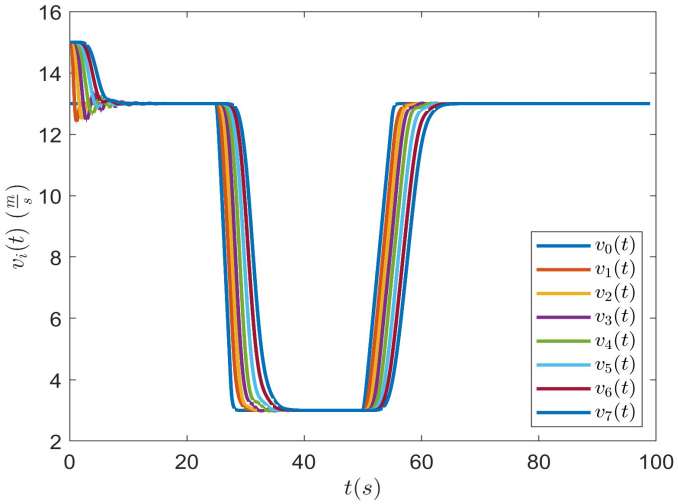

Figure 6.7: Speed of seven vehicles following a leader, with dynamics described by (6.1)–(6.3), under the predictor-feedback control laws from Section 6.2.2 for parameters and initial conditions as in Figure 6.4. The parameters available to the designers are $\tau_{0,\mathrm{r}} = 0.24$, $\tau_{1,\mathrm{r}} = 0.2$, $\tau_{2,\mathrm{r}} = 0.15$, $\tau_{3,\mathrm{r}} = 0.19$, $\tau_{4,\mathrm{r}} = 0.17$, $\tau_{5,\mathrm{r}} = 0.16$, $\tau_{6,\mathrm{r}} = 0.18$, $\tau_{7,\mathrm{r}} = 0.17$, $D_{0,\mathrm{r}} = 1.0$, $D_{1,\mathrm{r}} = 0.25$, $D_{2,\mathrm{r}} = 0.55$, $D_{3,\mathrm{r}} = 0.60$, $D_{4,\mathrm{r}} = 0.93$, $D_{5,\mathrm{r}} = 0.77$, $D_{6,\mathrm{r}} = 0.46$, $D_{7,\mathrm{r}} = 0.28$.

6.5.4 Validation with the OpenACC Dataset

We extract reconstructed data from [33] to demonstrate the controller's performance in real maneuvers of the leading vehicle, considering that the leading vehicle's trajectory is taken from the real trajectory of vehicle no. 2 in AstaZero platoon 2. This vehicle's trajectory is selected because it is characterized by several acceleration/deceleration maneuvers. We consider a heterogeneous platoon of three vehicles to clearly illustrate the benefits of (6.5) through a numerical example. For dataset implementation, we assume that the leading vehicle's dynamics satisfy $\dot{v}_{\mathrm{l}}(t) = a_{\mathrm{l}}(t)$ (and not the third-order system (6.1)–(6.3)), and thus, we have to modify slightly the predictor-feedback control law for the first vehicle accordingly. In this case, for implementation of the predictor-feedback law, because only velocity data are available from the OpenACC dataset, we obtain $a_l(t)$ by numerically computing $\dot{v}_l(t)$.

Figure 6.8 illustrates the results of implementing the predictor-feedback CACC, as discussed in Section 6.2.2, on the OpenACC dataset, which confirm the effectiveness of the CACC law developed in practically realistic scenarios. In the present scenario we consider a case in which $\tau_0 = 0.25$, $\tau_1 = 0.18$, $\tau_2 = 0.17$; the desired time-headways are $h_1 = 0.7$, $h_2 = 0.6$; and actuation delays are $D_0 = 0$, $D_1 = 0.3$, $D_2 = 1.0$. Moreover, we choose control gains $\alpha_i = 15$, $b_i = 5$, and $c_i = 1$ for $i = 1, 2$. We set $a_i(0) = 0$ and $u_i(s) = 0$, $s \in [-D_i, 0)$ for vehicles $i = 1, 2$. While we also set $v_{i_0} = 20\left(\frac{m}{s}\right)$, $i = 1, 2$ and $v_{\mathrm{l}_0} = 19.3\left(\frac{m}{s}\right)$ (to match with the initial speed of vehicle no. 2 in AstaZero platoon 2 from the OpenACC dataset); $s_{2_0} = h_2 v_{2_0} = 12$, $s_{1_0} = 14\ m$.

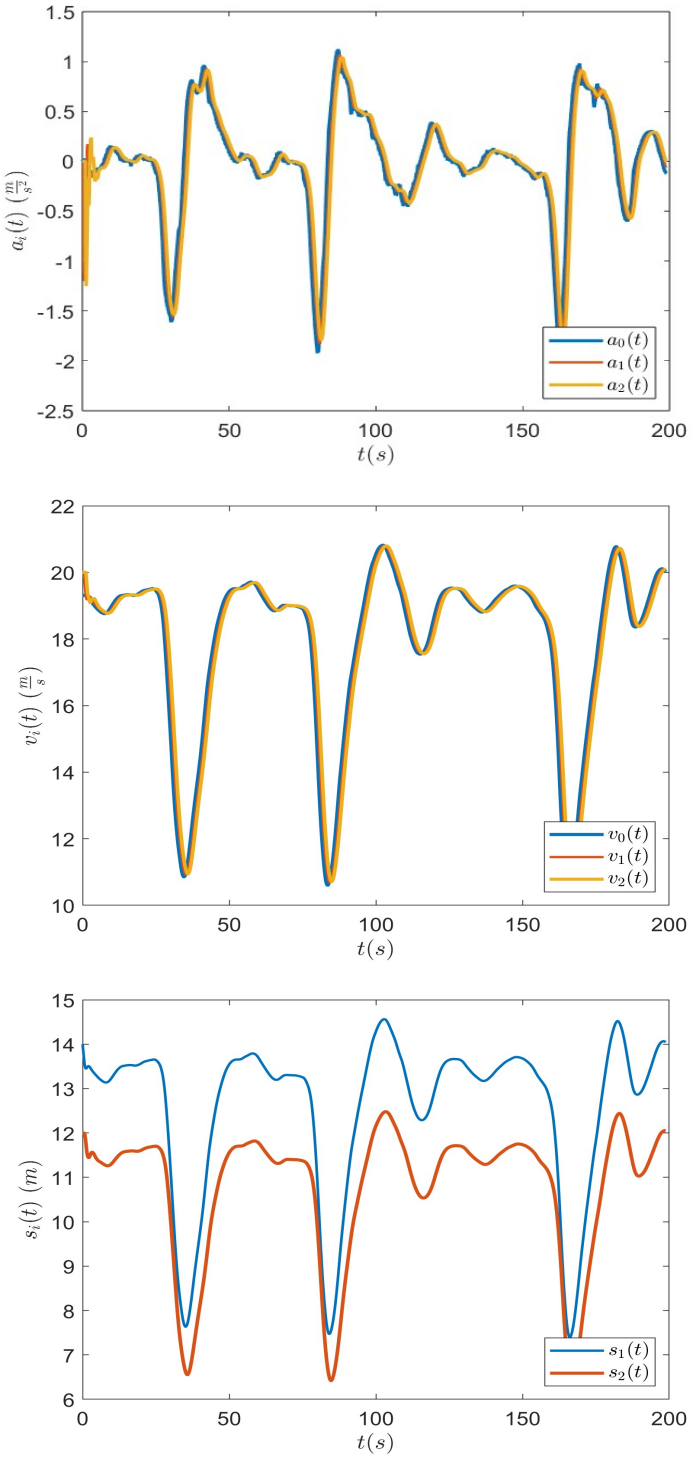

Figure 6.8: Acceleration (top), speed (middle), and spacing (bottom) of two vehicles following a leader, with dynamics described by (6.1)–(6.3), under the predictor-feedback control laws (6.40)–(6.59) in which $\tau_0 = 0.25$, $\tau_1 = 0.18$, $\tau_2 = 0.17$; the desired time-headways are $h_1 = 0.7$, $h_2 = 0.6$; and actuation delays are $D_0 = 0$, $D_1 = 0.3$, $D_2 = 1.0$. We choose control gains $\alpha_i = 15$, $b_i = 5$, and $c_i = 1$ for $i = 1, 2$. The speed (and acceleration) of the leading vehicle is taken from vehicle no. 2 in AstaZero platoon 2 in [33]. Initial conditions are $v_{i_0} = 20\left(\frac{m}{s}\right)$, $i = 1, 2$, $v_{0_0} = 19.3\left(\frac{m}{s}\right)$; $s_{2_0} = h_2 v_{2_0} = 12\ m$, $s_{1_0} = 14\ m$; $a_{i_0} = 0$, and $u_{i_0} \equiv 0$, for $i = 1, 2$.

6.5.5 Validation with NGSIM Dataset

Reconstructed data from [37] are also utilized to evaluate the controller's performance under heavily congested traffic conditions [37], with the leading vehicle's trajectory taken from vehicle no. 1601. We consider here a heterogeneous platoon of six vehicles and, as in the previous scenario, for implementation of the predictor-feedback law, because only velocity data are available from the NGSIM dataset, we obtain $a_l(t)$ by numerically computing $\dot{v}_l(t)$. Considering a larger number of vehicles it may be more illustrative of controller's performance in realistic traffic scenarios, the substance however of the validation, from the stability and string stability viewpoints, is not altered even with a smaller number of vehicles.

In Figure 6.9, we present the results of applying the predictor-feedback CACC law from Section 6.2.2 to the NGSIM dataset. We observe in particular the smoothing effect of our design manifested as reduction in oscillations' magnitudes in the responses, as result of the string stability guarantees. In this scenario, vehicles 1, 2, 3 implement a controller corresponding to the third case of Section 6.2.2 (as the leader's intentions are needed), while vehicles 4, 5 implement a controller corresponding to the first case of Section 6.2.2. The latter is because the following vehicle for vehicles 4 and 5 has a larger delay. In the present scenario we consider a case in which τ_i, time-headways h_i, actuation delays D_i are set according to Table 6.1. Moreover, we choose control gains $\alpha_i = 15$, $b_i = 5$, $c_i = 1$ for vehicles $i = 1, 2, 3, 4, 5$ accordingly. We set $a_i(0) = 0$ and $u_i(s) = 0$, $s \in [-D_i, 0)$ for vehicles $i = 1, 2, 3, 4, 5$. While we also set $v_{i_0} = 16 \left(\frac{m}{s}\right)$, $i = 1, 2, 3, 4, 5$ and $v_{l_0} = 14.9 \left(\frac{m}{s}\right)$ (to match the initial speed of vehicle 1601 from NGSIM data); $s_{i_0} = h_i v_{i_0} = h_i \times 16\ m$, $i = 2, 3, 4, 5$, $s_{1_0} = 11\ m$. Figures 6.8 and 6.9 illustrate that the performance of the predictor-feedback CACC law (6.4) is preserved even in more realistic traffic scenarios and in scenarios of heavily congested conditions.

Table 6.1: Parameters used for the simulation results in Figure 6.9.

Parameters / Vehicle No.	τ_i	h_i	D_i
0	–	–	–
1	0.18 s	0.7 s	0.3 s
2	0.17 s	0.6 s	0.7 s
3	0.2 s	0.8 s	1 s
4	0.25 s	0.6 s	0.8 s
5	0.17 s	0.8 s	0.5 s

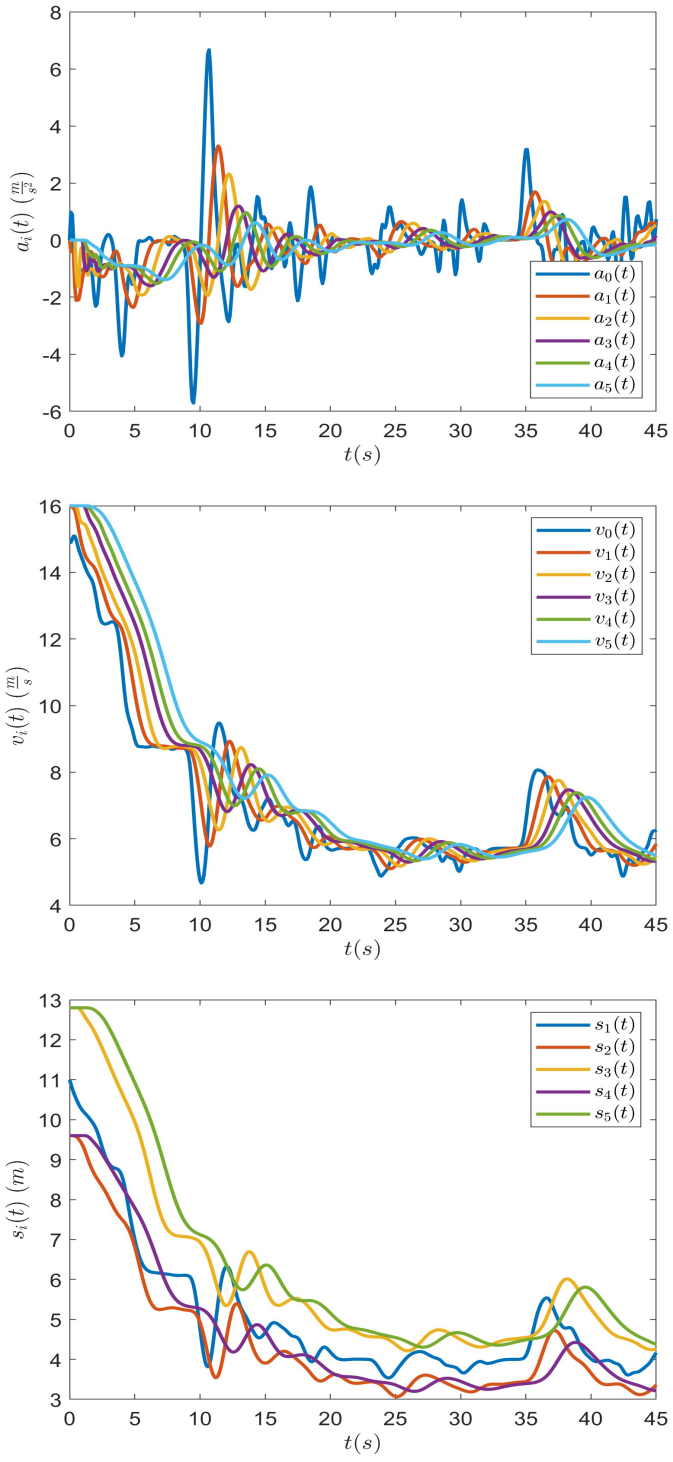

Figure 6.9: Acceleration (top), speed (middle), and spacing (bottom) of six vehicles, with dynamics described by (6.1)–(6.3), under the predictor-feedback control laws (6.5), (6.12), where the selected parameters are shown in Table 6.1. We choose control gains $\alpha_i = 15$, $b_i = 5$, $c_i = 1$ for vehicles $i = 1, 2, 3, 4, 5$. The speed (and acceleration) of the leading vehicle is taken from vehicle no. 1601 in NGSIM in [37]. Initial conditions are $v_{i_0} = 16\left(\frac{m}{s}\right)$, $i = 1, 2, 3, 4, 5$, $v_{l_0} = 14.9\left(\frac{m}{s}\right)$; $s_{i_0} = h_i v_{i_0} = h_i \times 16\ m$, $i = 2, 3, 4, 5$, $s_{1_0} = 11\ m$; $a_{i_0} = 0$, and $u_{i_0} \equiv 0$, for $i = 1, 2, 3, 4, 5$.

6.6 Chapter Conclusions and Related Publications

In the present chapter, we develop a predictor-feedback CACC law to fully compensate long actuation delays in heterogeneous platoons, where vehicles' dynamics are subject to distinct actuator delays. The control design introduced ensures string stability in terms of speed error propagation, individual vehicle stability, and spacing/speed regulation. We present consistent simulation results for a platoon, including a comparison with an existing predictor-based CACC law. Moreover, we provide simulations for realistic scenarios, utilizing real traffic data to model the trajectory of the leading vehicle. A potential limitation of the proposed approach is its reliance on exact knowledge of the delay values and time constants from preceding vehicles. However, the design method is robust to moderate mismatches in the knowledge of these parameters. In addition, another potential limitation is the need for communication of the states of a vehicle to all following vehicles. However, such communication topologies have been employed in existing literature for CACC design, see, e.g., [1], and thus, it can be considered as realistic such information to be available. We further expect that for large-scale platoons, computationally complexity of control implementation to grow. In such cases, an ego vehicle's controller could, in principle, utilize the predictor states computed from preceding vehicles (when these are transmitted to the following vehicles), rather than computing all predictor states required locally, to reduce computational burden.

This chapter is an adaptation of material appearing in

A. Samii and N. Bekiaris-Liberis, "Exact predictor-feedback CACC of heterogeneous vehicular platoons with distinct actuation delays," *IEEE Transactions on Intelligent Transportation Systems*, provisionally accepted, 2025.

A. Samii and N. Bekiaris-Liberis, "On Compensation of Distinct Input Delays in Heterogeneous Vehicular Platoons via Exact Predictor-Feedback CACC," *IFAC Workshop on Time Delay Systems*, Paris, 2025.

Chapter 7

Experimental Implementation and Validation of Predictor-Based CACC for Vehicular Platoons With Distinct Actuation Delays

We provide experimental validation, in a pair of vehicles, of a recently introduced predictor-based cooperative adaptive cruise control (CACC) design, developed for achieving delay compensation in heterogeneous vehicular platoons subject to long actuation delays that may be distinct for each individual vehicle. We provide the explicit formulae of the control design that is implemented, accounting for the effect of zero-order hold and sampled measurements; as well as we obtain vehicle and string stability conditions numerically, via derivation of the transfer functions relating the speeds of pairs of consecutive vehicles. We also present consistent simulation results for a platoon with a larger number of vehicles, under digital implementation of the controller. Both the simulation and experimental results confirm the effectiveness of the predictor-based CACC design in guaranteeing individual vehicle stability, string stability, and tracking, despite long/distinct actuation delays.

7.1 Chapter Organization

In Section 7.2 we present the model considered for control design, together with the basic, continuous predictor-based CACC law; as well as we provide the formulae of our design when it is applied with zero-order hold employing sampled measurements. In Section 7.3 we derive numerical conditions for vehicle and string stability, under digital

implementation of the controller, as well as we present simulation results. In Section 7.4 we present experimental results. We provide concluding remarks in Section 7.5.

7.2 CACC for Heterogeneous Platoons with Distinct Actuation Delays

7.2.1 Vehicle Model and Available Measurements

a) Vehicle dynamics: We consider a heterogeneous string of vehicles (see Figure 7.1) each one modeled by the following third-order, linear system with distinct actuator delays that describes vehicle dynamics (see, e.g., [45], [57], [58])

$$\dot{s}_i(t) = v_{i-1}(t) - v_i(t), \tag{7.1}$$

$$\dot{v}_i(t) = a_i(t), \tag{7.2}$$

$$\dot{a}_i(t) = -\frac{1}{\tau_i} a_i(t) + \frac{1}{\tau_i} u_i(t - D_i), \tag{7.3}$$

where $D_i \geq 0$ are input delays, and $t \geq 0$ is time.

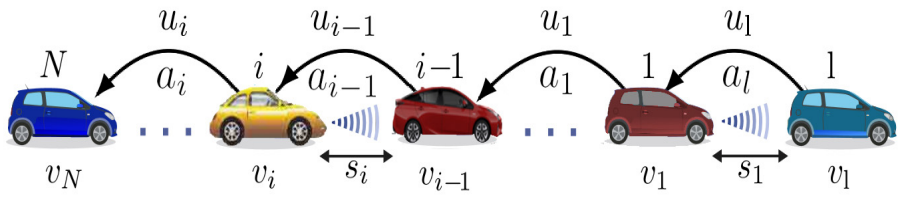

Figure 7.1: Platoon of $N+1$ heterogeneous vehicles following each other in a single lane without overtaking. The dynamics of each vehicle $i = 1, ..., N$ are governed by system (7.1)–(7.3). Each vehicle can measure its own speed, the relative speed with the preceding vehicle, and the spacing with respect to the preceding vehicle. The control input and acceleration of each vehicle is communicated to the following vehicle via V2V communication.

b) Available measurements: For the platoons considered here the measurements available to the ego vehicle i are its own spacing s_i, speed v_i, acceleration a_i, and control input u_i, as well as the speed of the preceding vehicle v_{i-1}. This information is obtained through on-board sensors. Furthermore, the control input of the preceding vehicle and its acceleration are also available, and they are denoted by u_{i-1} and a_{i-1}, respectively. These measurements are transmitted from the preceding vehicle, through vehicle-to-vehicle (V2V)

communication. Note that the speed of the preceding vehicle, v_{i-1}, can also be obtained via V2V communication.

7.2.2 Continuous Predictor-Based CACC Design

a) Nominal control design: Without input delay, the following control strategy is constructed (see, e.g., [1,11])

$$u_i(t) = \tau_i\alpha_i\left(\frac{s_i(t)-r_i}{h_i} - v_i(t)\right) + \tau_i b_i(v_{i-1}(t)-v_i(t)) + \tau_i c_i\left(a_{i-1}(t)-a_i(t)\right), \tag{7.4}$$

where $\alpha_i > 0$, $b_i > 0$, and $c_i \geq 0$ are design parameters, $h_i > 0$ is time-headway, and $r_i > 0$ is inter-vehicle distance at standstill.

b) Predictor-based CACC: The predictor-based control laws for system (7.1)–(7.3) in continuous time are given by (see [53])

$$u_i(t) = \frac{\tau_i\alpha_i}{h_i}q_{i,1}(t) - \tau_i(\alpha_i+b_i)q_{i,2}(t) + \tau_i b_i q_{i,3}(t) + \tau_i c_i\left(q_{i,5}(t)-q_{i,4}(t)\right), \tag{7.5}$$

where

$$q_i(t) = \mathrm{e}^{\Gamma_i D_i}\bar{x}_i(t) + \int_{t-D_i}^{t}\mathrm{e}^{\Gamma_i(t-\theta)}B_i u_i(\theta)\,d\theta + \int_{t-D_{i-1}}^{t}\mathrm{e}^{\Gamma_i(t+D_i-\theta-D_{i-1})}B_{1i}u_{i-1}(\theta)\,d\theta, \tag{7.6}$$

with

$$q_i = \begin{bmatrix} q_{i,1} & q_{i,2} & q_{i,3} & q_{i,4} & q_{i,5}\end{bmatrix}^{\mathrm{T}}, \quad \bar{x}_i = \begin{bmatrix} s_i - r_i & v_i & v_{i-1} & a_i & a_{i-1}\end{bmatrix}^{\mathrm{T}}, \tag{7.7}$$

$$B_i = \begin{bmatrix} 0 & 0 & 0 & \frac{1}{\tau_i} & 0\end{bmatrix}^{\mathrm{T}}, B_{1i} = \begin{bmatrix} 0 & 0 & 0 & 0 & \frac{1}{\tau_{i-1}}\end{bmatrix}^{\mathrm{T}}, \tag{7.8}$$

$$\Gamma_i = \begin{bmatrix} 0 & -1 & 1 & 0 & 0 \\ 0 & 0 & 0 & 1 & 0 \\ 0 & 0 & 0 & 0 & 1 \\ 0 & 0 & 0 & -\frac{1}{\tau_i} & 0 \\ 0 & 0 & 0 & 0 & -\frac{1}{\tau_{i-1}} \end{bmatrix}. \tag{7.9}$$

7.2.3 Predictor-Based CACC Design for Distinct Delays Implemented with Zero-Order Hold

Let $T_s > 0$ be the sampling period, with $D_i \geq 0$ be given and $l_i \in Z^+$ such that $D_i = l_i T_s$. Define the following quantities

$$u_i(t) = u_{i_k}, \quad t \in [kT_s, (k+1)T_s), \quad k \in Z^+, \tag{7.10}$$

$$\bar{x}_{i_k} = \bar{x}_i(kT_s), \tag{7.11}$$

$$\bar{x}_{i,\mathrm{m}_k} = \bar{x}_i(kT_s - D_{\mathrm{c},i}), \tag{7.12}$$

where $D_{\mathrm{c},i} = l_{i,\mathrm{c}} T_s$ is communication delay. Then, the control inputs (7.5) implemented with zero-order-hold are (see also [28])

$$u_{i_k} = \frac{\tau_i \alpha_i}{h_i} q_{i,1_k} - \tau_i(\alpha_i + b_i) q_{i,2_k} + \tau_i b_i q_{i,3_k} + \tau_i c_i \left(q_{i,5_k} - q_{i,4_k} \right), \tag{7.13}$$

$$q_{i_k} = \mathrm{e}^{\Gamma_i D_i} \bar{x}_{i_k} + \sum_{j=1}^{l_i} Q_{i_j} B_i u_{i_{k-j}} + \mathrm{e}^{\Gamma_i (D_i - D_{i-1})} \sum_{j=1}^{l_{i-1}} Q_{i-1_j} B_{1i} u_{i-1,\mathrm{m}_{k-j}}, \tag{7.14}$$

where

$$Q_{i_j} = \mathrm{e}^{\Gamma_i j T_s} \int_0^{T_s} \mathrm{e}^{-\Gamma_i \theta} d\theta, \quad j = 1, ..., l_i, \tag{7.15}$$

$$Q_{i-1_j} = \mathrm{e}^{\Gamma_i j T_s} \int_0^{T_s} \mathrm{e}^{-\Gamma_i \theta} d\theta, \quad j = 1, ..., l_{i-1}, \tag{7.16}$$

and

$$q_{i_k} = \begin{bmatrix} q_{i,1_k} \\ q_{i,2_k} \\ q_{i,3_k} \\ q_{i,4_k} \\ q_{i,5_k} \end{bmatrix}, \quad \bar{x}_{i_k} = \begin{bmatrix} s_{i_k} - r_i \\ v_{i_k} \\ v_{i-1,\mathrm{m}_k} \\ a_{i_k} \\ a_{i-1,\mathrm{m}_k} \end{bmatrix}, \tag{7.17}$$

$$\mathrm{e}^{\Gamma_i D_i} = \begin{bmatrix} 1 & -D_i & D_i & \tau_i^2 - D_i\tau_i - \tau_i^2 \mathrm{e}^{\frac{-D_i}{\tau_i}} & -\tau_{i-1}^2 + D_i\tau_{i-1} - \tau_{i-1}^2 \mathrm{e}^{\frac{-D_i}{\tau_{i-1}}} \\ 0 & 1 & 0 & \tau_i - \tau_i \mathrm{e}^{\frac{-D_i}{\tau_i}} & 0 \\ 0 & 0 & 1 & 0 & \tau_{i-1} - \tau_{i-1} \mathrm{e}^{\frac{-D_i}{\tau_{i-1}}} \\ 0 & 0 & 0 & \mathrm{e}^{\frac{-D_i}{\tau_i}} & 0 \\ 0 & 0 & 0 & 0 & \mathrm{e}^{\frac{-D_i}{\tau_{i-1}}} \end{bmatrix}, \tag{7.18}$$

$$\int_0^{T_s} \mathrm{e}^{-\Gamma_i \theta} d\theta =$$
$$\begin{bmatrix} T_s & \frac{T_s^2}{2} & -\frac{T_s^2}{2} & \frac{\tau_i}{2}\left(T_s^2+2T_s\tau_i-2\left(-1+\mathrm{e}^{\frac{T_s}{\tau_i}}\right)\tau_i^2\right) & \frac{\tau_{i-1}}{2}\left(T_s^2+2T_s\tau_{i-1}-2\left(-1+\mathrm{e}^{\frac{T_s}{\tau_{i-1}}}\right)\tau_{i-1}^2\right) \\ 0 & T_s & 0 & \tau_i\left(T_s+\tau_i-\tau_i\mathrm{e}^{\frac{T_s}{\tau_i}}\right) & 0 \\ 0 & 0 & T_s & 0 & \tau_{i-1}\left(T_s+\tau_{i-1}-\tau_{i-1}\mathrm{e}^{\frac{T_s}{\tau_{i-1}}}\right) \\ 0 & 0 & 0 & \tau_i\left(-1+\mathrm{e}^{\frac{T_s}{\tau_i}}\right) & 0 \\ 0 & 0 & 0 & 0 & \tau_{i-1}\left(-1+\mathrm{e}^{\frac{T_s}{\tau_{i-1}}}\right) \end{bmatrix}. \tag{7.19}$$

7.3 Numerical Investigation of String Stability in Discrete Time And Simulation Results

We start providing the definition of string stability employed in this chapter. A platoon of vehicles indexed by $i = 1, ..., N$, following each other within one lane without overtaking, is $\mathcal{L}_2$ string stable with reference to speed errors if the following condition holds (see, e.g., [39])

$$\sup_{\omega} |G_i\left(\mathrm{e}^{j\omega T_s}\right)| \leq 1, \qquad i = 1, ..., N, \tag{7.20}$$

where $G_i\left(\mathrm{e}^{j\omega T_s}\right)$ denotes the transfer function between the i-th vehicle's speed and the speed of its preceding vehicle $i-1$. Here we study $\mathcal{L}_2$ string stability with respect to speed errors propagation, as this is the most commonly used definition, see, for example, [12, 19, 21, 62]. Based on $G_i(z) = \frac{V_i(z)}{V_{i-1}(z)}$ we perform numerical studies to investigate the range of control parameters for which vehicle and string stability hold, also depending on the sampling period T_s. We next derive $G_i(z)$

In order to study string stability of speed errors propagation, we first recall the $\hat{G}_i(s)$ from [53], which is given by

$$\hat{G}_i(s) = \frac{\delta_i(s)}{s^3 + \left(\frac{1}{\tau_i} + c_i\right)s^2 + (\alpha_i + b_i)s + \frac{\alpha_i}{h_i}}, \tag{7.21}$$

where

$$\delta_i(s) = \mathrm{e}^{-(D_i-D_{i-1})s}\left(\left(\frac{\alpha_i}{h_i}\tau_{i-1}\left(D_i-D_{i-1}\right)+b_i\tau_{i-1}-\frac{\alpha_i}{h_i}\tau_{i-1}^2 + \mathrm{e}^{-\frac{(D_i-D_{i-1})}{\tau_{i-1}}}\left(\frac{\alpha_i}{h_i}\tau_{i-1}^2-b_i\tau_{i-1}+c_i\right)\right)s^2+\left(\left(D_i-D_{i-1}\right)\frac{\alpha_i}{h_i}+b_i\right)s+\frac{\alpha_i}{h_i}\right). \tag{7.22}$$

Then by applying Tustin approximation [26] and substituting $s = \frac{2}{T_s}\frac{z-1}{z+1}$, we derive its discrete-time counterpart

$$G_i(z) = z^{-(l_i-l_{i-1})}\frac{f_{1,i}z^3+f_{2,i}z^2+f_{3,i}z+f_{4,i}}{g_{1,i}z^3+g_{2,i}z^2+g_{3,i}z+g_{4,i}}, \tag{7.23}$$

where

$$\begin{aligned}
f_{1,i} =& 4\left(\frac{\alpha_i}{h_i}\tau_{i-1}\left(D_i-D_{i-1}\right)+b_i\tau_{i-1}-\frac{\alpha_i}{h_i}\tau_{i-1}^2+\mathrm{e}^{-\frac{(D_i-D_{i-1})}{\tau_{i-1}}}\left(\frac{\alpha_i}{h_i}\tau_{i-1}^2-b_i\tau_{i-1}+c_i\right)\right)\\
&\times h_i\tau_i T_s+2\left(\left(D_i-D_{i-1}\right)\frac{\alpha_i}{h_i}+b_i\right)h_i\tau_i T_s^2+\alpha_i\tau_i T_s^3, &(7.24)\\
f_{2,i} =& -4\left(\frac{\alpha_i}{h_i}\tau_{i-1}\left(D_i-D_{i-1}\right)+b_i\tau_{i-1}-\frac{\alpha_i}{h_i}\tau_{i-1}^2+\mathrm{e}^{-\frac{(D_i-D_{i-1})}{\tau_{i-1}}}\left(\frac{\alpha_i}{h_i}\tau_{i-1}^2-b_i\tau_{i-1}+c_i\right)\right)\\
&\times h_i\tau_i T_s+2\left(\left(D_i-D_{i-1}\right)\frac{\alpha_i}{h_i}+b_i\right)h_i\tau_i T_s^2+3\alpha_i\tau_i T_s^3, &(7.25)\\
f_{3,i} =& -4\left(\frac{\alpha_i}{h_i}\tau_{i-1}\left(D_i-D_{i-1}\right)+b_i\tau_{i-1}-\frac{\alpha_i}{h_i}\tau_{i-1}^2+\mathrm{e}^{-\frac{(D_i-D_{i-1})}{\tau_{i-1}}}\left(\frac{\alpha_i}{h_i}\tau_{i-1}^2-b_i\tau_{i-1}+c_i\right)\right)\\
&\times h_i\tau_i T_s-2\left(\left(D_i-D_{i-1}\right)\frac{\alpha_i}{h_i}+b_i\right)h_i\tau_i T_s^2+3\alpha_i\tau_i T_s^3, &(7.26)\\
f_{4,i} =& 4\left(\frac{\alpha_i}{h_i}\tau_{i-1}\left(D_i-D_{i-1}\right)+b_i\tau_{i-1}-\frac{\alpha_i}{h_i}\tau_{i-1}^2+\mathrm{e}^{-\frac{(D_i-D_{i-1})}{\tau_{i-1}}}\left(\frac{\alpha_i}{h_i}\tau_{i-1}^2-b_i\tau_{i-1}+c_i\right)\right)\\
&\times h_i\tau_i T_s-2\left(\left(D_i-D_{i-1}\right)\frac{\alpha_i}{h_i}+b_i\right)h_i\tau_i T_s^2+\alpha_i\tau_i T_s^3, &(7.27)\\
g_{1,i} =& 8h_i\tau_i+4h_iT_s+4c_ih_i\tau_iT_s+2\alpha_ih_i\tau_iT_s^2+2b_ih_i\tau_iT_s^2+\alpha_i\tau_iT_s^3, &(7.28)\\
g_{2,i} =& -24h_i\tau_i-4h_iT_s-4c_ih_i\tau_iT_s+2\alpha_ih_i\tau_iT_s^2+2b_ih_i\tau_iT_s^2+3\alpha_i\tau_iT_s^3, &(7.29)\\
g_{3,i} =& 24h_i\tau_i-4h_iT_s-4c_ih_i\tau_iT_s-2\alpha_ih_i\tau_iT_s^2-2b_ih_i\tau_iT_s^2+3\alpha_i\tau_iT_s^3, &(7.30)\\
g_{4,i} =& -8h_i\tau_i+4h_iT_s+4c_ih_i\tau_iT_s-2\alpha_ih_i\tau_iT_s^2-2b_ih_i\tau_iT_s^2+\alpha_i\tau_iT_s^3. &(7.31)
\end{aligned}$$

7.3.1 Choice of Control Parameters

We numerically analyze the $\mathcal{L}_2$ string stability properties of the closed-loop system concerning the propagation of speed errors. The transfer function $G_i(z)$ we consider, shown

in (7.23), corresponds to the closed-loop transfer function obtained in [53] and displayed in (7.21) (for the reader's convenience) after applying the Tustin approximation [26]. This is only an approximation of the actual transfer function one obtains in a closed-loop system consisting of (7.1)–(7.3), subject to zero-order hold, under (7.13)–(7.19). We use it however for simplicity as derivation of the actual transfer function would result in a quite complicated expression, which would make it quite difficult to obtain string stability conditions even numerically. The top plot of Figure 7.2 depicts $\sup_\omega |G_1(\mathrm{e}^{j\omega T_s})|$ as a function of α_1 and b_1 for choices of parameters corresponding to vehicles 0, 1 from Table 7.1. The region between the red lines indicates where $\mathcal{L}_2$ string stability holds. In addition, the bottom plot of Figure 7.2 demonstrates $\sup_\omega |G_1(\mathrm{e}^{j\omega T_s})|$ as a function of $D_1 - D_0$.

We note that for vehicle stability, under the zero-order hold implementation (7.13)–(7.19), we can use the condition in Corollary 3.4 from [17], which gives the (exact) condition that the eigenvalues of matrix

$$\mathrm{e}^{\bar{A}_i T_s}\left(I + \int_0^{T_s} \mathrm{e}^{-\bar{A}_i w} dw \bar{B}_i \bar{K}_i\right), \tag{7.32}$$

are within the unit circle, where

$$\bar{A}_i = \begin{bmatrix} 0 & -1 & 0 \\ 0 & 0 & 1 \\ 0 & 0 & -\frac{1}{\tau_i} \end{bmatrix}, \quad \bar{B}_i = \begin{bmatrix} 0 \\ 0 \\ \frac{1}{\tau_i} \end{bmatrix}, \tag{7.33}$$

$$\bar{K}_i = \begin{bmatrix} \tau_i \frac{\alpha_i}{h_i} & -\tau_i(\alpha_i + b_i) & -\tau_i c_i \end{bmatrix}. \tag{7.34}$$

This holds for the model/control parameters in Table 7.1. Furthermore, for the control/model parameters of vehicle 1, we show in Figure 7.3 the magnitude of the maximum eigenvalue of matrix (7.32) as function of T_s. We observe that vehicle stability is preserved for $T_s < 1.67$.

7.3.2 Simulation Results

For a platoon of five vehicles with third-order dynamics given by (7.1)–(7.3), we consider a case with parameters in Tables 7.1 and 7.2 taken from [21,22,53]. We consider a scenario in which $a_i(0) = 0$; $u_i(s) \equiv 0$, for each vehicle i. In Figure 7.4 we set $v_{i_0} = 10\left(\frac{m}{s}\right)$ and $v_{l_0} = 9\left(\frac{m}{s}\right)$; $s_{i_0} = h_i v_{i_0} + r_i\ (m)$ and $s_{1_0} = 9.5 + r_1\ (m)$. Additionally, we add noise to all measurements of acceleration, velocity, spacing, and control input of preceding vehicle, to more closely emulate experimental implementations. We observe that the platoon is $\mathcal{L}_2$ string stable, but it may not necessarily be $\mathcal{L}_\infty$ string stable, which may result

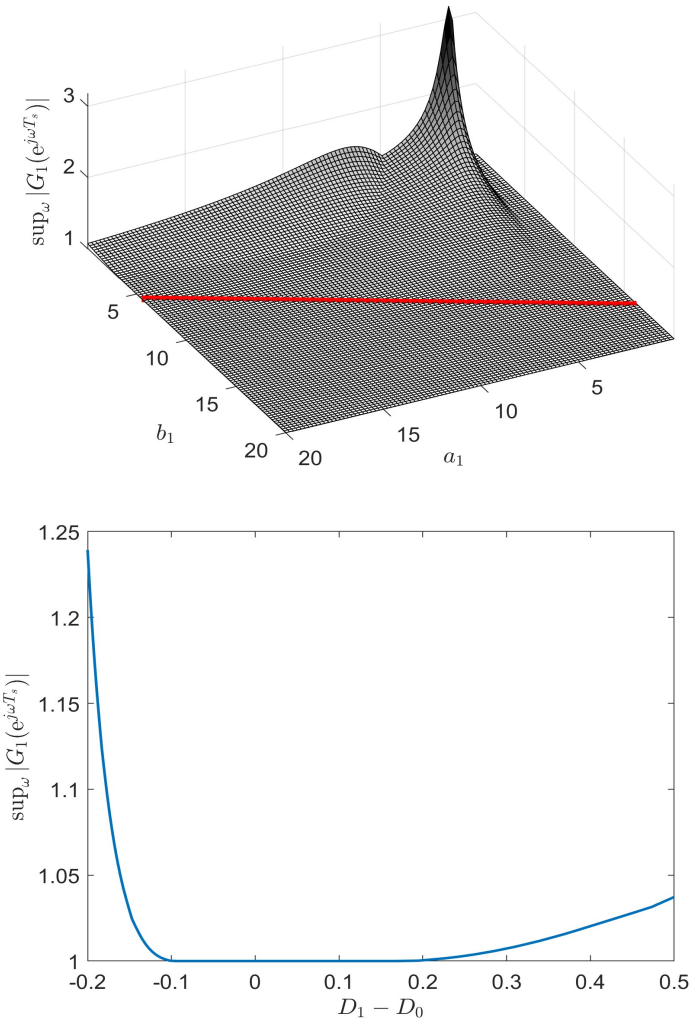

Figure 7.2: Magnitude $\sup_\omega |G_1(e^{j\omega T_s})|$ corresponding to transfer function (7.23), as a function of α_1 and b_1 for choices of parameters corresponding to vehicles 0, 1 from Table 7.1 (top) and $\sup_\omega |G_1(e^{j\omega T_s})|$ as a function of $D_1 - D_0$ (bottom).

in the small overshoots observed (that may appear also due to noise). We note that the nominal controller (7.4), without a delay compensation mechanism, would result in a highly oscillatory, string (and even vehicle) unstable behavior as actuation delays increase.

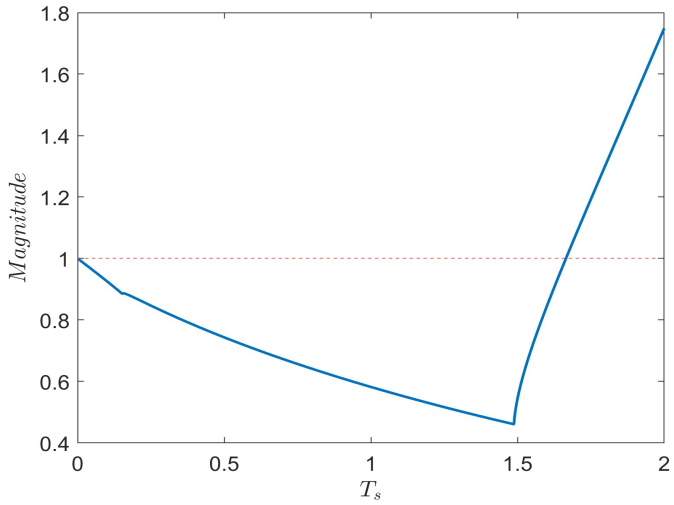

Figure 7.3: Magnitude of the maximum eigenvalue of matrix (7.32) for $i = 1$ as function of T_s.

Table 7.1: The parameters employed for the numerical/experimental investigations presented in Sections 7.3 and 7.4.

Parameters \ Vehicle No.	0	1	2	3	4
τ_i	0.067 s	0.067 s	0.1 s	0.2	0.15
h_i	–	1 s	1 s	0.8 s	0.8 s
D_i	0.15 s	0.3 s	0.6 s	0.4 s	0.3 s
$D_{c,i-1}$	–	0.02 s	0.05 s	0.04 s	0.03 s
α_i	–	7.5	7.5	5	5
b_i	–	12.5	12.5	10	10
c_i	–	0	0	1	1

Table 7.2: The parameters employed for numerical/experimental illustration.

Parameter	Value
T_s	0.01 s
Simulation step	0.001 s
r_i	10 m

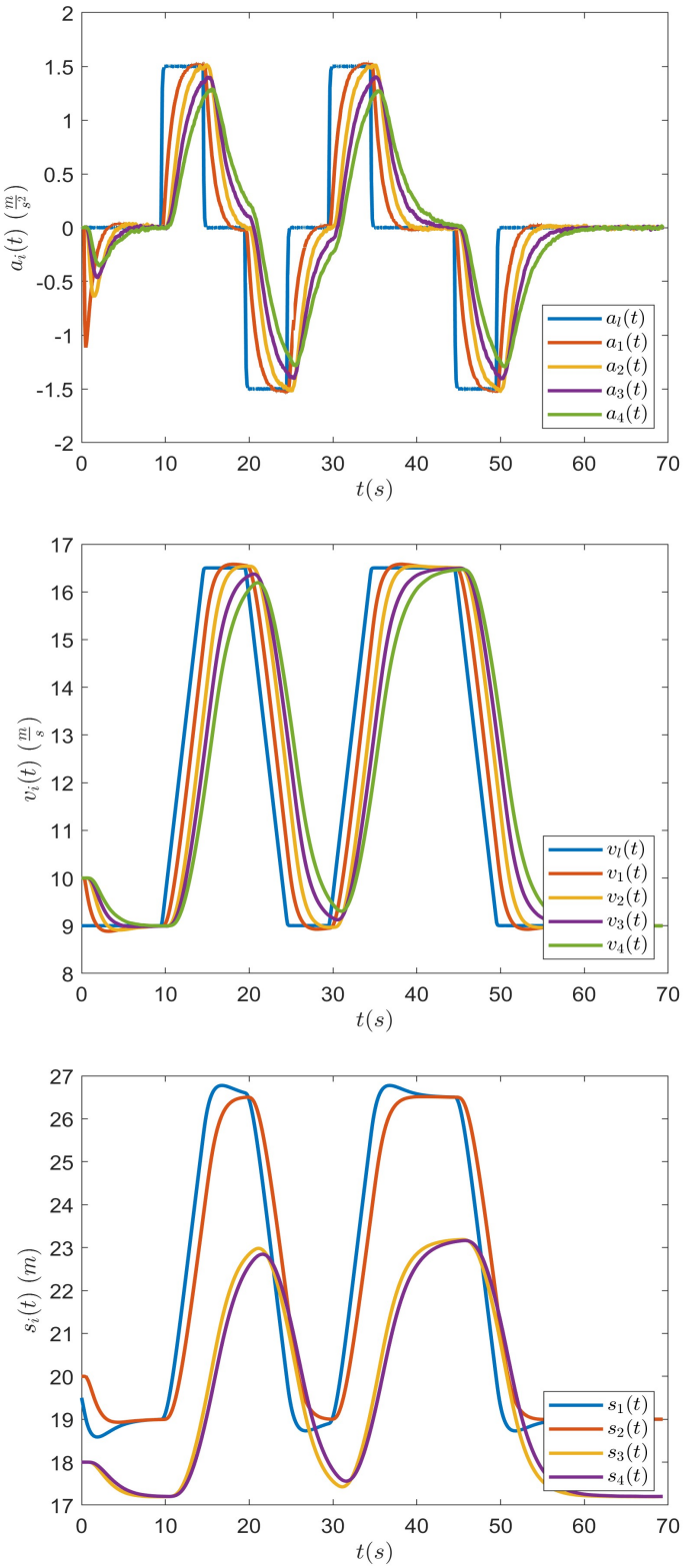

Figure 7.4: Acceleration (top), speed (middle), and spacing (bottom) of five vehicles, with dynamics described by (7.1)–(7.3), under the predictor-based CACC laws (7.13), (7.14), where the selected parameters and control gains are shown in Table 7.1 and Table 7.2, respectively. Initial conditions are $v_{i_0} = 10\left(\frac{m}{s}\right)$, $i = 1, 2, 3, 4$, $v_{l_0} = 9\left(\frac{m}{s}\right)$; $s_{i_0} = h_i \times 10 + r_i$ (m), $i = 2, 3, 4$, $s_{1_0} = 9.5 + r_1$ (m); and $a_i(0) = 0$; $u_i(s) \equiv 0$, for each vehicle i.

7.4 Experimental Implementation and Validation

7.4.1 Description of the Experimental Setup

To experimentally validate the controller, we use a platoon of two full-scale electric vehicles as shown in Figure 7.5. Details on the automation of the vehicles and associated sensors for a (predictor-based) CACC controller, can be found in [22] and [23], respectively. The resulting experimental platform exhibits drive-by-wire functionality that results in a longitudinal vehicle response according to (7.3), with lag $\tau_i = 0.067$ s and input delay $D_i = 0.15$ s. To create distinct input delays for both vehicles, we add an additional input delay in the software of the ego vehicle, to obtain an input delay $D_1 = 0.3$ s. The resulting parameters of the experimental setup are identical to vehicles 0 and 1 in Table 7.2.

To implement the predictor-feedback controller, the measurements $\bar{x}_{ik}$ from (7.17) and u_{i-1,m_k} are required. The inter-vehicle distance s_i is directly measured by the automotive radar. To obtain the ego vehicle's longitudinal velocity v_i, the rear-axle rotational speed of the vehicle is measured. The longitudinal acceleration a_i of the vehicle is obtained through an Inertial Measurement Unit (IMU). The exact specifications of the sensors can be found in [21]. The preceding vehicle's velocity v_{i-1} and acceleration a_{i-1}, as well as its control input u_{i-1} are obtained through V2V communication. During the experiments, the mode of the experienced communication latency $D_{c,i-1}$ was 20 ms.

Figure 7.5: Platoon of experimental vehicles that are used to perform the experiments. The vehicles used in this study both belong to the Technical University of Eindhoven. Access was obtained through collaboration with the Group of Vehicle Dynamics and Control at TU Eindhoven.

7.4.2 Experimental Results

To perform the experiments, the vehicles are initialized in an equilibrium position with both vehicles at standstill. Next, the leader vehicle is controlled to a cruise speed of $v_{i-1} = 3\left(\frac{m}{s}\right)$, while the follower vehicle is controlled with the predictor-based CACC controller (7.13), with the tuning of vehicle 1 from Table 7.1. Once the cruise speed is reached, positive and negative acceleration steps with an amplitude of $1.5\left(\frac{m}{s^2}\right)$ are prescribed to the leader vehicle. The measured velocity and acceleration response of the platoon is shown in Figure 7.6.

At the start of the experiment (from 230 to 232.5 seconds), a negative acceleration setpoint of the ego vehicle can be observed. This negative acceleration setpoint is the result of the initialization of the platoon, which has a slightly smaller inter-vehicle distance than the desired inter-vehicle distance at standstill, as can be seen in Figure 7.6a. Since the experimental vehicle cannot drive backward (without physically changing the gear), this results in a negative acceleration setpoint which keeps the ego vehicle stationary until the leader vehicle starts driving. The measured experimental response indicates the controller and adopted tuning indeed result in string stability, as the there is essentially no overshoot in both the velocity and acceleration response. In steady state situations, when the leader vehicle is driving with constant velocity, the ego vehicle's speed converges to the leader vehicle's speed. Consequently, the experimental results confirm the theoretical results and show that the controller can operate in practice.

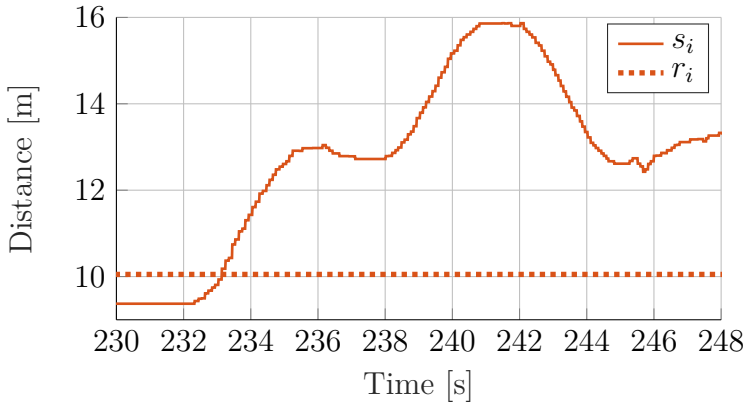

(a) Inter vehicle distance s_i, as measured by radar.

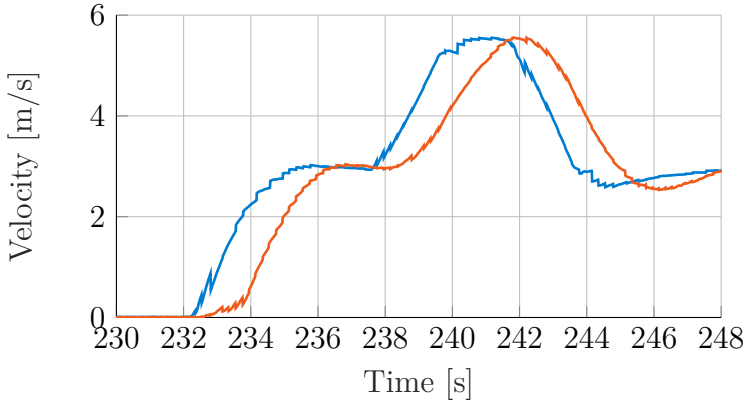

(b) Platoon velocity response.

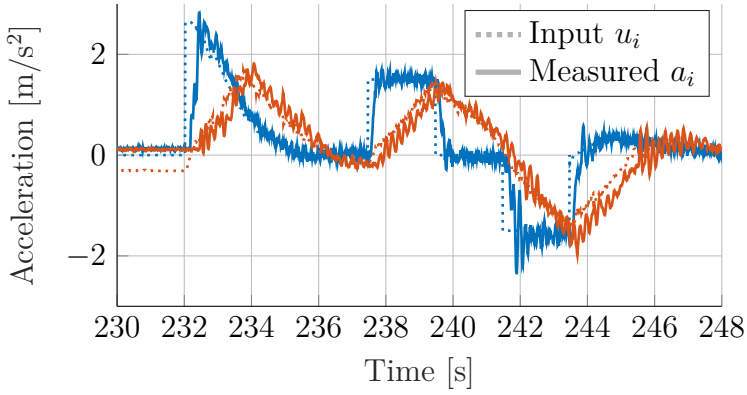

(c) Platoon acceleration response.

Figure 7.6: Measured experimental response of vehicle (—) deploying predictor-based controller (7.13), (7.14), to follow leader vehicle (—). The ego and leader vehicles' parameters and tuning correspond to vehicles 0 and 1 from Table 7.1, respectively.

7.5 Chapter Conclusions and Related Publications

We provided experimental results, validating in actual implementations, the delay-compensating CACC design from [53]. The implementation relied on explicit, zero-order hold formulae of the predictor-based CACC law, which was employed in the case of a pair of vehicles with different actuation delays. We also provided consistent simulation results, also studying numerically vehicle and string stability, depending on control/model parameters. Both the simulation and experimental results confirm the effectiveness of the design in guaranteeing vehicle stability, string stability, and tracking, consistently with the respective theoretical results from [53].

This chapter is an adaptation of material appearing in

A. Samii, R. de Haan, and N. Bekiaris-Liberis, "Experimental implementation and validation of predictor-based CACC for vehicular platoons with distinct actuation delays," *IEEE Conference on Decision and Control*, Rio de Janeiro, 2025.

Chapter 8

Perspectives

As an extension, future research will focus on implementing the exact predictor-feedback CACC design from Chapter 6 in a ring-road scenario, which is a theoretically important problem. Furthermore, we aim to develop an exact predictor-feedback approach that explicitly accounts for the effect of control inputs applied via zero-order hold, which better reflects practical implementation constraints. In addition, we plan to extend the predictor-based CACC framework to accommodate various platoon communication topologies, while integrating alternative nominal (for the delay-free case) control strategies that , e.g., incorporate safety criteria within the platoon.

A more challenging, but promising, avenue is the development of nonlinear, predictor-based CACC designs, accounting for model nonlinearities and relying on nonlinear nominal controllers. This framework can be further extended to incorporate actuation delays in vehicle dynamics and communication delays across the CACC vehicular network. In addition to showing string and vehicle stability, studying the safety properties of the platoon is a challenging, but important, problem related to development of nonlinear, predictor-based CACC laws.

In addition, future work could explore mixed traffic scenarios involving both automated and human-driven vehicles. Within such contexts, applying ACC/CACC strategies under varying network topologies would enable investigation of methods for reducing the constant time-headway in light traffic conditions. Furthermore, developing adaptive time-headway strategies tailored to heavy traffic could help increase overall road throughput. Critical criteria, such as head-to-tail string stability, should be examined alongside optimization objectives that are vital in automated vehicle systems, including fuel efficiency, passenger comfort, and overall performance.

Bibliography

[1] E. Abolfazli, B. Besselink, and T. Charalambous, "Minimum time headway in platooning systems under the MPF topology for different wireless communication scenario", *IEEE Transactions on Intelligent Transportation Systems*, vol. 24, no. 4, pp. 4377–4390, 2023.

[2] R. Akcelik and D. C. Biggs, "Acceleration profile models for vehicles in road traffic", *Transportation Science*, vol. 21, pp. 36–54, 1987.

[3] Z. Artstein, "Linear systems with delayed controls: A reduction", *IEEE Transactions on Automatic Control*, vol. 27, pp. 869–879, 1982.

[4] N. Bekiaris-Liberis, "Robust string stability and safety of CTH predictor-feedback CACC", *IEEE Transactions on Intelligent Transportation Systems*, vol. 24, pp. 8209-8221, 2023.

[5] N. Bekiaris-Liberis and M. Krstic, *Nonlinear Control Under Nonconstant Delays*, SIAM, 2013.

[6] N. Bekiaris-Liberis and M. Krstic, "Predictor-feedback stabilization of multi-input nonlinear systems," *IEEE Transactions on Automatic Control*, vol. 62, no. 2, pp. 516–531, Feb. 2017.

[7] N. Bekiaris-Liberis, C. Roncoli, and M. Papageorgiou, "Predictor-based adaptive cruise control design", *IEEE Transactions on Intelligent Transportation Systems*, vol. 19, pp. 3181–3195, 2018.

[8] N. Bekiaris-Liberis, "Robustness of string stability to delay mismatch and safety of CTH predictor-feedback CACC", *IEEE Conference on Decision and Control*, Cancun, Mexico, 2022.

[9] N. Bekiaris-Liberis, C. Roncoli, and M. Papageorgiou, "Predictor-based adaptive cruise control design", *IEEE Transactions on Intelligent Transportation Systems*, vol. 19, pp. 3181–3195, 2018.

[10] M. di Bernardo, A. Salvi, and S. Santini, "Distributed consensus strategy for platooning of vehicles in the presence of time-varying heterogeneous communication delays", *IEEE Transactions on Intelligent Transportation Systems*, vol. 16, pp. 102–112, 2015.

[11] Y. Bian, Y. Zheng, W. Ren, S. Eben Li, J. Wang, K. Li, "Reducing time headway for platooning of connected vehicles via V2V communication", *Transportation Research Part C: Emerging Technologies*, vol. 102, pp. 87–105, 2019.

[12] A. Bose and P. A. Ioannou, "Analysis of traffic flow with mixed manual and semiautomated vehicles", *IEEE Transactions on Intelligent Transportation Systems*, vol. 4, pp. 173–188, 2003.

[13] B. Caiazzo, F. Di Rosa, D. Giuseppe Lui, A. Petrillo, and S. Santini, "Distributed resilient control for autonomous connected vehicles platoon over uncertain V2X communication links", *IEEE International Conference on Intelligent Transportation Systems*, Bilbao, Spain, 2023.

[14] B. Caiazzo, D. Giuseppe Lui, A. Mungiello, A. Petrillo, and S. Santini, "On the resilience of autonomous connected vehicles platoon under DoS attacks: a predictor-based sampled data control", *IEEE International Conference on Intelligent Transportation Systems*, Bilbao, Spain, 2023.

[15] L. Chen, "Triangular angle rigidity for distributed localization in 2D", *Automatica*, vol. 143, paper no. 110414, 2022.

[16] L. Chen, M. Cao and C. Li, "Angle rigidity and its usage to stabilize multiagent formations in 2-D", *IEEE Transactions on Automatic Control*, vol. 66, pp. 3667–3681, 2021.

[17] L. Chen, K. Cao, L. Xie, X. Li and M. Feroskhan, "3-D network localization using angle measurements and reduced communication", *IEEE Transactions on Signal Processing*, vol. 70, pp. 2402–2415, 2022.

[18] L. C. Davis, "Method of compensation for the mechanical response of connected adaptive cruise control vehicles", *Physica A: Statistical Mechanics and its Applications*, vol. 562, paper no. 125402, 2021.

[19] J. I. Ge and G. Orosz "Dynamics of connected vehicle systems with delayed acceleration feedback", *Transportation Research Part C: Emerging Technologies*, vol. 46, pp. 46–64, 2014.

[20] S. Guo, G. Orosz, and T. G. Molnar, "Connected cruise and traffic control for pairs of connected automated vehicles", *IEEE Transactions on Intelligent Transportation Systems*, vol. 24, pp. 12648–12658, 2023.

[21] R. de Haan, T. van der Sande, E. Lefeber, "Cooperative adaptive cruise control for heterogeneous platoons with actuator delay", *IFAC-PapersOnLine*, vol. 56, pp. 5579–5584, 2023.

[22] R. de Haan, L. Redi, T. van der Sande, and E. Lefeber, "Platooning of heterogeneous vehicles with actuation delays: Experimental results," *IFAC-PapersOnLine*, vol. 58, no. 27, pp. 131–136, 2024.

[23] F. N. Hoogeboom, *Safety of Automated Vehicles: Design, Implementation, and Analysis*. Ph.D. thesis, Eindhoven University of Technology, 2020.

[24] S. Huang and W. Ren, "Autonomous intelligent cruise control with actuator delays", *Journal of Intelligent & Robotic Systems*, vol. 23, pp. 27-–43, 1998.

[25] O. Hutník and J. Molnárová, "On Flett's mean value theorem," *Aequationes Mathematicae*, vol. 89, pp. 1133–1165, 2015.

[26] K. B. Janiszowski, "A modification and the Tustin approximation," *IEEE Transactions on Automatic Control*, vol. 38, no. 8, pp. 1313–1316, 1993.

[27] I. Karafyllis and M. Krstić, *Predictor Feedback for Delay Systems: Implementations and Approximations*, Springer International Publishing, 2017.

[28] I. Karafyllis and M. Krstic, "Nonlinear stabilization under sampled and delayed measurements, and with inputs subject to delay and zero-order hold", *IEEE Transactions on Automatic Control*, vol. 57, no. 5, pp. 1141–1154, 2012.

[29] H. K. Khalil, *Nonlinear Control*, Pearson, 2015.

[30] Z. H. Khattak, B. L. Smith and M. D. Fontaine, "Cyberattack monitoring architectures for resilient operation of connected and automated vehicles", *IEEE Open Journal of Intelligent Transportation Systems*, vol. 5, pp. 322–341, 2024.

[31] D. Liu, B. Besselink, S. Baldi, W. Yu and H. L. Trentelman, "On structural and safety properties of head-to-tail string stability in mixed platoons", *IEEE Transactions on Intelligent Transportation Systems*, vol. 24, pp. 6614–6626, 2023.

[32] F. Ma, J. Wang, S. Zhu, S. Gelbal, Y. Yang, B. Aksun-Guvenc, and L. Guvenc, "Distributed control of cooperative vehicular platoon with nonideal communication condition", *IEEE Transactions on Vehicular Technology*, vol. 69, pp. 8207–8220, 2020.

[33] M. Makridis, K. Mattas, A. Anesiadou, and B. Ciuffo, "OpenACC. An open database of car-following experiments to study the properties of commercial ACC systems", *Transportation Research Part C: Emerging Technologies*, vol. 125, 2021.

[34] J. J. Martinez and C. Canudas-de-Wit, "A safe longitudinal control for adaptive cruise control and stop-and-go scenarios", *IEEE Transactions on Control Systems Technology*, vol. 15, pp. 246–258, 2007.

[35] T. G. Molnar, W. B. Qin, T. Insperger, and G. Orosz, "Application of predictor feedback to compensate time delays in connected cruise control," *IEEE Transactions on Intelligent Transportation Systems*, vol. 19, pp. 545–559, 2018.

[36] T. G. Molnar, A. K. Kiss, A. D. Ames, and G. Orosz, "Safety-critical control with input delay in dynamic environment," *IEEE Transactions on Control Systems Technology*, vol. 31, pp. 1507–1520, 2023.

[37] M. Montanino and V. Punzo, "Trajectory data reconstruction and simulation-based validation against macroscopic traffic patterns," *Transportation Research Part B: Methodological*, vol. 80, pp. 82–106, 2015.

[38] S. Öncü, N. van de Wouw, W. P. M. H. Heemels, and H. Nijmeijer, "String stability of interconnected vehicles under communication constraints", *IEEE Conference on Decision and Control*, Maui, USA, 2012.

[39] S. Öncü, J. Ploeg, N. van de Wouw, and H. Nijmeijer, "Cooperative adaptive cruise control: Network-aware analysis of string stability", *IEEE Transactions on Intelligent Transportation Systems*, vol. 15, pp. 1527–1537, 2014.

[40] T. Pati, S. Hwang, and S. Z. Yong, "Control barrier functions for linear continuous-time input-delay systems with limited-horizon previewable disturbances," in *American Control Conference*, Toronto, ON, Canada, pp. 2412–2419, 2024.

[41] A. Petrillo, A. Salvi, S. Santini, and A. S. Valente, "Adaptive multi-agent synchronization for collaborative driving of autonomous vehicles with multiple communication delays," *Transportation Research Part C: Emerging Technologies*, vol. 86, pp. 372–392, 2018.

[42] J. Ploeg, N. van de Wouw, and H. Nijmeijer, "$\mathcal{L}_p$ string stability of cascaded systems: Application to vehicle platooning", *IEEE Transactions on Control Systems Technology*, vol. 22, pp. 786–793, 2014.

[43] A. Salvi, S. Santini, and A. S. Valente, "Design, analysis and performance evaluation of a third order distributed protocol for platooning in the presence of time-varying delays and switching topologies", *Transportation Research Part C: Emerging Technologies*, vol. 80, pp. 360–383, 2017.

[44] A. Samii and N. Bekiaris-Liberis, "Robustness of string stability of linear predictor-feedback CACC to communication delay", *IEEE International Conference on Intelligent Transportation Systems*, Bilbao, Spain, 2023.

[45] A. Samii and N. Bekiaris-Liberis, "Simultaneous compensation of actuation and communication delays for heterogeneous platoons via predictor-feedback CACC with integral action," *IEEE Transactions on Intelligent Vehicles*, vol. 9, pp. 5618–5630, 2024.

[46] A. Samii and N. Bekiaris-Liberis, "Numerical investigation of head-to-tail string stability and performance of predictor-based ACC in a mixed traffic scenario", *Mediterranean Conference on Control and Automation*, Chania, Greece, 2024.

[47] R. A. Shet and S. Yao, "Cooperative driving in mixed traffic: an infrastructure-assisted approach", *IEEE Open Journal of Intelligent Transportation Systems*, vol. 2, pp. 429–447, 2021.

[48] L. Shir-Kuan and F. Chang-Jia, "Nonovershooting and monotone nondecreasing step responses of a third-order SISO linear system", *IEEE Transactions on Automatic Control*, vol. 42, pp. 1299-1303, 1997.

[49] M. Sun, "A Barbalat-like lemma with its application to learning control", *IEEE Transactions on Automatic Control*, vol. 54, pp. 2222–2225, 2009.

[50] B. van Arem, C. J. G. van Driel and R. Visser, "The impact of cooperative adaptive cruise control on traffic-flow characteristics", *IEEE Transactions on Intelligent Transportation Systems*, vol. 7, pp. 429–436, 2006.

[51] M. Wang, S. P. Hoogendoorn, W. Daamen, B. van Arem, B. Shyrokau, and R. Happee, "Delay-compensating strategy to enhance string stability of autonomous vehicle platoons", *Transport metrica B: Transport Dynamics*, vol. 6, pp. 211–229, 2016.

[52] H. M. Wang et al., "Conflict analysis for cooperative maneuvering with status and intent sharing via V2X communication," *IEEE Transactions on Intelligent Vehicles*, vol. 8, no. 2, pp. 1105–1118, 2023.

[53] K. Watanabe and M. Ito, "An observer for linear feedback control laws of multi variable systems with multiple delays in controls and outputs", *Systems & Control Letters*, vol. 1, pp. 54–59, 1981.

[54] S. Wong, L. Jiang, R. Walters, T. G. Molnár, G. Orosz, and R. Yu, "Traffic forecasting using vehicle-to-vehicle communication," *Proceedings of the 3rd Conference on Learning for Dynamics and Control, Proceedings of Machine Learning Research*, vol. 144, pp. 917–929, 2021.

[55] L. Xiao and F. Gao, "Practical string stability of platoon of adaptive cruise control vehicles", *IEEE Transactions on Intelligent Transportation Systems*, vol. 12, pp. 1184–1194, 2011.

[56] H. Xie, Y. Wang, X. Su, S. Wang and L. Wang, "Safe driving model based on V2V vehicle communication", *IEEE Open Journal of Intelligent Transportation Systems*, vol. 3, pp. 449–457, 2022.

[57] H. Xing, J. Ploeg, and H. Nijmeijer, "Smith predictor compensating for vehicle actuator delays in cooperative ACC systems", *IEEE Transactions on Vehicular Technology*, vol. 68, pp. 1106–1115, 2018.

[58] H. Xing, J. Ploeg, and H. Nijmeijer, "Compensation of communication delays in a cooperative ACC system", *IEEE Transactions on Vehicular Technology*, vol. 69, pp. 1177–1189, 2019.

[59] H. Xing, J. Ploeg, and H. Nijmeijer, "Robust CACC in the presence of uncertain delays", *IEEE Transactions on Vehicular Technology*, vol. 71, pp. 3507–3518, 2022.

[60] D. Yanakiev and I. Kanellakopoulos, "Longitudinal control of automated CHVs with significant actuator delays", *IEEE Transactions on Vehicular Technology*, vol. 50, pp. 1289-1297, 2001.

[61] Y. Zhang, Y. Bai, J. Hu, and M. Wang, "Control design, stability analysis, and traffic flow implications for cooperative adaptive cruise control systems with compensation of communication delay", *Transportation Research Record*, vol. 2674, pp. 638-–652, 2020.

[62] Y. Zhang, Y. Bai, J. Hu, D. Cao, and M. Wang, "Memory-anticipation strategy to compensate for communication and actuation delays for strings-stable platooning", *IEEE Transactions on Intelligent Vehicles*, vol. 8, pp. 1145–1155, 2022.

[63] H. Zhang, J. Liu, Z. Wang, C. Huang and H. Yan, "Adaptive switched control for connected vehicle platoon with unknown input delays", *IEEE Transactions on Cybernetics*, vol. 53, pp. 1511–1521, 2023.

[64] Y. Zhang, M. Wang, J. Hu, and N. Bekiaris-Liberis, "Semi-constant spacing policy for leader-predecessor-follower platoon control via delayed measurements synchronization", *IFAC World Congress*, vol. 53, pp. 15096–15103, 2020.

[65] C. Zhao, H. Yu, and T. G. Molnar, "Safety-critical traffic control by connected automated vehicles", *Transportation Research Part C: Emerging Technologies*, vol. 154, paper no. 104230, 2023.

[66] Y. Zheng, S. Eben Li, J. Wang, D. Cao, and K. Li, "Stability and scalability of homogeneous vehicular platoon: Study on the influence of information flow topologies," *Transportation Research Part C: Emerging Technologies*, vol. 17, pp. 14–26, 2016.

[67] Y. Zhang, Z. Xu, Z. Wang, X. Yao, and Z. Xu, "Impacts of communication delay on vehicle platoon string stability and its compensation strategy: A review", *Journal of Traffic and Transportation Engineering (English Edition)*, vol. 10, pp. 508–529, 2023.

Complete List of Publications

Journal Papers

1. **A. Samii** and N. Bekiaris-Liberis, "Exact predictor-feedback CACC of heterogeneous vehicular platoons with distinct actuation delays", *IEEE Transactions on Intelligent Transportation Systems*, provisionally accepted, 2025.

2. **A. Samii** and N. Bekiaris-Liberis, "Predictor-based CACC design for heterogeneous vehicles with distinct input delays", *IEEE Open Journal of Intelligent Transportation Systems*, vol. 5, pp. 783–796, 2024.

3. **A. Samii** and N. Bekiaris-Liberis, "Simultaneous compensation of actuation and communication delays for heterogeneous platoons via predictor-feedback CACC with integral action", *IEEE Transactions on Intelligent Vehicles*, vol. 9, pp. 5618–5630, 2024.

Conference Papers

1. **A. Samii**, R. de Haan, and N. Bekiaris-Liberis, "Experimental implementation and validation of predictor-based CACC for vehicular platoons with distinct actuation delays", *IEEE Conference on Decision and Control*, Rio de Janeiro, 2025.

2. **A. Samii** and N. Bekiaris-Liberis, "On Compensation of Distinct Input Delays in Heterogeneous Vehicular Platoons via Exact Predictor-Feedback CACC", *IFAC Workshop on Time Delay Systems*, Paris, 2025.

3. **A. Samii** and N. Bekiaris-Liberis, "Compensation of distinct actuator delays for heterogeneous vehicular platoons via predictor-based CACC", *European Control Conference*, Thessaloniki, 2025.

4. **A. Samii** and N. Bekiaris-Liberis,"Simultaneous compensation of actuation and communication delays for heterogeneous platoons via predictor-feedback CACC

with integral action", *European Control Conference*, Stockholm, 2024.

5. **A. Samii**, P. Karafotis, and N. Bekiaris-Liberis, "Numerical Investigation of Head-to-Tail String Stability and Performance of Predictor-Based ACC in a Mixed Traffic Scenario", *Mediterranean Conference on Control and Automation*, Chania, Greece, 2024.

6. **A. Samii** and N. Bekiaris-Liberis, "Simultaneous compensation of actuation and communication delays for heterogeneous platoons via predictor-feedback CACC with integral action", *IEEE Transactions on Intelligent Vehicles*, vol. 9, pp. 5618–5630, 2024.